



City Research Online

City, University of London Institutional Repository

Citation: Marian, Laurentiu (2015). The tuned mass damper inerter for passive vibration control and energy harvesting in dynamically excited structural systems. (Unpublished Doctoral thesis, City University London)

This is the accepted version of the paper.

This version of the publication may differ from the final published version.

Permanent repository link: <https://openaccess.city.ac.uk/id/eprint/14884/>

Link to published version:

Copyright: City Research Online aims to make research outputs of City, University of London available to a wider audience. Copyright and Moral Rights remain with the author(s) and/or copyright holders. URLs from City Research Online may be freely distributed and linked to.

Reuse: Copies of full items can be used for personal research or study, educational, or not-for-profit purposes without prior permission or charge. Provided that the authors, title and full bibliographic details are credited, a hyperlink and/or URL is given for the original metadata page and the content is not changed in any way.

City Research Online:

<http://openaccess.city.ac.uk/>

publications@city.ac.uk

**THE TUNED MASS DAMPER INERTER FOR PASSIVE
VIBRATION CONTROL AND ENERGY HARVESTING
IN DYNAMICALLY EXCITED STRUCTURAL SYSTEMS**

by

Laurentiu Marian

Dissertation submitted in fulfilment of the requirements for the award of

DOCTOR OF PHILOSOPHY

in

STRUCTURAL ENGINEERING

School of Engineering and Mathematical Sciences

City University London

October 2015

TABLE OF CONTENTS

TABLE OF CONTENTS.....	ii
LIST OF TABLES	vi
LIST OF FIGURES	viii
ACKNOWLEDGMENTS	viiiiv
DECLARATION.....	xv
ABSTRACT.....	xvi
CHAPTER 1 :INTRODUCTION.....	1
1.1 MOTIVATION AND OBJECTIVES	1
1.2 THESIS ORGANISATION AND OUTLINE	6
CHAPTER 2 :A REVIEW ON THE CLASSICAL TUNED-MASS-DAMPER AND MASS AMPLIFICATION DEVICES FOCUSING ON APPLICATIONS IN EARTHQUAKE ENGINEERING	8
2.1 PASSIVE TUNED-MASS-DAMPER BASED VIBRATION CONTROL	8
2.2 THE INERTER AND OTHER MASS AMPLIFICATION DEVICES IN EARTHQUAKE ENGINEERING APPLICATIONS.....	14
CHAPTER 3 :THE TUNED-MASS-DAMPER-INERTER PASSIVE CONTROL SOLUTION FOR SINGLE-DEGREE-OF-FREEDOM PRIMARY SYSTEMS.....	19
3.1 PRELIMINARY REMARKS	19

3.2	GOVERNING EQUATIONS OF MOTION	20
3.3	OPTIMUM DESIGN OF THE TUNED-MASS-DAMPER-INERTER FOR HARMONIC EXCITATION.....	25
3.3.1	<i>Derivation of closed form solutions for optimum design parameters</i>	<i>25</i>
3.3.2	<i>Quantification of the performance enhancement and weight reduction of the Tuned-Mass-Damper-Inerter vis-à-vis the classical Tuned-Mass-Damper.....</i>	<i>30</i>
3.4	OPTIMUM DESIGN OF THE TUNED-MASS-DAMPER-INERTER FOR STOCHASTIC WHITE NOISE EXCITATION	36
3.4.1	<i>Derivation of closed form solutions for optimum design parameters.....</i>	<i>36</i>
3.4.2	<i>Quantification of performance enhancement and weight reduction of the Tuned-Mass-Damper-Inerter vis-à-vis the classical Tuned-Mass-Damper.</i>	<i>40</i>
CHAPTER 4 :THE TUNED MASS DAMPER – INERTER FOR SUPPORT- EXCITED MULTI-DEGREE-OF-FREEDOM PRIMARY SYSTEMS		45
4.1	PRELIMINARY REMARKS	45
4.2	GOVERNING EQUATIONS OF MOTION	47
4.3	OPTIMUM DESIGN OF THE TUNED-MASS-DAMPER-INERTER CONFIGURATION FOR DAMPED MULTI-DEGREE-OF-FREEDOM PRIMARY SYSTEMS.....	52
4.4	NUMERICAL APPLICATION OF THE TUNED-MASS-DAMPER-INERTER FOR DAMPED MULTI-DEGREE-OF-FREEDOM PRIMARY SYSTEMS: OPTIMUM DESIGN FOR STATIONARY COLOURED NOISE SUPPORT EXCITATION.....	55

4.4.1	<i>Optimum design of the classical Tuned-Mass-Damper as a special case of the Tuned-Mass-Damper-Inerter configuration</i>	57
4.4.2	<i>Optimum design of the Tuned-Mass-Damper-Inerter configuration</i>	60
CHAPTER 5:DESIGN AND ASSESMENT OF THE TUNED-MASS-DAMPER-INERTER FOR SEISMIC PROTECTION OF MULTI-STOREY BUILDINGS.		64
5.1	PRELIMINARY REMARKS	64
5.2	EUROCODE 8 COMPATIBLE OPTIMUM TUNED-MASS-DAMPER-INERTER DEISGN OF BUILDING STRUCTURES	68
5.2.1	<i>Optimum Tuned-Mass-Damper-Inerter design parameters</i>	71
5.2.2	<i>Top floor displacement variance of optimally designed Tuned-Mass-Damper-Inerter ($b>0$) versus the Tuned-Mass-Damper ($b=0$) for Eurocode 8 compatible stochastic excitation.</i>	79
5.2.3	<i>On the weight reduction of the Tuned-Mass-Damper Inerter ($b>0$) versus the classical Tuned-Mass-Damper ($b=0$)</i>	86
5.3	PERFORMANCE ASSESMENT OF OPTIMALLY DESIGNED TUNED-MASS-DAMPER-INERTER EQUIPPED STRUCTURES USING FIELD RECORDED EUROCODE 8 COMPATIBLE ACCELEROGRAMS	89
5.4	ON THE CONTROL OF HIGHER MODES USING THE TUNED-MASS-DAMPER-INERTER PASSIVE CONTROL SOLUTION.....	95
CHAPTER 6 :SIMULTANEOUS VIBRATION SUPRESSION AND ENERGY HARVESTING USING THE TUNED-MASS-DAMPER-INERTER.....		99
6.1	PRELIMINARY REMARKS	99

6.2	MECHANICAL DESCRIPTION AND CHARACTERISATION OF THE PROPOSED ENERGY HARVESTING ENABLED TUNED-MASS-DAMPER-INERTER.....	101
6.3	QUANTIFICATION OF ENERGY SCAVENGED BY THE PROPOSED TUNED-MASS-DAMPER-INERTER ELECTRO-MAGNETIC HARVESTER DEVICE.....	104
6.4	SIMULTANIOUS ENERGY HARVESTING AND VIBRATION SUPPRESSION FOR TUNED-MASS-DAMPER-INERTER EQUIPPED SYSTEMS WITH VARYING INERTANCE	107
	CHAPTER 7 :CONCLUDING REMARKS.....	111
	APPENDIX I: ALTERNATIVE CONNECTIVITY ARRANGEMENTS OF SPRINGS, DAMPERS AND INERTERS	120
	APPENDIX II : TUNED-MASS-DAMPER-INERTER EQUATIONS OF MOTION USING A SYSTEM NETWORK APPROACH.....	123
	REFERENCES	126

LIST OF TABLES

Table 1.1 Matrix of Thesis Contribution	5
Table 3.1. Closed-form expressions for optimal TMDI for undamped SDOF harmonically excited primary structures vis-à-vis the classical TMD case	29
Table 3.2. Closed-form expressions for optimal tuning of the proposed TMDI configuration for undamped SDOF primary structures subject to white noise base excitation vis-à-vis the classical TMD case.	39
Table 4.1 Inertial and elastic properties of the considered 3-DOF primary structure.....	56
Table 4.2. Optimal TMDI parameters, Performance Index (PI) and percentage difference of PI achieved for different values of the attached TMDI mass and the inerter constant b compared to the classical TMD ($b=0$).	61
Table 5.1. Inertial and elastic properties of the considered primary structure	69
Table 5.2. Undamped natural frequencies of the considered primary structure.	69
Table 5.3. Parameters for the definition of C-P evolutionary power spectrum compatible with EC8 spectra	71
Table 5.4. The normalized by the top floor value of the first mode shape vector and the corresponding generalised masses	72
Table 5.5. TMDI parameters and Performance Index for different values of the additional m_{TMDI} mass and of the inerter constant b	82
Table 5.6. Maximum top floor displacements (cm) for 3DOF Structure IIa	90
Table 5.7. Maximum top floor acceleration (g) for 3DOF Structure IIa	93
Table 5.8. Maximum m_{TMDI} mass displacements (cm)	94
Table 5.9. Inertial and elastic properties of the considered primary structure.....	95
Table 5.10. Undamped natural frequencies of the considered primary structure.	95
Table 5.11. Inertial and elastic properties of the considered primary structure	96

Table 5.12. Maximum top floor and next-to-top floor displacements (cm) and accelerations for the 10DOF primary structure.....	98
Table 6.1 Optimal TMDI parameters derived for $\beta=0.6$ and several mass ratio μ values	109

LIST OF FIGURES

Figure 2.1 A structural frame model of multi-storey (a) and single-storey (b) building structures (primary systems) equipped with Tuned-Mass-Damper (TMD) classical passive control solution.....	9
Figure 2.2 Schematic representation of the two-terminal flywheel device (b is the mass-equivalent constant of proportionality	14
Figure 2.3. Single-degree-of-freedom (SDOF) primary structure ground-connected via an inerter element.....	16
Figure 2.4. Possible mechanical realisation of the inerter comprising a plunger that drives a rotating flywheel through a rack, pinion and gearing system with n gears.....	16
Figure 3.1. Single-degree-of-freedom (SDOF) primary structure equipped with a tuned mass-damper-inerter (TMDI) system (a) force excited; (b) base-excited.....	21
Figure 3.2. Single-degree-of-freedom (SDOF) primary structure (modelled as a frame structure) ground-connected via an inerter element (a) force excited (b) base excited. .	21
Figure 3.3 Relative displacement response amplitude of undamped support excited TMDI equipped SDOF primary structure with mass ratio $\mu=0.1$, inertance ratio $\beta=0.1$, frequency ratio $\nu_{TMDI}=0.5$, and for various TMDI damping ratios ζ_{TMDI}	26
Figure 3.4. Optimum TMDI frequency ratio ν_{TMDI} and damping ratio ζ_{TMDI} as a function of the inertance ratio β and for several mass ratio values μ	31
Figure 3.5. Dynamic amplification factor spectra for various optimally designed TMDI ($b>0$) systems and for the classical TMD ($b=0$).	32
Figure 3.6. Normalized dynamic amplification factor at the “fixed” point ω_{PI} for optimally designed TMDI systems as functions of the inertance ratio β	32

Figure 3.7. Dynamic amplification factor spectra for various optimally designed TMD (b=0) equipped undamped SDOF systems.....	34
Figure 3.8. Dynamic amplification factor spectra for various optimally designed TMD (b=0) equipped undamped SDOF systems.....	35
Figure 3.9. Optimum TMDI frequency ratio for various values of β and several mass ratio values	41
Figure 3.10. Optimum TMD damping ratio for various values of β and several mass ratio values.....	41
Figure 3.11. Minimum variance ratio between the proposed model (b>0) and the classical TMD (b=0).....	42
Figure 3.12 Additional m_{TMDI} mass values required for achieving the same level of performance in terms of displacement response variance for the proposes TMDI configuration and classical TMD (b=0).....	44
Figure 4.1. Multi-degree-of-freedom (MDOF) primary structure incorporating the proposed tuned mass-damper-inerter (TMDI) configuration.....	46
Figure 4.2. One-sided power spectrum representing the acceleration support excitation $\alpha_g(t)$	57
Figure 4.3. Optimum frequency ratio as a function of the TMD mass for various values of the inerter constant b to control the fundamental mode of vibration of the 3-DOF primary structure of Table 4.1.....	58
Figure 4.4. Optimum damping ratio as a function of the TMD mass for various values of the inerter constant b to control the fundamental mode of vibration of the 3-DOF primary structure of Table 4.1.	58
Figure 4.5. Achieved performance index versus the TMD mass for various values of the inerter constant b	59

Figure 5.1. Tuned mass-damper-inerter (TMDI) equipped n -storey frame building.....	66
Figure 5.2. Considered EC8 compatible evolutionary power spectrum $S(\omega, t)$ for design purposes	70
Figure 5.3. Three DOF primary structure (I). Optimum TMDI parameters. Frequency ratio (a) and TMDI damping ratio (b), versus the additional m_{TMDI} mass for various values of b	73
Figure 5.4. Three DOF primary structure (IIa). Optimum TMDI parameters. Frequency ratio (a) and TMDI damping ratio (b), versus the additional m_{TMDI} mass for various values of b	74
Figure 5.5. Three DOF primary structure (IIIa). Optimum TMDI parameters. Frequency ratio (a) and TMDI damping ratio (b), versus the additional m_{TMDI} mass for various values of b	74
Figure 5.6. Three DOF primary structure (I). Optimum TMDI parameters. TMDI stiffness value (a) and TMDI damping value (b), versus the additional m_{TMDI} mass for various values of b	75
Figure 5.7. Three DOF primary structure (IIa). Optimum TMDI parameters. TMDI stiffness value (a) and TMDI damping value (b), versus the additional m_{TMDI} mass for various values of b	76
Figure 5.8. Three DOF primary structure (IIIa). Optimum TMDI parameters. TMDI stiffness value (a) and TMDI damping value (b), versus the additional m_{TMDI} mass for various values of b	77
Figure 5.9. Optimum TMDI parameters. Comparison of TMDI stiffness value versus the additional m_{TMDI} mass for all primary structures considered.	78
Figure 5.10. Optimum TMDI parameters. Comparison of TMDI damping value versus the additional m_{TMDI} mass for all primary structures considered	78

Figure 5.11. Three DOF primary structure - 3DOF (I). Performance index versus the additional m_{TMDI} mass for various values of b	79
Figure 5.12. Three DOF primary structure - 3DOF (IIa). Performance index versus the additional m_{TMDI} mass for various values of b	80
Figure 5.13. Three DOF primary structure - 3DOF (IIb). Performance index versus the additional m_{TMDI} mass for various values of b	80
Figure 5.14. Three DOF primary structure - 3DOF (IIIa). Performance index versus the additional m_{TMDI} mass for various values of b	81
Figure 5.15. Three DOF primary structure - 3DOF (IIIb). Performance index versus the additional m_{TMDI} mass for various values of b	81
Figure 5.16. Performance index ratio between an optimum designed TMD and an optimum designed TMDI for an m_{TMDI} mass of 10% from the total mass of the primary structure and for various values of b	84
Figure 5.17. Three DOF primary structure - 3DOF (IIa). Performance index versus the additional m_{TMDI} mass for various values of b . Robustness assessment of optimal TMDI on structures with uncertainty in natural frequency.	85
Figure 5.18. Absolute transfer function between the input ground acceleration and the output top floor displacement for the uncontrolled (primary) structure 3DOF IIa, structure equipped with optimal TMD and structure equipped with optimal TMDI.	86
Figure 5.19. Additional m_{TMDI} mass values required for achieving the same level of performance index for the proposed TMDI configuration ($b>0$) and for classical TMD ($b=0$). Three DOF primary structure - 3DOF (I).	87
Figure 5.20. Additional m_{TMDI} mass values required for achieving the same level of performance index for the proposed TMDI configuration ($b>0$) and for classical TMD ($b=0$). Three DOF primary structure - 3DOF (IIa).	88

Figure 5.21. Additional m_{TMDI} mass values required for achieving the same level of performance index for the proposed TMDI configuration ($b>0$) and for classical TMD ($b=0$). Three DOF primary structure - 3DOF (IIIa).	88
Figure 5.22. Response spectra of the considered EC8 compatible field recorded accelerograms listed in Table 5.6.....	90
Figure 5.23. Three DOF primary structure IIa. Top floor displacement responses for uncontrolled structure, structure equipped with optimal TMD and structure equipped with optimal TMD and TTF device.	91
Figure 5.24. Three DOF primary structure IIa. Top floor acceleration responses for uncontrolled structure, structure equipped with optimal TMD and structure equipped with optimal TMD and TTF device.	92
Figure 5.25. Absolute transfer function between the input ground acceleration and the output top floor displacement for the 10DOF uncontrolled (primary) structure, structure equipped with optimal TMD and structure equipped with optimal TMDI.....	96
Figure 5.26. Absolute transfer function between the input ground acceleration and the output top floor acceleration for the regular 10DOF uncontrolled (primary) structure, structure equipped with optimal TMD and structure equipped with optimal TMDI.....	97
Figure 6.1 Single-degree-of-freedom (SDOF) primary structure incorporating the proposed tuned mass-damper-inerter-harvester (TMDI-H) configuration.	102
Figure 6.2. Normalized relative velocity amplitude for an undamped structure equipped with optimal TMDI configuration.....	105
Figure 6.3. Normalized power harvested from various TMDI systems optimally designed for vibration suppression.....	106

Figure 6.4. Dynamic amplification factor spectra (left panel) for an optimally designed TMDI system for vibration suppression with $\mu=0.1$ and $\beta=0.6$ (fixed $v_{TMDI}=0.5651$ and $\zeta_{TMDI}=0.4132$) and for several values of inertance.....	108
Figure 6.5. Normalized power harvested spectra for an optimally designed TMDI system for vibration suppression with $\mu=0.1$ and $\beta=0.6$ (fixed $v_{TMDI}=0.5651$ and $\zeta_{TMDI}=0.4132$) and for several values of inertance.....	108
Figure 6.6. Peak dynamic amplification factor for the <i>non-optimal</i> TMDI configurations normalized by the maximum of the dynamic amplification factor for optimally designed TMDI (for $\beta=0.6$) as functions of the inertance ratio β	109
Figure 6.7. Peak normalized potential harvesting power for the <i>non-optimal</i> TMDI configurations normalized by the maximum of the dynamic amplification factor for optimally designed TMDI (for $\beta=0.6$) as functions of the inertance ratio β	110
Figure 0.1. Alternative connectivity arrangements of TMD-inerter considered.....	120
Figure 0.2. Dynamic amplification factor for the system equipped with TMD and for the same system equipped with TMD-inerter, for varying values of b	122

ACKNOWLEDGMENTS

First and foremost, I would like to express my sincere gratitude to my supervisor, Dr Agathoklis Giaralis for his invaluable continuous support, advice and guidance. He is indeed the most rigorous, supportive and dedicated supervisor anyone would hope to have and has been an inspiration throughout my research work and our close collaboration.

Further, the financial support provided by City University London is gratefully acknowledged.

A heartfelt thanks to all my former research colleges at City University for their support and friendship.

In addition, I would also like to express my appreciation to my family's unconditional love. This work would not have been possible without their support and understanding.

DECLARATION

I grant powers of discretion to the University Librarian to allow this dissertation to be copied in whole or in part without further reference to me. This permission covers only single copies made for study purposes, subject to normal conditions of acknowledgements.

ABSTRACT

A novel passive vibration control configuration, namely the Tuned-Mass-Damper-Inerter (TMDI) is proposed in this work. The TMDI combines the “inertor”, a mechanical two-terminal flywheel device developing resisting forces proportional to the relative acceleration of its terminals, with the well-known and widely used in various passive vibration control applications Tuned-Mass-damper (TMD). Introduced as a generalization of the TMD, the TMDI takes advantage of the “mass amplification effect” of the inertor to achieve enhanced performance compared to the classical TMD. For linear harmonically excited primary systems, analytical closed-form expressions are derived for optimal TMDI design/tuning parameters using the well-established and widely applied for the case of the classical TMD semi-empirical fixed-point theory. It is shown that for the same attached mass the TMDI system is more effective than the classical TMD to suppress vibrations close to the natural frequency of the uncontrolled primary system, while it is more robust to de-tuning effects. Moreover, it is analytically shown that optimally designed TMDI outperforms the classical TMD in minimizing the displacement variance of undamped linear single-degree-of-freedom (SDOF) white-noise excited primary systems. For this particular case, optimal TMDI parameters are derived in closed-form as functions of the additional oscillating mass and the inertor constant.

Furthermore, pertinent numerical data are furnished, derived by means of a numerical optimization procedure, for classically damped mechanical cascaded chain-like primary systems base excited by stationary colored noise. This exemplifies the effectiveness of the TMDI over the classical TMD to suppress the fundamental mode of vibration for linear MDOF structures. It is concluded that the incorporation of the inertor in the proposed TMDI configuration can either replace part of the TMD vibrating mass to achieve lightweight passive vibration control solutions, or improve the performance of the classical TMD for a given TMD mass.

The TMDI is further applied for passive vibration control of seismically excited building structures. An input non-stationary stochastic process compatible with the elastic design spectrum of the European aseismic code provisions (EC8) is assumed. The effectiveness of the proposed TMDI configuration over the classical TMD is assessed by performing response history analyses for an ensemble of EC8 spectrum compatible field recorded strong ground motions. The optimally tuned TMDI solution achieves considerable reduction of the peak average top floor displacement and peak average top floor accelerations of the considered primary structures compared to the one achieved by the optimally designed classical TMD, assuming the same additional mass in both cases. Furthermore, the TMDI configuration achieves significant reduction in the maximum displacement of the additional oscillating mass. In this study, the primary structures are assumed to behave linearly in alignment with current trends in performance based requirements for minimally damaged structures protected by passive control devices.

Furthermore, optimally designed TMDI is applied for vibration suppression and energy harvesting via an electromagnetic device which transforms the mechanical kinetic

energy into electrical energy. Unlike the case of traditional energy harvesting enabled TMD systems, the amount of available energy to be harvested by the herein proposed TMDI-based harvester is leveraged by changing the intensity of the mass amplification effect of the inerter, through mechanical gearing, without changing the weight of the TMDI system. Therefore, the inclusion of the inerter adds a “degree of freedom” or a design parameter to the classical TMD-based harvesters allowing to control the trade-off between vibration suppression and energy harvesting in a more flexible manner.

Overall, the herein reported numerical data and analytical work provide evidence that the TMDI offers a novel promising solution for passive vibration control and energy harvesting. Most importantly, it opens several new research paths involving numerical/parametric work, as well as, prototyping, experimental testing and field deployment.

CHAPTER 1 : INTRODUCTION

1.1 MOTIVATION AND OBJECTIVES

Depending on their location certain civil structured facilities can be subjected to dynamic loads due to gusty wind fronts and/or strong ground motion associated with earthquake events of different intensity/severity during their life service. At high levels of intensity these naturally occurring dynamic loads may induce permanent structural damage and, in extreme cases, total structural failure/collapse. During the past three decades the incorporation of various devices such as base isolators, energy dissipation equipment (e.g. viscous dampers, friction dampers, etc.), and tuned-mass dampers (TMDs) has been considered by various researchers and has been applied in practice to passively control the vibratory motion of structures maintaining its amplitude below certain acceptable thresholds (Martelli & Forni, 2011; Spencer Jr, 2002; Soong & Dargush, 1999; Chang, 1999). Typically, such “non-conventional” means of mitigating the hazard posed to structures due to the action of winds and earthquakes are applied to protect critical civil infrastructure such as high-rise buildings, hospitals, and long-span (foot)bridges. Furthermore, the employment of such passive devices is commonly considered to upgrade/reinforce existing/historical structures to meet the contemporary safety criteria and to retrofit damaged structures in the aftermath of severe seismic events. These practical applications have sustained the important and active research field of passive vibration control for new and for existing/damaged structures. Admittedly, it is noted that improved structural performance can be achieved by using active/semi-active control solutions relying on the integration of sensors, controllers and real-time data

processing (Spencer & Nagarajaiah, 2003; Yoshioka et al, 2002; Ozbulut et al, 2011). However, due to reliability issues and the installation cost of such solutions, the use of active control systems is not as wide spread as the passive control solutions.

In the context of passive vibration control, the concept of the dynamic vibration absorber is historically one of the first and most widely used strategies for passive vibration mitigation of dynamically excited mechanical and civil engineering structures and structural components (Frahm, 1911 and Ormondroyd & Den Hartog, 1928). It relies on attaching an additional free-to-vibrate mass to the structural system (primary or host structure) whose motion is to be suppressed via certain mechanical devices. These devices are appropriately designed (or “tuned”) such that a resonant out-of-phase motion of the attached mass is achieved compared to the primary structure. Arguably, the most commonly used dynamic vibration absorber is the so-called “tuned mass-damper” (TMD). In its simplest form, the TMD considers a linear spring and a viscous damper to link the additional mass to the primary structure. The effectiveness of this classical TMD relies on tuning its stiffness and damping properties such that significant kinetic energy is transferred from the vibrating primary structure to the TMD mass and is absorbed through the viscous damper.

Despite being widely used due to the relatively simple and well-established design procedures, the TMD suffers the problem of “detuning” (e.g. due to non-linear response or a change in the dynamic properties of the primary structure) which may significantly affect its vibration suppression performance especially for the case of narrow band or harmonic excitations. Moreover, the TMD is not robust to uncertainties in estimating the properties of the primary structure from which the optimal TMD design parameters depend on. To address these issues, various different strategies have been employed such as the use of multiple TMDs (e.g. Yamaguchi & Harnpornchai, 1993) and of hysteretic

dampers in place of the linear dashpot (e.g. Ricciardelli & Vickery, 1999). These strategies do offer enhanced performance compared to the classical TMD, however, they add a further layer of complexity; optimum design/tuning becomes a challenging and computationally involved task. In this regard, it should be noted that, perhaps, the most straightforward way to enhance the performance and robustness of the TMD is to increase the attached mass for which optimum TMD design is sought. Indeed, the larger the attached mass considered, the more effective an optimally designed TMD becomes to suppress excessive primary structure vibrations at the cost of an increase total weight of the structural system (see e.g. Angelis et al, 2012; Hoang et al, 2008 and references therein).

Motivated by the latter observations, this thesis considers the addition of a mass amplification mechanical device, dubbed the “inertor” by Smith (2002), to enhance the performance of the classical TMD configuration. The thus proposed Tuned-Mass-Damper Inertor (TMDI) exploits the apparent mass amplification effect of the inertor, a two-terminal device developing a resisting force proportional to the relative acceleration of its terminals, to achieve improved vibration control compared to the TMD for the same attached mass.

In this context, the underlying equations of motion for linear SDOF and MDOF TMDI equipped primary structures are first introduced in the thesis. It is shown that the TMDI constitutes a generalization of the classical TMD. Next, standard optimisation techniques used for the classical TMD are applied to derive optimum TMDI parameters. Focus is given to the vibration control performance of the TMDI over the one achieved by the TMD. In particular, a significant part of this thesis is focused on deriving analytical closed-form expressions for optimal TMDI design/tuning parameters for harmonically and stochastically excited single-degree-of-freedom (SDOF) primary systems.

For multi-degree-of freedom (MDOF) cascaded chain-like mechanical systems, pertinent numerical data are furnished, derived by means of a numerical optimization procedure when considering stationary “coloured noise” base excitation.

Next, the TMDI is utilized to achieve a lightweight passive vibration solution for seismically excited building structures, focusing as well on the reduction of the peak average top floor displacements/accelerations and on the reduction of the required additional oscillating mass stroke. For this purpose, an input non-stationary stochastic process compatible with the elastic design spectrum of the European aseismic code provisions (EC8) is assumed. Furthermore, the effectiveness of the proposed optimum designed TMDI configuration over the classical TMD is assessed through response history analyses for an ensemble of 7 EC8 spectrum compatible field recorded strong ground motions.

Further, optimally designed TMDIs are applied for simultaneous vibration control and energy harvesting .The latter study is motivated by the fact that in considering a passive TMD-based harvester device, as the oscillating TMD mass increases, better primary structure response reduction is achieved but at the cost of reduced available energy for harvesting (Gonzalez-Buelga et al, 2014; Tang & Zuo, 2012; Adhikari & Ali, 2013).

In view of the above, Table 1.1 summarises for clarity the main contribution of this thesis within a matrix format. Furthermore, the same table provides a location map of each TMDI development/application within the thesis’s chapters. Several publications derived from this thesis are also enumerated.

Table 1.1 Matrix of Thesis Contribution

		TYPE OF PRIMARY SYSTEMS CONSIDERED	
		Single Degree of Freedom Primary System	Multi Degree of Freedom Primary Systems
DEVELOPMENT OF THE TMDI	Governing equations of motion	- In time and frequency domain. ^{(2) (3)} <i>(Chapter 2)</i>	- In time and frequency domain. ⁽¹⁾ -State Space Formulation. -Admittance Matrix Formulation ⁽¹⁾ <i>(Chapter 4), (Appendix II)</i>
	Optimum design	- Closed form Expression for Undamped primary systems. ⁽³⁾ <i>(Chapter 3)</i>	- Numerical Optimisation – “min-max” constraint optimization algorithm employing a sequential programming method. ^{(1), (2)} <i>(Chapter 4 & Chapter 5)</i>
APPLICATIONS		Simultaneous vibration suppression and energy harvesting. ⁽³⁾ <i>(Chapter 6)</i>	- Earthquake protection for multi-storey buildings. ⁽¹⁾ <i>(Chapter 5)</i>

⁽¹⁾ Marian, L. & Giaralis, A. 2013. Optimal design of inerter devices combined with TMDs for vibration control of buildings exposed to stochastic seismic excitations. In: *Proceedings of the 11th ICOSSAR International Conference on Structural Safety and Reliability for Integrating Structural Analysis, Risk and Reliability*; New York, US (eds: Deodatis G, Ellingwood BR and Frangopol DM), CRC Press.

⁽²⁾ Marian, L. & Giaralis, A. 2014. Optimal design of a novel tuned mass-damper-inerter (TMDI) passive vibration control configuration for stochastically support-excited structural systems. *Probabilistic Engineering Mechanics* 2014; DOI:/10.1016/j.probengmech.2014.03.007.

⁽³⁾ Marian, L. & Giaralis, A. 2014. Vibration suppression and energy harvesting in tuned mass-damper – inerter (TMDI) equipped harmonically support-excited structures. In: *Proceedings of the 6th International Conference on Structural Control and Health Monitoring* 2014; Barcelona, Spain.

1.2 THESIS ORGANISATION AND OUTLINE

This dissertation comprises seven chapters and one appendix followed by the list of cited references. The introductory *first chapter* presents the motivation and the objectives of the undertaken work. It outlines the chapters within the thesis with a short summary of their content.

Chapter 2 provides a brief review on the classical tuned-mass-damper (TMD) and on the inerter, focusing on applications in structural engineering.

In Chapter 3 the governing equations of motion and relevant transfer functions of the proposed tuned-mass-damper- inerter (TMDI) configuration are derived for the case of linear single-degree-of-freedom (SDOF) primary systems. Analytical expressions are derived in closed form for optimum TMDI parameters minimizing the displacement amplitude response for the special case of undamped harmonically base-excited SDOF primary systems. Furthermore, analytical expressions for optimum TMDI parameters minimizing the displacement variance for the special case of undamped white noise excited SDOF primary systems are obtained.

Chapter 4 introduces the TMDI configuration to suppress oscillations following the fundamental mode of vibration of support-excited damped multi-degree-of-freedom (MDOF) chain-like primary systems. A numerical optimization procedure for optimum design of the TMDI for these primary systems is also discussed. Numerical data is provided to demonstrate the effectiveness and applicability of the TMDI vis-à-vis the classical TMD for classically damped support excited MDOF chain-like primary systems.

Chapter 5 applies the TMDI system to achieve a lightweight passive vibration solution for seismically excited building structures. For optimum TMDI parameters design, a non-stationary power spectrum compatible in the “mean sense” with the elastic

spectrum of the current European aseismic code provisions (EC8) is considered. Moreover, the effectiveness of the proposed TMDI configuration over the classical TMD is assessed by performing response history analyses for an ensemble of Eurocode 8 spectrum compatible field recorded strong ground motions.

In Chapter 6 the TMDI is applied for simultaneous vibration suppression and energy harvesting. Analytical and numerical results are reported on the capabilities of optimally designed TMDIs for vibration suppression to harvest energy by transferring the kinetic energy from harmonically base excited SDOF primary structures into electrical energy via a particular electromagnetic energy harvester.

Finally, Chapter 7 summarizes the main conclusions of the work.

CHAPTER 2 : A REVIEW ON THE CLASSICAL TUNED MASS DAMPER (TMD) AND MASS AMPLIFICATION DEVICES FOCUSING ON APPLICATIONS IN EARTHQUAKE ENGINEERING

2.1 PASSIVE TUNED MASS DAMPER BASED VIBRATION CONTROL

The idea of attaching an additional free-to-vibrate mass to dynamically excited structural systems (primary structures) to suppress their oscillatory motion is historically among the first passive vibration control strategies in the area of structural dynamics (Frahm, 1911; Ormondroyd & Den Hartog, 1928; Den Hartog, 1956; Brock, 1946). This idea relies on designing or “tuning” the mechanical devices that link the added mass to the primary structure to achieve a “resonant” out-of-phase motion of the mass. In this context, (Frahm, 1911) introduced the use of a linear spring-mass attachment to suppress the oscillations of harmonically excited primary structural systems in naval and mechanical engineering applications. This early “dynamic vibration absorber” was able to reduce the oscillations of single-degree-of-freedom (SDOF) primary structures within a narrow range centred at a particular (pre-specified) frequency of excitation. Later, Ormondroyd and Den Hartog (1928) enhanced the effectiveness of the above absorber to dissipate the kinetic energy of primary structures by appending a viscous damper (dashpot) in parallel to the linear spring. This is known as the Tuned Mass Damper (TMD) shown in Figure 2.1 for single-degree-of-freedom (SDOF) and multi-degree-of-freedom (MDOF) primary structures.

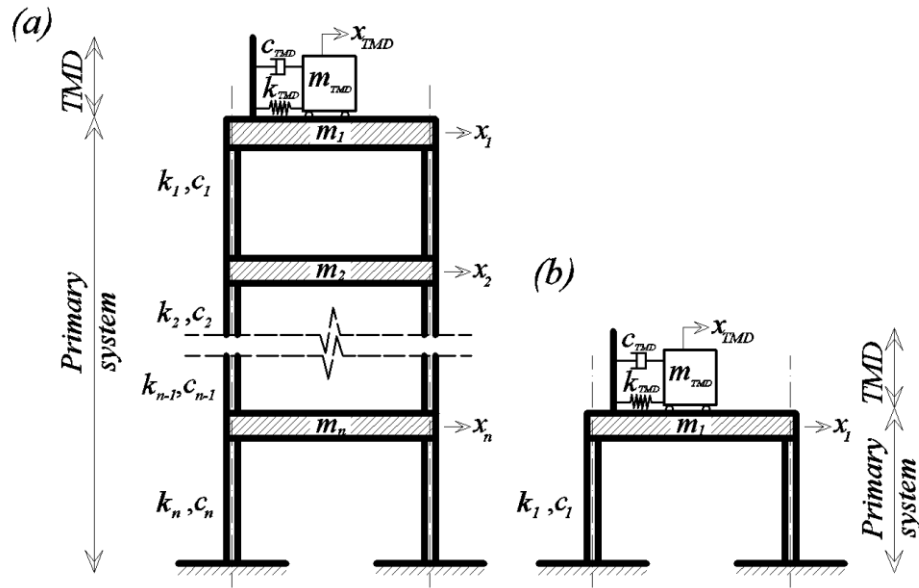


Figure 2.1 A structural frame model of multi-storey (a) and single-storey (b) building structures (primary systems) equipped with Tuned-Mass-Damper (TMD) classical passive control solution

A semi-empirical “optimum” design procedure has been established by Den Hartog (Den Hartog, 1956) and Brock (Brock, 1946) to “tune” the damping and stiffness properties for an *a priori* specified mass of this spring-mass-damper attachment such that the peak displacement of harmonically excited undamped SDOF primary structures is minimized (see Krenk, 2005). This design/tuning procedure relies on the “fixed point” assumption which states that all frequency response curves of the resulting two-DOF dynamical system pass through two specific points; the location of these points being independent of the damping coefficient of the dashpot. Thus the tuned spring-mass-damper attachment, commonly termed in the literature as the “tuned mass-damper” (TMD), achieves the suppression of the oscillatory motion of harmonically excited primary structures over a wider range of exciting frequencies compared to a spring-mass attachment. Recently, the fixed point-based tuning procedure was shown to be very close to the “exact” solution for the optimal tuning of the classical TMD (Nishihara & Asami, 2002). However, for the case of damped SDOF primary structures, the fixed point theory

does not strictly hold and the derivation of optimal TMD parameters in closed form becomes a challenging task (e.g. Nishihara & Asami, 2002; Asami et al, 2002). In this respect, numerical optimization techniques are applied in practice for optimal design of TMDs (e.g. Leung & Zhang, 2009). Motivated mostly by earthquake engineering applications, Warburton (1982) derived optimum TMD parameters based on the fixed point theory for the case of harmonically base excited undamped SDOF structures. Further, substantial research work has been devoted to investigate the potential of using the classical TMD to mitigate the motion of stochastically support-excited primary structures. Using standard analytical techniques, optimal TMD parameters can be readily obtained in closed-form as functions of the TMD mass to minimise the response variance of undamped SDOF primary structures subject to white noise support excitation (Ayorinde & Warburton, 1980; Warburton, 1982). However, for the case of damped SDOF primary structures subjected to stochastic support excitations, the derivation of optimal TMD parameters by analytical approaches becomes a challenging task. To this end, numerical optimization techniques are commonly employed for optimum design of TMDs to minimize the response variance for such primary structures (see e.g. Bakre & Jangid, 2005; Hoang et al, 2008; Leung & Zhang, 2009; Salvi & Rizzi, 2011). Alternatively, simplified approximate solutions for the problem at hand have been reached by making the assumption of “lightly” damped primary structures (e.g. Ghosh & Basu, 2005; Krenk & Høgsberg, 2008). Along similar lines, several researchers proposed different approximate simplified and numerical methods for the design of TMDs for damped linear multi-degree-of-freedom (MDOF) primary structures under stochastic base excitation widely used to model seismically excited multi-storey building structures (see e.g. Sadek et al, 1997, Rana & Soong, 1998, Moutinho, 2012, Angelis et al, 2012 and references therein). Note that, TMD optimum design for vibration suppression of linear

multi degree-of-freedom (MDOF) primary structures is a straightforward task since, in common practice, the aim is to control vibrations according to a single (the dominant) structural mode shape (e.g. Rana & Soong, 1998).

Although alternative arrangements of linear springs and dashpots (viscous dampers) have been considered in the literature to attach a mass to primary structures (see e.g. Liu & Liu, 2005, Cheung & Wong, 2011 and references therein), the above discussed “classical” TMD configuration (mass attached via a spring and a dashpot in parallel) is the most widely studied in the literature and the most commonly used one for passive vibration control of various mechanical and civil engineering structures and structural components.

In recent years, several different strategies have been employed to enhance the performance of the classical TMD for passive vibration suppression of structural systems including the use of multiple classical TMDs (see e.g. Hoang & Warnitchai, 2005; Lee et al, 2006 and references therein), the incorporation of non-linear viscous dampers to the classical TMD configuration (Rudinger, 2006), and the consideration of hysteretic TMDs (see e.g. Ricciardelli & Vickery, 1999). These strategies do offer enhanced performance compared to the classical TMD, however, optimum design/tuning becomes a challenging and computationally involved task, especially for damped MDOF primary structures. Furthermore, analytical and numerical results reported in the extensive relevant literature suggest that the effectiveness of the TMD for vibration mitigation of base-excited structures increases by increasing the attached TMD mass. This is particularly the case for high intensity support excitations (e.g. Hoang et al, 2008; Angelis et al, 2012).

Indeed, the larger the attached mass considered, the more effective an optimally designed TMD becomes to suppress excessive primary structure vibrations at the cost of an increase total weight of the structural system (e.g. Feng & Mita, 1995). In this respect,

recent studies focus towards non-conventional configurations which have in common the employment of significantly large TMD masses, which can reach the order of 15% to 100% of the primary structure total mass (Feng & Mita, 1995; Moutinho, 2012; Angelis et al, 2012; Hoang et al, 2008; Matta & DeStefano, 2009a; 2009b). This can be accomplished by the use of substructures utilized as self-contained vibration absorbers in tall buildings, as proposed by Feng & Mita (1995) where it is shown that the use of this ‘mega-substructure configuration’ with masses that can reach 100% of the mass of the structure’s main body significantly improves the seismic response of primary structures. Moreover, in (Moutinho, 2012) it is proposed to use the top floor of a five storey shear building as a large mass TMD to reduce induced seismic vibrations, assuming TMD masses which can reach the total mass of the primary structure. This is accomplished through the use of rubber bearings which are interposed between the top of the columns on the last floor and the roof. It is proven that the use of large mass TMDs improves robustness in terms of parameter uncertainties. In a similar manner, large TMDs are also proposed in (Angelis et al, 2012) with masses equal to 72% of the primary system’s mass. The study is carried out by means of both numerical analyses and experimental tests. It is concluded that large mass TMDs lead to greater reductions of the structural response compared to conventional ones. The proposed solution is also found to be more robust against deviations of optimum parameters resulting from uncertainties in structural properties. Large mass TMDs are also employed in Hoang et al (2008) for the case of a SDOF structure on a design example for seismic retrofitting of a long-span truss bridge. A TMD mass equal to 77% of the total mass of the primary structure is proposed. Its performance is proved to be robust with respect to uncertainties in the system structural parameters as well as the excitation frequency content. Furthermore, the concept of the rolling-pendulum roof-garden TMD (RPTMD) is introduced by Matta & DeStefano

(2009) where non-structural large masses already available atop buildings are turned into TMDs. The occurring TMD mass-uncertainties are inspected through a robust analysis. The same authors (Matta & DeStefano, 2009b) provide a comparison between the previously proposed rolling-pendulum and the classical translational TMD configuration.

Given that large mass TMD lead to an undesirable increase of the weight which needs to be accommodated by the primary structure using structurally sophisticated solutions, there is scope in seeking ways to reduce the attached TMD mass to facilitate practical structural design, while maintaining the well-documented effectiveness of large mass TMDs to mitigate seismic risk associated with moderate-to-severe earthquake induced ground shaking. In this regard, in this thesis the classical TMD is coupled with mass amplification devices, reviewed in the following section, aiming to achieve enhanced structural performance with reduced weight.

2.2 THE INERTER AND OTHER MASS AMPLIFICATION DEVICES IN EARTHQUAKE ENGINEERING APPLICATIONS

Conceptually introduced by Smith (2002), the ideal inerter is a two terminal mechanical element of negligible mass/weight developing an internal (resisting) force proportional to the relative acceleration of its terminals which are free to move independently. Figure 2.2 depicts an inerter device whose terminals are subject to an equal and opposite externally applied force F in equilibrium with the internally developed force. By definition the following relationship holds for the ideal linear inerter (e.g. Smith, 2002; Chuan et al, 2011a):

$$F = b(\ddot{u}_1 - \ddot{u}_2), \quad (2-1)$$

where u_1 and u_2 are the displacement coordinates of the two terminals and a dot over symbol signifies differentiation with respect to time t . In the above equation, the constant of proportionality b attains mass units and fully characterizes the behaviour of the inerter. Still, the physical mass of an actual inerter device is orders of magnitude lower than b .

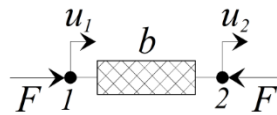


Figure 2.2 Schematic representation of the two-terminal flywheel device (b is the mass-equivalent constant of proportionality)

Employing rack and pinion gearing arrangements or ball screw mechanisms to drive a rotating flywheel several such devices have been built and prototyped (Smith, 2002; Chuan et al, 2011a; Papageorgiou & Smith, 2005). In fact, TTF devices/inerters have been

successfully used for vibration control of suspension systems in high performance vehicles (e.g. Evangelou et al, 2004; Chuan et al, 2011b and others). More, recently, fluid inerter implementations have been proposed (Swift et al, 2013; Wang et al, 2011) which use the mass of a fluid flowing through a helical channel to generate the required resistive force. Inerter devices can be viewed and modelled as a linear mechanical element which complements the ideal linear spring element (i.e. two-terminal device developing an internal force proportional to the relative displacement of its terminals) and the linear dashpot (i.e. two-terminal device developing an internal force proportional to the relative velocity of its terminals). To this end, the concept of the inerter allows for a one-to-one mapping of dynamical mechanical systems for passive vibration control analogously to the electrical network synthesis. In fact, the concept of the inerter allows for designing mechanical systems for passive vibration control analogously to the electrical network synthesis. To this end, various topologies of springs, dampers, and inerters have been tested for vibration isolation of vehicles. (Chuan et al, 2011b, Evangelou et al, 2004)

Of particular importance for the purpose of this thesis is the mass amplification effect of the inerter which has been noted in the original paper of Smith (2002). This effect can be readily understood by examining a seismically excited linear spring-inerter-mass system. Specifically, consider the single storey portal frame building of Figure 2.3 having an inerter device exposed to a horizontal seismic excitation and modelled as a linear single-degree-of-freedom system with k_l lateral stiffness, m_l mass assumed to be lumped at the girder. Let the girder be connected to the ground by means of an ideal inerter device. The equation of motion of this structure written in terms of the horizontal floor displacement relative to the ground motion is given as:

$$(m_1 + b)\ddot{x}_1 + c_1\dot{x}_1 + kx_1 = -m_1a_g \quad (2-2)$$

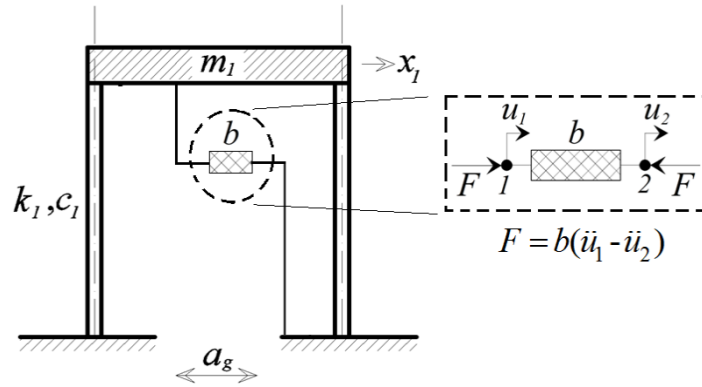


Figure 2.3. Single-degree-of-freedom (SDOF) primary structure ground-connected via an inerter element.

Clearly, the inclusion of the inerter increases the “apparent” mass of the portal frame by b . However, the physical mass of the inerter is assumed to be negligible compared to the mass m_1 , in accordance with the definition of the concept of the inerter as defined in Smith (2002). To further elaborate on this matter, Figure 2.4 provides a mechanical realisation of the inerter comprising a plunger that drives a rotating flywheel through a rack, pinion, and a gearing system with n gears (e.g. Smith, 2002).

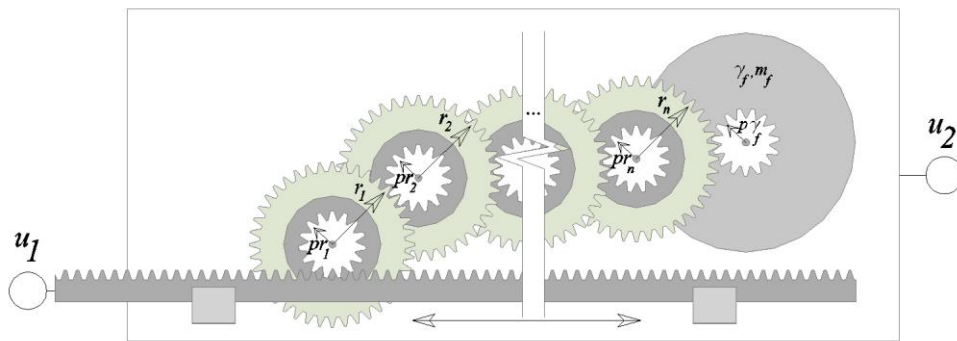


Figure 2.4. Possible mechanical realisation of the inerter comprising a plunger that drives a rotating flywheel through a rack, pinion and gearing system with n gears

The inertance b achieved from such a mechanical device is expressed as:

$$b = m_f \frac{\gamma_f^2}{\gamma_{pr}^2} \left(\prod_{i=1}^n \frac{r_i^2}{pr_i^2} \right) \quad (2-3)$$

where m_f is the mass of the flywheel and γ_f is the radius of gyration of the flywheel; r_f represents the radius of the flywheel pinion and n represents the number of gears with radius r_i and pinion radius r_j chained together between the input gear and the output flywheel pinion. It can be easily deduced from Equation (2-3) that, as the number of gears considered in the mechanical realization of the inerter increases, the inertance b and implicitly the mass amplification effect increases proportional.

Importantly, the inclusion of the inerter changes (reduces) the natural frequency of the system. This issue has been recently examined in (Chen et al, 2014). Further, the amplitude of the effective horizontal force is also reduced, consideration which has been extensively discussed in (Takewaki et al 2012).

The use of mass amplification devices/inerters for vibration mitigation in seismically excited buildings has recently attracted some attention in the literature. Wang et al. (2007; 2010) propose various passive vibration control configurations, assessing the performance of several suspension layouts employing inerters placed in between the ground and the superstructure in a base isolation type of arrangement. It has been established that inerter devices are effective in controlling the response of rigid superstructures exposed to vertical band-limited white noise ground motions. Passive vibration control systems comprising inerters in conjunction with springs and dampers have been considered by Lazar et al. (2013a; 2013b) for vibration isolation of primary systems subjected to recorded earthquake excitations applied along the vertical direction. Furthermore, a number of energy dissipation devices combining an apparent “mass

amplifier”, which achieves a similar dynamic effect as the inerter, in parallel with a viscous damper have been discussed in the literature (e.g. Hwang et al, 2007; Ikago et al, 2012 and others). These rotational inertia dampers are usually arranged as diagonal bracing members in multi-story framed buildings to provide supplemental damping and inertia properties to structures (e.g. Ikago et al, 2012). In this manner, passive control of seismically excited buildings is achieved by increase of the inherent to all structures damping and mass properties. Furthermore, a new vibration control device is proposed in (Garrido et al, 2013) called rotational inertia double-tuned mass damper (RIDTMD), consisting of a classical TMD and a rotational inertia element similar to the inerter. The efficiency of the proposed configurations vis-à-vis the classical TMD is assessed via a numerical optimisation for SDOF primary structures subjected to harmonic load. In (Takewaki et al, 2012) it is shown that inerters distributed along the height of a seismically excited structure are effective for the reduction of the maximum absolute horizontal acceleration of floors by reducing the applied to the structure horizontal load.

It is noted that, the TMDI discussed in the following chapters is significantly different than the TDI in (Lazar et al., 2013) and the solutions of (Ikago et al, 2012) as in all these cases the inerter is placed as a strut within the storeys of buildings in combination with spring and damping elements. Further, in a similar manner, Takewaki uses inerters allocated within the structure and connected from one storey to another.

CHAPTER 3 : THE TUNED-MASS-DAMPER-INERTER PASSIVE CONTROL SOLUTION FOR SINGLE-DEGREE-OF-FREEDOM PRIMARY SYSTEMS

3.1 PRELIMINARY REMARKS

This chapter introduces the Tuned Mass Damper-Inerter (TMDI) for vibration control of harmonically and stochastically excited single-degree-of-freedom (SDOF) primary systems. The herein proposed TMDI configuration takes advantage of the “mass amplification effect” of the inerter by using it as an additional connective element between the TMD oscillating mass and the ground for SDOF primary systems. Importantly, the TMDI can be viewed as a generalization of the classical TMD. Thus, all established in the literature procedures for optimum design (tuning) of the classical TMD are readily applicable to achieve optimal performance for the TMDI configuration.

In addition to the herein considered TMDI configuration, several other spring-mass-damper and inerter connectivity arrangements have been studied, as exemplified in Appendix I. However, as detailed in Chapter 2.2, the most beneficial way in which the mass-amplification effect of the inerter can be exploited is to have one of its terminal connected to a fixed points in the inertial frame of reference. The latter thus motivates the choice of the proposed TMDI arrangement.

This chapter presents the governing differential equations of motion in the time and in the frequency domain for TMDI equipped damped linear SDOF primary structures. Closed-form analytical expressions for optimal TMDI parameters are derived by application of a semi-empirical approach extensively used for the “optimum”

design/tuning of the classical TMD to suppress the motion of harmonically excited undamped SDOF primary structures. Moreover, optimal TMDI design parameters minimizing the relative displacement variance of undamped SDOF primary structures under white noise support excitation are analytically derived in closed form as functions of the TMD mass and the inerter constant b ; based on the computed optimum design parameters, the performance of the novel TMDI is analytically assessed vis-à-vis the classical TMD.

3.2 GOVERNING EQUATIONS OF MOTION

Consider a linear damped single-degree-of-freedom (SDOF) dynamical system (primary structure) modelled by a linear spring of stiffness k_1 , a mass m_1 , and a viscous damper with damping coefficient c_1 , excited by an externally mass-applied force P or based-excited by an acceleration stochastic process $a_g(t)$ as shown in Figure 3.1a and Figure 3.1b, respectively. Alternatively, the mechanical dynamical systems of Figure 3.1 can be viewed as one storey high frame structure buildings as suggested in Figure 3.2.

To suppress the oscillatory motion of this primary structure it is herein proposed to consider the classical tuned mass-damper (TMD), in conjunction with a two terminal flywheel (inerter) device as shown in Figure 3.2. The TMDI consists of a mass m_{TMDI} attached to the primary structure via a linear spring of stiffness k_{TMDI} and a viscous damper with damping coefficient c_{TMDI} along with a two-terminal flywheel - inerter device which connects the attached mass to the ground.

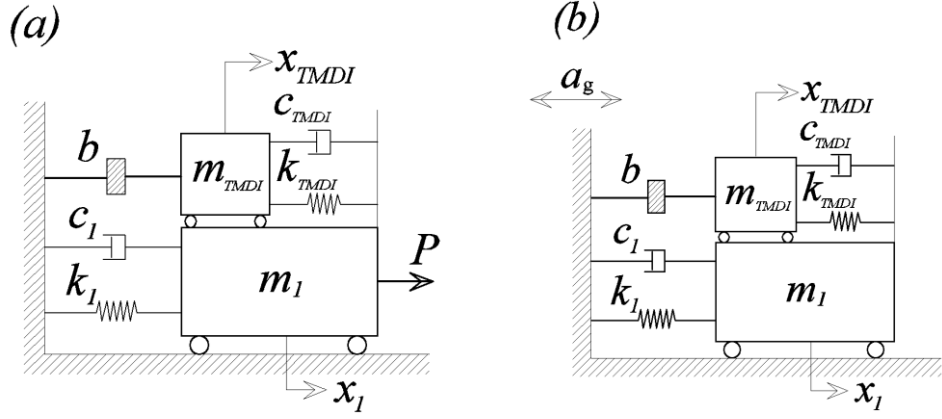


Figure 3.1. Single-degree-of-freedom (SDOF) primary system equipped with a tuned mass-damper-inerter (TMDI) system (a) force excited; (b) base-excited.

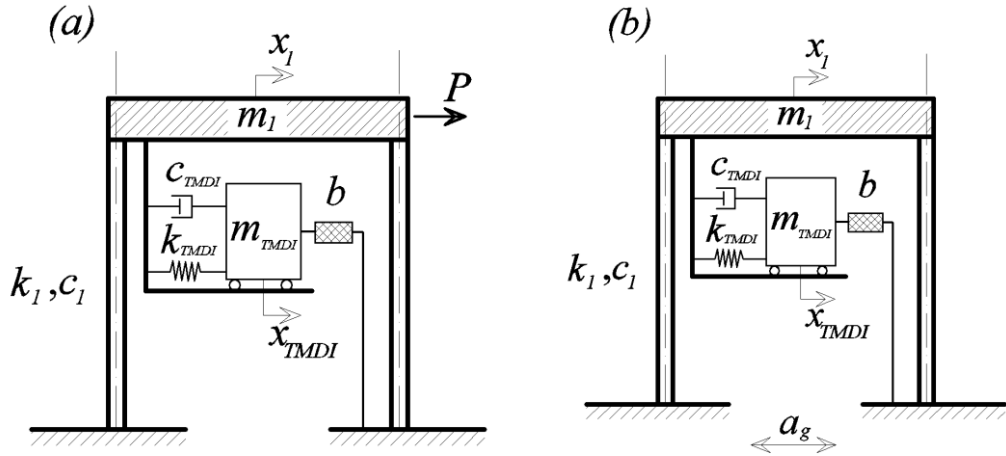


Figure 3.2. Single-degree-of-freedom (SDOF) primary system (modelled as a frame structure) ground-connected via an inerter element (a) force excited (b) base excited.

Under the assumption that the physical mass of the inerter, the damper, and the spring are negligible compared to the masses m_1 and m_{TMDI} , the equations of motion of the TMDI equipped SDOF primary structure considered are written in matrix form as:

$$\begin{aligned}
 & \begin{bmatrix} m_{TMDI} + b & 0 \\ 0 & m_1 \end{bmatrix} \begin{Bmatrix} \ddot{x}_{TMDI} \\ \ddot{x}_1 \end{Bmatrix} + \begin{bmatrix} c_{TMDI} & -c_{TMDI} \\ -c_{TMDI} & c_1 + c_{TMDI} \end{bmatrix} \begin{Bmatrix} \dot{x}_{TMDI} \\ \dot{x}_1 \end{Bmatrix} + \\
 & \begin{bmatrix} k_{TMDI} & -k_{TMDI} \\ -k_{TMDI} & k_1 + k_{TMDI} \end{bmatrix} \begin{Bmatrix} x_{TMDI} \\ x_1 \end{Bmatrix} = \begin{Bmatrix} F_2(t) \\ F_1(t) \end{Bmatrix} \quad (3-1)
 \end{aligned}$$

In the above equations, x_I and x_{TMDI} are the displacement response histories relative to the motion of the ground of the primary structure mass and of the attached mass, respectively (see also Figure 3.2). For force excitation, $F_2(t)=0$ in Eq. (3-1) and $F_2(t)=P(t)$. In this case, the incorporation of the inerter contribution to an increase of the attached mass m_{TMDI} by the inertance b (mass amplification effect). Therefore, the resulting TMDI will have the same dynamical behaviour as a classical TMD with attached mass equal to $m_{TMDI}+b$, though the added weight of the TMDI will only be equal to $m_{TMDI}g$, where g is the acceleration of gravity. In this regard, the case of a force excited TMDI equipped SDOF primary systems coincides with the classical TMD in terms of equation of motion and, thus, with optimum design. To this end, it will not be explicitly treated in this thesis.

For ground excitation, the following forcing vector applies in Equation (3-1):

$$\begin{Bmatrix} F_2(t) \\ F_1(t) \end{Bmatrix} = - \begin{Bmatrix} m_{TMDI} \\ m_1 \end{Bmatrix} a_g \quad (3-2)$$

Notably, this is different than the case of a base-excited classical TMD with $m_{TMDI}+b$ attached mass. In this respect, the remainder of this section focuses on the case of support-excited TMDI.

Denote by ω_{TMDI} and ζ_{TMDI} the natural frequency and the critical damping ratio of the TMDI system, respectively, defined as

$$\omega_{TMDI} = \sqrt{\frac{k_{TMDI}}{m_{TMDI} + b}}, \quad \zeta_{TMDI} = \frac{c_{TMDI}}{2(m_{TMDI} + b)\omega_{TMDI}} \quad (3-3)$$

Further, consider the dimensionless mass ratio μ , the dimensionless frequency ratio ν_{TMDI} and the dimensionless ‘‘inertance’’ ratio β expressed as:

$$\mu = \frac{m_{TMDI}}{m_1}, \quad \nu_{TMDI} = \frac{\omega_{TMDI}}{\omega_1}, \quad \beta = \frac{b}{m_1} \quad (3-4)$$

where ω_1 is the natural frequency of the primary structure, that is, $\omega_1 = (k_1/m_1)^{1/2}$. Using the above definitions, the complex frequency response function (FRF) in terms of the relative lateral sway x_1 of the frame structure in Figure 3.2 can be written as:

$$\begin{aligned} G_1(\omega) &= \frac{x_1}{a_g} \omega_1^2 \\ &= \frac{(1+\mu)\omega_{TMDI}^2 - \omega^2 + i2\zeta_{TMDI}(1+\mu)\omega_{TMDI}\omega}{\left(1 - \frac{\omega^2}{\omega_1^2} + i2\zeta_1 \frac{\omega}{\omega_1}\right) \left(\omega_{TMDI}^2 - \omega^2 + i2\zeta_{TMDI}\omega_{TMDI}\omega\right) - \frac{\beta+\mu}{\omega_1^2} \left(\omega_{TMDI}^2 + i2\zeta_{TMDI}\omega_{TMDI}\omega\right) \omega^2} \end{aligned} \quad (3-5)$$

in the domain of frequency ω by considering the normalized acceleration input a_g/ω_1^2 . In the latter equation and hereafter $i = \sqrt{-1}$. Furthermore, the complex FRF in terms of the relative displacement x_{TMDI} of the attached mass is written as:

$$\begin{aligned} G_2(\omega) &= \frac{x_2}{a_g} \omega_1^2 \\ &= \frac{(1+\mu)\left(\omega_{TMDI}^2 + i2\zeta_{TMDI}\omega_{TMDI}\omega\right) + \frac{\mu}{\beta+\mu}\left(\omega_1^2 - \omega^2 + i2\zeta_1\omega\omega_1\right)}{\left(1 - \frac{\omega^2}{\omega_1^2} + i2\zeta_1 \frac{\omega}{\omega_1}\right) \left(\omega_{TMDI}^2 - \omega^2 + i2\zeta_{TMDI}\omega_{TMDI}\omega\right) - \frac{\beta+\mu}{\omega_1^2} \left(\omega_{TMDI}^2 + i2\zeta_{TMDI}\omega_{TMDI}\omega\right) \omega^2} \end{aligned} \quad (3-6)$$

It is noted that by setting $b=\beta=0$ in Eq. (3-5) and Eq. (3-6) the FRFs in terms of the relative displacements x_1 and x_{TMDI} , respectively, for an undamped SDOF primary system equipped with the classical TMD are retrieved. In this respect, *it is seen that the proposed*

tuned mass-damper-inerter (TMDI) configuration for passive vibration control can be interpreted as a generalization of the classical TMD.

In the next section, optimal TMDI design is sought by considering the minimization of the magnitude of the FRF G_I (i.e., $|G_I(\omega)|$), commonly referred to as the “dynamic amplification factor”. This is the most common design criterion for vibration suppression of harmonically excited primary structures by means of the classical TMD system (e.g. Krenk, 2005).

3.3 OPTIMUM DESIGN OF THE TUNED-MASS-DAMPER-INERTER FOR HARMONIC EXCITATION

Assume that the TMDI equipped structure of Figure 3.2 is subjected to a harmonic support excitation. Given fixed values for the μ and β ratios in (3-4), it is sought to determine “optimum” values for the TMDI stiffness and damping constants k_{TMDI} and c_{TMDI} , respectively, or equivalently for the ν_{TMDI} and ζ_{TMDI} dimensionless parameters in (3-4) and (3-3) respectively, such that the amplitude of the lateral sway of the primary structure is minimized.

3.3.1 DERIVATION OF CLOSED FORM SOLUTIONS FOR OPTIMUM DESIGN PARAMETERS

The tuning design approach proposed by (Den Hartog, 1956) for harmonically force excited undamped SDOF primary structures equipped with the classical TMD (i.e. TMDI with $b=\beta=0$) is herein adopted. This approach is based on the “fixed point” theory which relies on the empirical observation that the magnitude of the FRF curves $|G_I(\omega)|$ in Equation (3-5) for $b=\beta=0$ passes through two specific points, the location of which is independent of the damping coefficient c_{TMDI} . Importantly, this observation holds for the TMDI system and for harmonically base-excited primary structures, as well. For example, in Figure 3.3, the dynamic amplification factor $|G_I(\omega)|$ is plotted for several values of the TMDI damping ratio ζ_{TMDI} and for fixed values of the ratios μ , β , and ν_{TMDI} .

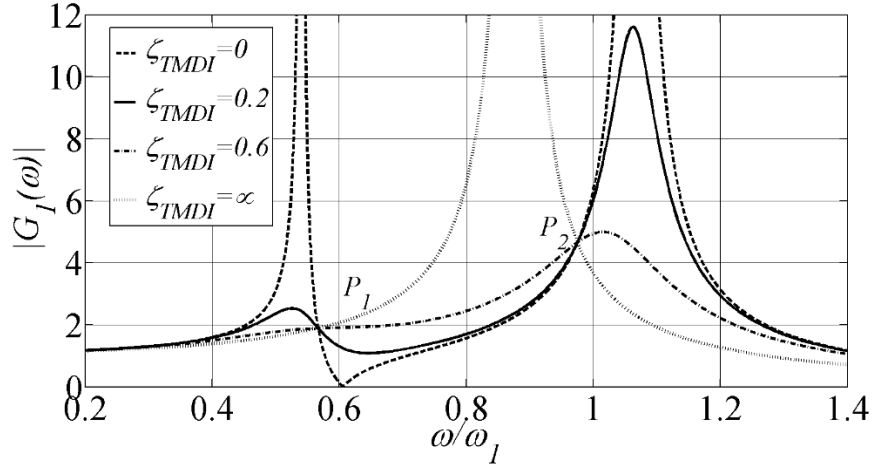


Figure 3.3 Relative displacement response amplitude of undamped support excited TMDI equipped SDOF primary structure with mass ratio $\mu=0.1$, inertance ratio $\beta=0.1$, frequency ratio $\nu_{TMDI}=0.5$, and for various TMDI damping ratios ζ_{TMDI} .

Evidently, there exist two “stationary” points, denoted by P_1 and P_2 , where G_I FRF curves intersect for all damping coefficient values c_{TMDI} , or equivalently TMDI damping ratios ζ_{TMDI} . Following the classical TMD design approach of Den Hartog, the amplitude of $|G_I(\omega)|$ at points P_1 and P_2 must be equal (Den Hartog, 1956; Brock, 1946; Krenk, 2005) for achieving optimum response. Furthermore, $|G_I(\omega)|$ must attain a local maximum at these two points and, thus, the slope of $|G_I(\omega)|$ at P_1 and P_2 must be equal to zero. Therefore, according to Den Hartog approach, the minimum response of a TMDI equipped harmonically support excited undamped primary structure may be achieved by enforcing that there exist two local maxima of $|G_I(\omega)|$ with equal amplitudes at the stationary points P_1 and P_2 .

Collecting the real and imaginary parts, the square magnitude of the FRF in (3-5) is written as:

$$|G_I(\omega)|^2 = \frac{A^2 + 4\zeta_{TMDI}^2 B^2}{C^2 + 4\zeta_{TMDI}^2 D^2} \quad (3-7)$$

Where:

$$A = (1 + \mu)\omega_{TMDI}^2 - \omega^2, \quad B = (1 + \mu)\omega_{TMDI}\omega, \quad (3-8)$$

$$C = \frac{\omega^4}{\omega_1^2} - \omega^2 \left[1 + \frac{\omega_{TMDI}^2}{\omega_1^2} (1 + \beta + \mu) \right] + \omega_{TMDI}^2, \quad \text{and} \quad D = \omega\omega_{TMDI} \left[1 - \frac{\omega^2}{\omega_1^2} (1 + \beta + \mu) \right].$$

By imposing the condition:

$$\lim_{\zeta_{TMDI} \rightarrow \infty} |G_1(\omega)|^2 = \lim_{\zeta_{TMDI} \rightarrow 0} |G_1(\omega)|^2 \quad (3-9)$$

to enforce that the dynamic amplification factor $|G_1(\omega)|$ is independent of ζ_{TMDI} , one obtains:

$$AD = \pm BC \quad (3-10)$$

Substitution of A, B, C , and D in the above equation adopting the positive sign leads to the trivial solution $\omega=0$. However, use of the negative sign yields the following quadratic equation in ω^2 :

$$\omega^4(2\mu + \beta + 2) - \omega^2[\omega_1^2(2 + \mu) + 2\omega_{TMDI}^2(1 + \beta + \mu)(1 + \mu)] + 2(1 + \mu)\omega_1^2\omega_{TMDI}^2 = 0 \quad (3-11)$$

whose roots ω_{P_1} and ω_{P_2} are the natural frequencies corresponding to the stationary points P_1 and P_2 ; the response amplitude is independent of the TMDI damping coefficient ζ_{TMDI} at these frequencies. The sum of the roots ω_{P_1} and ω_{P_2} can be expressed as the ratio between the coefficient of the linear term and the coefficient of the quadratic term in (3-11) with a negative sign, that is,

$$\omega_{P_1}^2 + \omega_{P_2}^2 = \frac{\omega_1^2(2 + \mu) + 2\omega_{TMDI}^2(1 + \beta + \mu)(1 + \mu)}{(2\mu + \beta + 2)} \quad (3-12)$$

Enforcing equal dynamic amplification at points P_1 and P_2 for the limit $\zeta_{TMDI} \rightarrow \infty$, that is,

$$\lim_{\zeta_{TMDI} \rightarrow \infty} |G_1(\omega_{P_1})| = \lim_{\zeta_{TMDI} \rightarrow \infty} |G_1(\omega_{P_2})| \quad (3-13)$$

the following equation in ω_{P_1} and ω_{P_2} is obtained

$$\omega_{P_1}^2 + \omega_{P_2}^2 = \frac{2\omega_1^2}{1 + \beta + \mu} \quad (3-14)$$

Solving the system of equations in (3-12) and (3-14), the value of the following (optimum) frequency ratio ν_{TMDI} is obtained in closed form:

$$\nu_{TMDI} = \frac{1}{1 + \beta + \mu} \sqrt{\frac{(1 + \mu)(2 - \mu) - \mu\beta}{2(1 + \mu)}} \quad (3-15)$$

which achieves equal dynamic amplification at points P_1 and P_2 .

Moreover, the optimum TMDI damping ratio can be obtained by requiring that the dynamic amplification at the two stationary points P_1 and P_2 is maximized locally. This condition is achieved by setting:

$$\left. \frac{\partial |G_1(\omega)|}{\partial \nu_{TMDI}} \right|_{\omega=\omega_{P_1}} = \left. \frac{\partial |G_1(\omega)|}{\partial \nu_{TMDI}} \right|_{\omega=\omega_{P_2}} = 0 \quad (3-16)$$

Using the above equation, the ‘‘optimal’’ TMDI parameter ζ_{TMDI} is found in terms of the ratios μ and β as:

$$\zeta_{TMDI} = \sqrt{\frac{\beta^2 \mu + 6\mu(1+\mu)^2 + \beta(1+\mu)(6+7\mu)}{8(1+\mu)(1+\beta+\mu)[2+\mu(1-\beta-\mu)]}} \quad (3-17)$$

By substitution of the above optimal TMDI tuning parameters in (3-5), the following expression for the dynamic amplification factor at points P_1 and P_2 is obtained:

$$\max_{\omega} \{|G_1(\omega)\}| = |G_1(\omega_{P_1})| = |G_1(\omega_{P_2})| = \sqrt{\frac{(1+\mu)(\beta+2\mu+2)}{\beta+\mu}} \quad (3-18)$$

Note that by setting $\beta=b=0$ in Equations (3-16), (3-17) and (3-18) the closed-form expressions for optimal parameters and dynamic amplification factor of the classical TMD for undamped harmonically support excited SDOF systems are retrieved (Warburton, 1982; Rana & Soong, 1998) as shown in Table 3.1. Closed-form expressions corresponding to the force excitation case are also included in the latter table for the sake of completeness. In this case, the optimal TMDI parameters and dynamic amplification factor for harmonically forced excited undamped SDOF structures follows trivially from the known expressions of the classical TMD with attached mass m_2+b (see Figure 3.2 and Eq. (3-1)). However, these expressions need to be slightly modified to be consistent with the definitions of the parameters v_{TMDI} and ζ_{TMDI} in Eq. (3-3).

Table 3.1. Closed-form expressions for optimal TMDI for undamped SDOF harmonically excited primary structures vis-à-vis the classical TMD case

	Frequency ratio (v_{TMDI})	Damping ratio (ζ_{TMDI})	Dynamic amplification factor ($\max_{\omega} \{ G_1(\omega)\} $)
Force excited TMD ($b=0$)	$\frac{1}{1+\mu}$	$\sqrt{\frac{3\mu}{8(1+\mu)}}$	$\sqrt{\frac{2+\mu}{\mu}}$
Force excited TMDI ($b>0$)	$\frac{1}{1+\beta+\mu}$	$\sqrt{\frac{3(\mu+\beta)}{8(1+\mu+\beta)}}$	$\sqrt{\frac{2+\mu+\beta}{\mu+\beta}}$

Base excited <i>TMD</i> ($b=0$)	$\frac{1}{1+\mu} \sqrt{\frac{2-\mu}{2}}$	$\sqrt{\frac{6\mu}{8(1+\mu)(2-\mu)}}$	$(1+\mu) \sqrt{\frac{2}{\mu}}$
Base excited <i>TMDI</i> ($b>0$)	$\frac{1}{1+\beta+\mu} \sqrt{\frac{(1+\mu)(2-\mu)-\mu\beta}{2(1+\mu)}}$	$\sqrt{\frac{\beta^2\mu+6\mu(1+\mu)^2+\beta(1+\mu)(6+7\mu)}{8(1+\mu)(1+\beta+\mu)[2+\mu(1-\beta-\mu)]}}$	$\sqrt{\frac{(1+\mu)(\beta+2\mu+2)}{\beta+\mu}}$

3.3.2 QUANTIFICATION OF THE PERFORMANCE ENHANCEMENT AND WEIGHT REDUCTION OF THE TUNED-MASS-DAMPER-INERTER VIS-À-VIS THE CLASSICAL TUNED-MASS-DAMPER

The optimum TMDI properties ν_{TMDI} and ζ_{TMDI} given by the above derived expressions (3-15) and (3-17) minimize the peak dynamic amplification factor $|G_I(\omega)|$ at frequencies ω_{p1} and ω_{p2} (and consequently the peak response at those frequencies) of TMDI equipped harmonically base excited undamped primary structures for any given value of the ratios μ and β following the Den Hartog approach for optimal design/tuning of TMDs. In Figure 3.4 the expressions in (3-15) and (3-17) are plotted, for four different values of the mass ratio μ , as a function of the inertance ratio β . The latter quantity takes values within a suggested interval of practical interest $[0,1]$, with $\beta=0$ being the limiting value for which the TMDI degenerates to the classical TMD. It is observed that the optimal frequency ratio ν_{TMDI} decreases as β increases for all values of μ considered, while it also decreases as the attached m_2 mass increases. Further, the computed optimum damping ratio ζ_{TMDI} increases monotonically (and almost linearly) with the normalized inerter constant β for all considered values of μ , while it also increases as the attached m_{TMDI} mass increases.

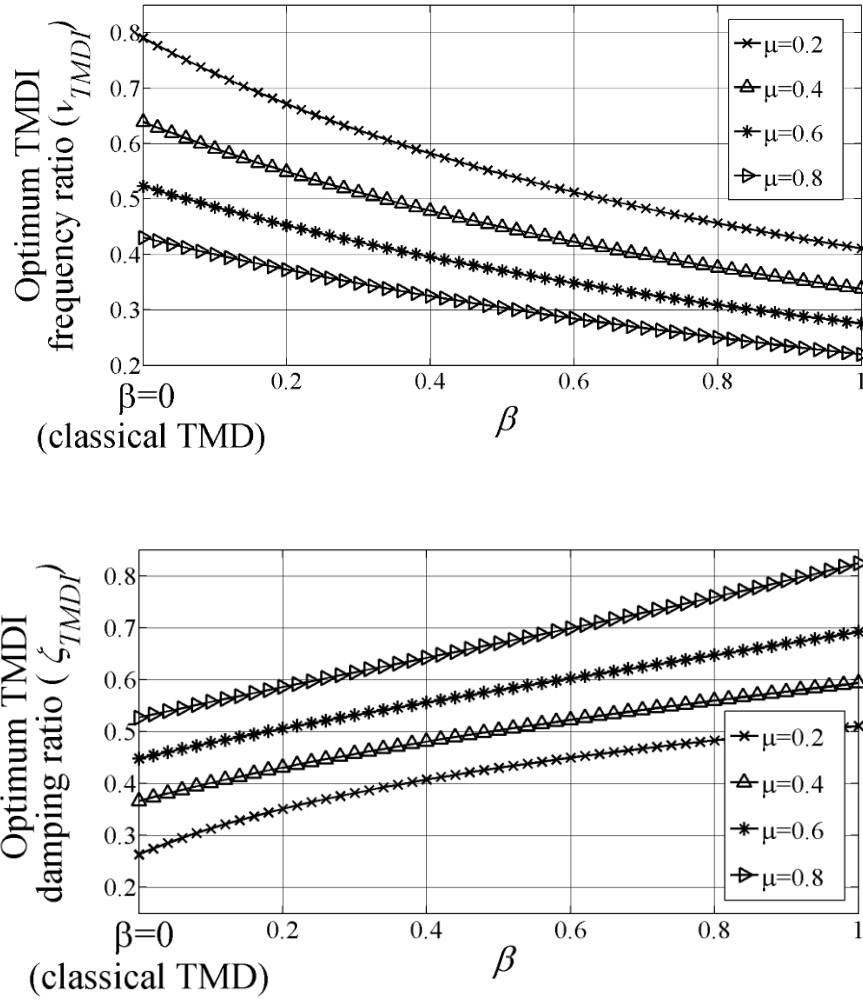


Figure 3.4. Optimum TMDI frequency ratio ν_{TMDI} and damping ratio ζ_{TMDI} as a function of the inertance ratio β and for several mass ratio values μ .

More importantly, Figure 3.5 plots the dynamic amplification factor $|G_I(\omega)|$ as a function of the input harmonic excitation normalized by the natural frequency of the uncontrolled primary structure ω_I for an optimally designed TMDI equipped undamped SDOF primary structure with mass ratio $\mu = 0.1$. Different values of the inertance ratio β , including the $\beta=0$ value which corresponds to the optimally designed classical TMD, are considered. As expected, all FRF curves plotted attain two local maxima of equal height at the frequencies ω_{p1} and ω_{p2} whose location depend on the ratio β . Compared to the case of the classical TMD, the incorporation of the inerter in the considered TMDI arrangement

reduces significantly the peak dynamic amplification factor of the primary structure at the resonant frequency ω_1 of the uncontrolled primary structure, as well as at frequencies ω_{p1} and ω_{p2} . The rate of this reduction saturates as the ratio β increases. This trend can be clearly seen in Figure 3.6 which plots the peak response amplitude of the optimally designed TMDI equipped primary structure at ω_{p1} normalized by the peak response amplitude of the optimally designed classical TMD equipped primary structure ($b=0$) at the same frequency against the inertance ratio β for four different values of the mass ratio.

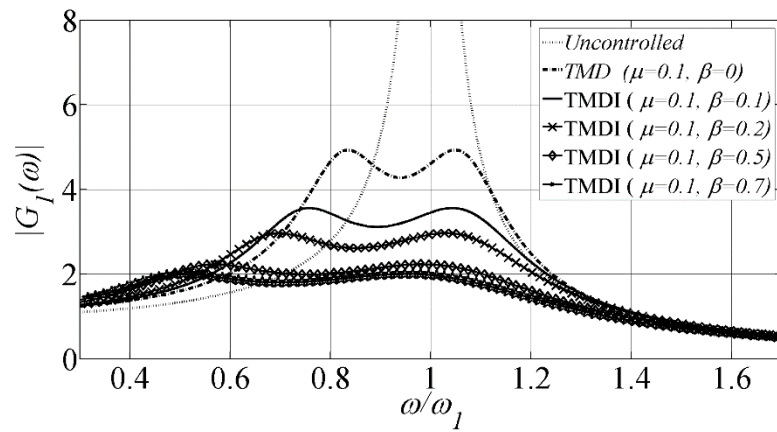


Figure 3.5. Dynamic amplification factor spectra for various optimally designed TMDI ($b>0$) systems and for the classical TMD ($b=0$).

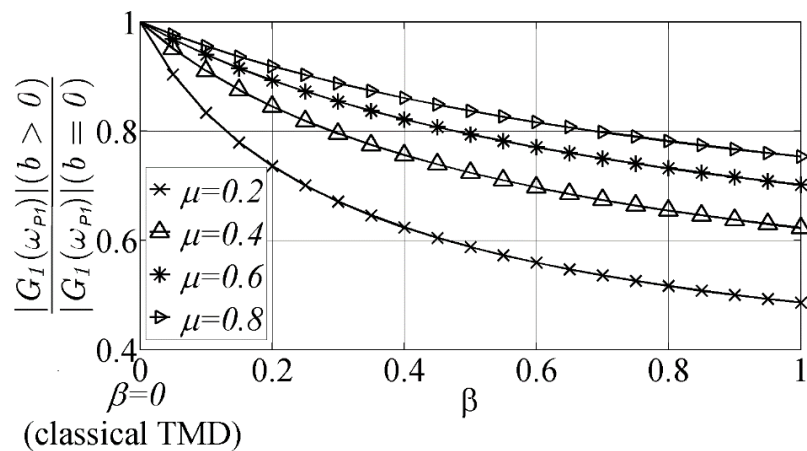


Figure 3.6. Normalized dynamic amplification factor at the “fixed” point ω_{p1} for optimally designed TMDI systems as functions of the inertance ratio β .

Figure 3.6 also suggests that the incorporation of the inerter to the classical TMD system is more effective for vibration suppression for smaller attached masses m_{TMDI} . Nevertheless, it is also observed in Figure 3.5 that for a certain interval of frequencies lower than ω_{p1} the classical TMD performs better than the TMDI. Even so, the upper bound of this interval reduces as β increases. For example, for the particular case of $\mu=0.1$ shown in Figure 3.5, this upper bound becomes as low as 60% of the resonant frequency of the uncontrolled primary structure for $\beta>0.5$. Furthermore, the dynamic amplification factor $|G_I(\omega)|$ becomes flatter as the inertance ratio β increases and exhibits practically insignificant fluctuations for $\beta>0.7$ (and $\mu=0.1$) over a considerable range of frequencies. Similar observations hold true for other values of mass ratio μ as well.

In view of the above observations, it is concluded that the consideration of larger inertance ratio values β is beneficial as it significantly reduces the peak response within a wide range of frequencies about the natural frequency of the uncontrolled primary structure compared to the classical TMD. Therefore, the TMDI is more robust for vibration suppression vis-à-vis the classical TMD of the same mass ratio μ (and consequently of the same weight) as it is less affected by detuning and uncertainties in estimating the structural properties of the primary structure.

It is important to point out that the previously reported benefits of incorporating an inerter to the classical TMD following the arrangement of Figure 3.2 are similar to considering classical TMDs with larger attached mass. This effect is demonstrated in Figure 3.7 which plots the dynamic amplification factor of harmonically base excited undamped SDOF structures equipped with the classical TMD for different values of the attached mass (i.e. different μ values).

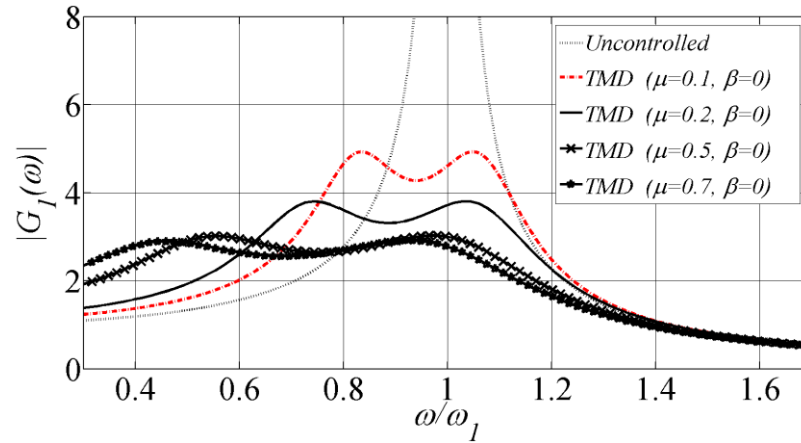


Figure 3.7. Dynamic amplification factor spectra for various optimally designed TMD ($b=0$) equipped undamped SDOF systems.

Though the curves are different than those of Figure 3.6 (see also the last column of Table 3.1) the effect of increasing the TMD mass is similar to that of a TMDI with a fixed attached mass but with increase inertance. In this regard, an important practical advantage of the TMDI is that it achieves similar levels of vibration suppression compared to the classical TMD with significantly smaller additive weight. This aspect is quantified in Figure 3.8 using a bar chart diagram of the required attached mass ratio to achieve specific peak dynamic amplification factors for different values of inertance including the limiting case of $\beta=b=0$ corresponding to the classical TMD.

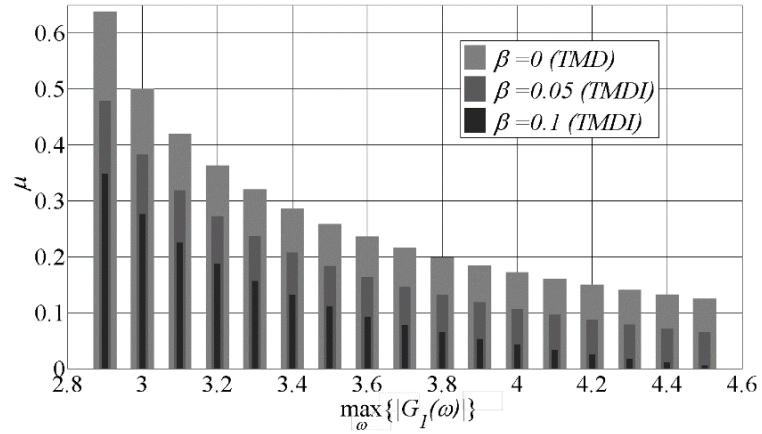


Figure 3.8. Dynamic amplification factor spectra for various optimally designed TMD ($b=0$) equipped undamped SDOF systems.

For example, a peak dynamic amplification factor of 3 can be achieved by a TMDI with inertance equal to 10% of the mass of the primary structure and with almost half the total weight of a classical TMD. Assuming a primary structure with $m_1= 360t$ mass, an inerter with inertance $b= 36t$ can be achieved by a flywheel with mass equal to 10kg and ratio $\gamma_f/\gamma_{pr}= 3$ connected to the rack by two gears ($n=2$ in Eq. (2-1) one having a transmission ratio r/pr equal to 5 and the other equal to 4 (see also Figure 2.4).

3.4 OPTIMUM DESIGN OF THE TUNED-MASS-DAMPER-INERTER FOR STOCHASTIC WHITE NOISE EXCITATION

3.4.1 DERIVATION OF CLOSED FORM SOLUTIONS FOR OPTIMUM DESIGN PARAMETERS

Assume that the TMDI system of Figure 3.2b is subjected to a stationary stochastic support excitation process $a_g(t)/\omega_1^2$ represented in the frequency domain by a double-sided spectral density function (power spectrum) $S(\omega)$. The variance of the relative displacement process x_1 of the primary structure is written as:

$$\sigma_1^2 = \int_{-\infty}^{+\infty} |G_1(\omega)|^2 S(\omega) d\omega \quad (3-19)$$

In the latter equation, the “transfer function” $|G_1(\omega)|^2$ is the squared modulus of the FRF defined in Equation (3-5). Given μ and β mass ratios, it is sought to determine optimum values for the stiffness k_{TMDI} and damping c_{TMDI} constants of the considered TMDI configuration, or equivalently ν_{TMDI} and ζ_{TMDI} dimensionless parameters (see Equations (3-3) and (3-4)), which minimize the variance σ_1^2 in Equation (3-19) for the case of the undamped ($\zeta_1 = 0$) TMDI equipped SDOF primary structures under white noise support excitation.

The latter is a well-studied in the literature special case for which analytical formulae for the optimal “tuning” of the classical TMD exist (see e.g. Warburton, 1982).

For this purpose, considering an undamped primary structure ($\zeta_1=0$) the transfer function in Equation (3-5) can be written by grouping its coefficients as:

$$|G_1(\omega)|^2 = \frac{b_2\omega^4 + b_1\omega^2 + b_0}{(a_4\omega^4 + a_3\omega^3 + a_2\omega^2 + a_1\omega + a_0)(a_4\omega^4 - a_3\omega^3 + a_2\omega^2 - a_1\omega + a_0)} \quad (3-20)$$

where the numerator coefficients are expressed as:

$$\begin{aligned} b_0 &= \omega_1^4 \nu_{TMDI}^4 (1 + \mu)^2 ; \\ b_1 &= 4\zeta_{TMDI}^2 (1 + \mu)^2 \omega_1^2 \nu_{TMDI}^2 - 2\omega_1^2 \nu_{TMDI}^2 \frac{(\beta + \mu)(1 + \mu)}{\mu} ; \\ b_2 &= \left(\frac{\beta + \mu}{\mu} \right)^2 ; \end{aligned} \quad (3-21)$$

and the denominator coefficients are expressed as:

$$\begin{aligned} a_0 &= \omega_1^2 \nu_{TMDI}^2 ; a_1 = -i2\zeta_{TMDI} \omega_1 \nu_{TMDI} ; a_2 = -\left(\frac{\beta + \mu}{\mu} + \nu_{TMDI}^2 (1 + \beta + \mu) \right) ; \\ a_3 &= \frac{i2\zeta_{TMDI} (1 + \beta + \mu) \nu_{TMDI}}{\omega_1} ; a_4 = \frac{\beta + \mu}{\mu \omega_1^2} . \end{aligned} \quad (3-22)$$

Assuming a constant power spectrum over all frequencies $S(\omega)=S_0$ (ideal white noise) and using standard analytical techniques to evaluate the integral in Equation (3-19) (see e.g. Roberts & Spanos, 2003) the variance σ_1^2 for an undamped primary system equipped with a TMDI is expressed as:

$$\sigma_1^2 = \pi S_0 \omega_1 \frac{\mu^2 C_1 + \beta^2 C_2 + 2\beta\mu C_3}{2\zeta_{TMDI} \nu_{TMDI} \mu (\beta + \mu)^2} \quad (3-23)$$

in which:

$$\begin{aligned}
C_1 &= 1 + v_{TMDI}^4 (1 + \mu)^4 + v_{TMDI}^2 (1 + \mu)^2 [\mu - 2 + 4\zeta_{TMDI}^2 (1 + \mu)]; \\
C_2 &= 1 + v_{TMDI}^2 \mu (1 + \mu) [\mu (1 + v_{TMDI}^2 (1 + \mu)) - 1]; \\
C_3 &= 1 + v_{TMDI}^2 (1 + \mu) [\mu (\mu + 2\zeta_{TMDI}^2 (1 + \mu) + v_{TMDI}^2 (1 + \mu)^2 - 1)].
\end{aligned} \tag{3-24}$$

Assuming constant mass ratios μ and β , the variance σ_1^2 of Eq. (3-23) is minimized in terms of the TMD frequency ratio v_{TMDI} and damping ratio ζ_{TMDI} by enforcing the following two conditions:

$$\frac{\partial \sigma_1^2}{\partial v_{TMDI}} = 0 \quad \text{and} \quad \frac{\partial \sigma_1^2}{\partial \zeta_{TMDI}} = 0 \tag{3-25}$$

These conditions yield a system of two equations from which the “optimal” tuning parameters v_{TMDI} and ζ_{TMDI} of the proposed TMDI configuration are found in terms of the mass ratios μ and β as:

$$v_{TMDI} = \frac{1}{1 + \beta + \mu} \frac{\sqrt{[\beta(\mu - 1) + (2 - \mu)(1 + \mu)]}}{\sqrt{2(1 + \mu)}} \tag{3-26}$$

and:

$$\zeta_{TMDI} = \frac{\sqrt{(\beta + \mu)} \sqrt{\beta(3 - \mu) + (4 - \mu)(1 + \mu)}}{2\sqrt{2(1 + \beta + \mu)[\beta(1 - \mu) + (2 - \mu)(1 + \mu)]}} \tag{3-27}$$

Further, by substitution of the above optimal TMDI tuning parameters into Equation (3-23) the following expression for the achieved minimum variance of the relative displacement process x_1 is obtained

$$\sigma_{1,\min}^2 = \pi S_0 \omega_1 (1 + \mu) \sqrt{\frac{(1 + \mu)[\beta(3 - \mu) + (4 - \mu)(1 + \mu)]}{(\beta + \mu)(1 + \beta + \mu)}} \quad (3-28)$$

It is important to note that by setting $b = \beta = 0$ in Equations (3-26), (3-27) and (3-28) the optimal tuning formulae of the classical TMD which minimize the relative displacement variance of an undamped SDOF primary structure subjected to white noise support excitation reported in the literature (Warburton, 1982) can be retrieved.

To facilitate comparison between the proposed TMDI configuration of Figure 3.2b and the TMD, the previously derived formulae for the optimal tuning of the TMDI are juxtaposed with the known formulae corresponding to the classical TMD in Table 3.2. Similar to the case of harmonic excitation TMDI presented in subchapter 3.3, closed-form expressions corresponding to the force excitation are also included in Table 3.2 for the sake of completeness. In this case, the optimal TMDI parameters and minimum achieved variance for white noise forced excited undamped SDOF structures follows from the known expressions of the classical TMD with attached mass.

Table 3.2. Closed-form expressions for optimal tuning of the proposed TMDI configuration for undamped SDOF primary structures subject to white noise base excitation vis-à-vis the classical TMD case.

	Frequency ratio (ν_{TMDI})	Damping ratio (ζ_{TMDI})	Minimum achieved variance of x_1
Force excited TMD ($b=0$)	$\frac{\sqrt{1 + \mu/2}}{1 + \mu}$	$\frac{\sqrt{\mu(1 + 3\mu/4)}}{\sqrt{4(1 + \mu)(1 + \mu/2)}}$	$\pi S_0 \omega_1 \sqrt{\frac{1 + \frac{3}{4}\mu}{\mu(1 + \mu)}}$
Force excited TMDI ($b>0$)	$\frac{\sqrt{1 + (\beta + \mu)/2}}{1 + \beta + \mu}$	$\frac{\sqrt{(\mu + \beta)(1 + 3(\mu + \beta)/4)}}{\sqrt{4(1 + (\mu + \beta))(1 + (\mu + \beta)/2)}}$	$\pi S_0 \omega_1 \sqrt{\frac{1 + \frac{3}{4}(\mu + \beta)}{(\mu + \beta)(1 + \mu + \beta)}}$
Base excited TMD ($b=0$)	$\frac{\sqrt{1 - \mu/2}}{1 + \mu}$	$\frac{\sqrt{\mu(1 - \mu/4)}}{\sqrt{4(1 + \mu)(1 - \mu/2)}}$	$\pi S_0 \omega_1 (1 + \mu) \sqrt{\frac{(1 + \mu)(4 - \mu)}{\mu}}$
Base excited TMDI ($b>0$)	$\frac{1}{1 + \beta + \mu} \frac{\sqrt{(\beta + \mu)[\beta(\mu - 1) + (2 - \mu)(1 + \mu)]}}{\sqrt{2\mu(1 + \mu)}}$	$\frac{(\beta + \mu)\sqrt{\beta(3 - \mu) + (4 - \mu)(1 + \mu)}}{2\sqrt{2\mu(1 + \beta + \mu)[\beta(1 - \mu) + (2 - \mu)(1 + \mu)]}}$	$\pi S_0 \omega_1 (1 + \mu) \sqrt{\frac{(1 + \mu)[\beta(3 - \mu) + (4 - \mu)(1 + \mu)]}{(\beta + \mu)(1 + \beta + \mu)}}$

In the following section, the potential of the TMDI to suppress the oscillatory motion of white noise support excited undamped SDOF primary structures is assessed vis-à-vis the classical TMD.

3.4.2 QUANTIFICATION OF PERFORMANCE ENHANCEMENT AND WEIGHT REDUCTION OF THE TUNED-MASS-DAMPER-INERTER VIS-À-VIS THE CLASSICAL TUNED-MASS-DAMPER.

In Figure 3.9 and Figure 3.10, Equations (3-26) and (3-27) are plotted, respectively, for four different values of the mass ratio μ and for β ratios within a suggested interval of practical interest $[0,1]$, with $\beta=0$ being the limiting value for which the TMDI degenerates to the classical TMD. It is observed that the influence of the apparent “mass amplification” effect due to the additional inerter device incorporated in the proposed TMDI is more prominent for lower values of the mass ratio μ . Specifically, for $\mu>0.6$ the “optimum” frequency ratio ν decreases slightly as β increases, while for $\mu<0.4$ the ratio ν increases significantly for values of β up to about 0.3 to 0.4 and then decays for higher values of β . More importantly, the achieved “optimum” damping ratio ζ_{TMDI} increases monotonically (and almost linearly) for all considered values of μ as the normalized inerter constant β increases. However, the rate of this increase deteriorates for higher values of μ . These trends suggest that the incorporation of an inerter device to the classical TMD is more beneficial for relatively smaller values of the mass ratio μ (i.e. for relatively lower vibrating TMD masses) as it allows for “driving” viscous dampers with higher kinetic energy absorption capabilities (i.e. damping ratios).

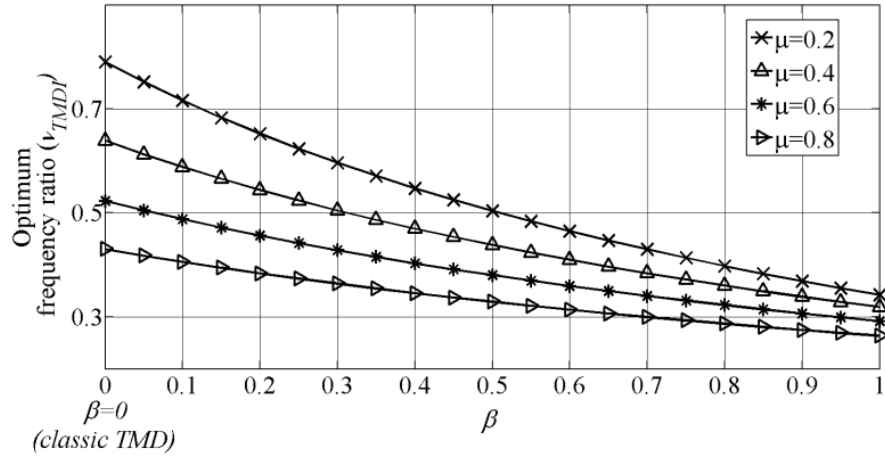


Figure 3.9. Optimum TMDI frequency ratio for various values of β and several mass ratio values

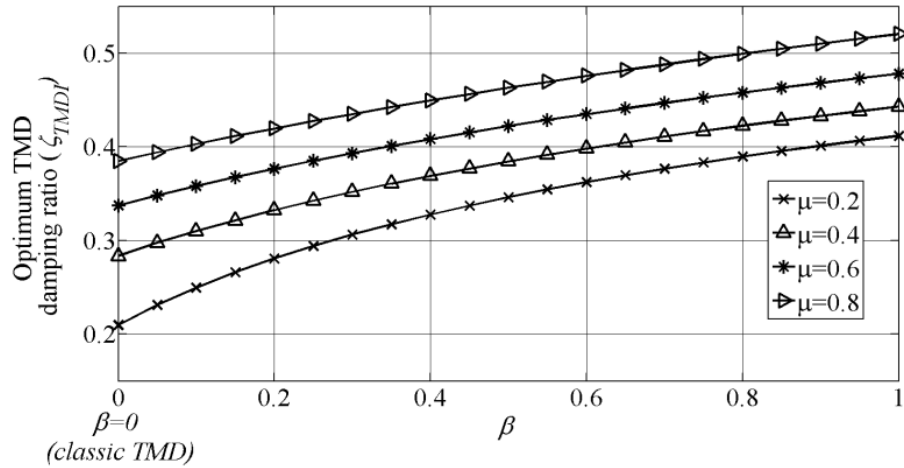


Figure 3.10. Optimum TMD damping ratio for various values of β and several mass ratio values

The above argument is confirmed by the numerical data of Figure 3.11 in which the minimum relative displacement variance of the primary structure achieved by means of TMDI $\sigma_{1,\min}^2(b > 0)$ is plotted (Equation (3-28)), normalized by the minimum variance achieved via the classical TMD $\sigma_{1,\min}^2(b = 0)$ for the same values of the mass ratios μ and β as previously considered. In all cases, the displacement response variance decreases significantly as the parameter β increases demonstrating that the proposed TMDI configuration is more effective to suppress oscillations compared to the classical TMD.

Further, the effectiveness of the TMDI increases considerably as lower values of the mass ratio μ ($\mu < 0.4$) are considered, commonly adopted in practical TMD implementations.

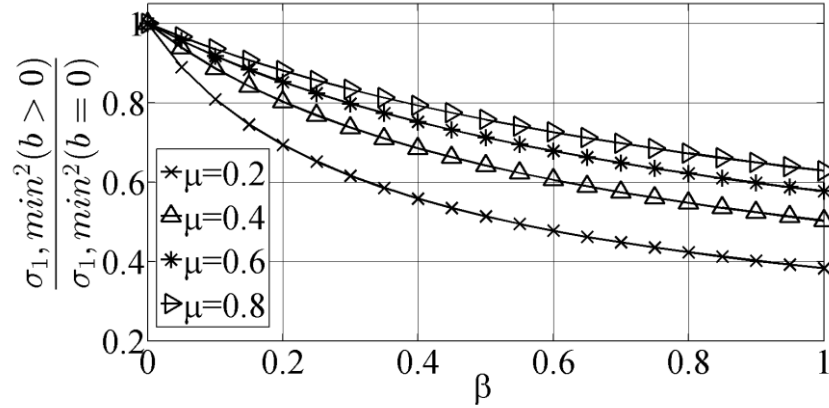


Figure 3.11. Minimum variance ratio between the proposed model ($b > 0$) and the classical TMD ($b = 0$)

In fact, although in most practical applications of the TMD the considered mass ratio μ rarely exceeds values of 0.2~0.3, it can be shown that the proposed TMDI configuration is more effective than the classical TMD in suppressing the relative displacement variance of the primary structure for all values of the mass ratio μ within the interval (0,4]. Specifically, by relying on Eq. (3-28), it can be shown that:

$$\frac{\sigma_{1,\min}^2(b > 0)}{\sigma_{1,\min}^2(b = 0)} < 1 \quad (3-29)$$

for

$$0 < \mu \leq 3 \text{ and } \beta > 0 \quad (3-30)$$

and for:

$$3 < \mu \leq 4 \quad \text{and} \quad 0 < \beta \leq \frac{4 + 3\mu - \mu^2}{\mu - 3} \quad (3-31)$$

In view of the above analytical and numerical data, it can be concluded that the use of the inerter in the proposed configuration reduces significantly the minimum variance of an undamped SDOF subjected to white noise base acceleration in comparison with classical TMD.

It has already been showed in the previous sub-chapter that the optimum designed TMDI configuration is more effective than the classical TMD for a fixed value of the TMD mass in suppressing the displacement variance of white noise excited undamped SDOF primary structures. In all cases, the displacement response variance decreases significantly as the parameter β increases demonstrating that the proposed TMDI configuration is more effective to suppress oscillations compared to the classical TMD. Herein, to emphasize on the mass reduction capabilities of the inerter, Figure 3.12 reports the required additional m_{TMDI} mass values for achieving pre-imposed levels of structural response for both TMDI passive control configuration and for the classical TMD solution. These are obtained by numerically solving for μ in Equation (3-28) for the case of $\beta=0$ (classical TMD) and for $\beta>0$ (TMDI configuration).

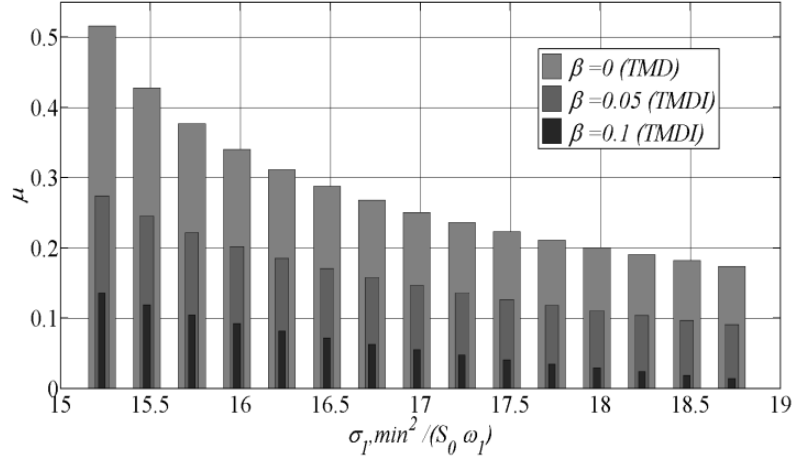


Figure 3.12 Additional m_{TMDI} mass values required for achieving the same level of performance in terms of displacement response variance for the proposed TMDI configuration and classical TMD ($b=0$)

It is observed that the same level of response amplitude evaluated by means of the normalized response variance $\sigma_{1,min}^2 / S_0 \omega_1$ can be achieved by adopting e.g. the classical TMD solution with a mass ratio $\mu=0.51$ or by employing a TMDI solution with $\beta=0.1$ and with a mass ratio $\mu=0.13$. It is important to mention that, the physical mass of the considered inerter might be up to two orders of magnitude smaller than its b constant (implicitly β ratio) as detailed in Section 2.2 and thus the TMDI configuration represents a much lighter passive control solution compared to the case of classical TMD.

As a final remark, it is noted that the optimum tuning parameters v_{TMDI} and ζ_{TMDI} obtained for undamped SDOF primary structures (Equations (3-26) and (3-27)) can be used to facilitate the optimum design of a novel TMDI configuration to suppress the oscillatory motion of support excited multi-degree-of-freedom (MDOF) primary structures.

CHAPTER 4 : THE TUNED-MASS-DAMPER-INERTER FOR SUPPORT EXCITED MULTI-DEGREE-OF-FREEDOM PRIMARY SYSTEMS

4.1 PRELIMINARY REMARKS

This chapter develops the TMDI for passive vibration control of mechanical chain-like (cascaded) damped multi-degree-of-freedom (MDOF) primary systems. In particular, consider a linear proportionally (classically) damped multi-degree-of-freedom (MDOF) system with masses m_j ($j=1,2,\dots,n$), linked together by linear springs of stiffness coefficients k_j ($j=1,2,\dots,n$) and viscous dampers with damping coefficients c_j ($j=1,2,\dots,n$) as shown in Figure 4.1., where n is the number of the DOFs of the system, based-excited by an acceleration stochastic process $a_g(t)$.

To suppress the motion of this chain-like MDOF primary structure according to its, presumably dominant, fundamental (first) mode shape of vibration, it is proposed to consider a tuned mass-damper (TMD) attached to the “lead” m_1 mass in conjunction with an inerter device connecting the TMD mass to the penultimate m_2 of the primary structure (Fig. 6). Note that by eliminating the inerter ($b=0$), the above tuned mass-damper-inerter (TMDI) configuration coincides with TMD arrangements commonly used to control the fundamental mode of vibration of base excited “regular” MDOF structures. This arrangement is motivated by earthquake engineering applications where TMD attached to the top building floor are used for seismic protection of multi-storey buildings (e.g. Rana & Soong, 1998). In this regard, as in the case of the SDOF primary structure presented in previous sections, *the herein proposed TMDI configuration can be*

interpreted as a generalization of the commonly used TMD arrangements for passive vibration control of support-excited MDOF primary structures. In the remainder of this chapter, the governing differential equations of motion of TMDI equipped system in Figure 4.1 are derived in the time and Laplace domain. Further, a standard optimization procedure is considered to obtain optimum TMDI and classical TMD designs (as a special case of a TMDI with $b=0$) which minimize the displacement variance of the “lead” mass (most remote mass from the support) of the primary structure base excited. Coloured noise base excitations are considered for the ensuing numerical applications.

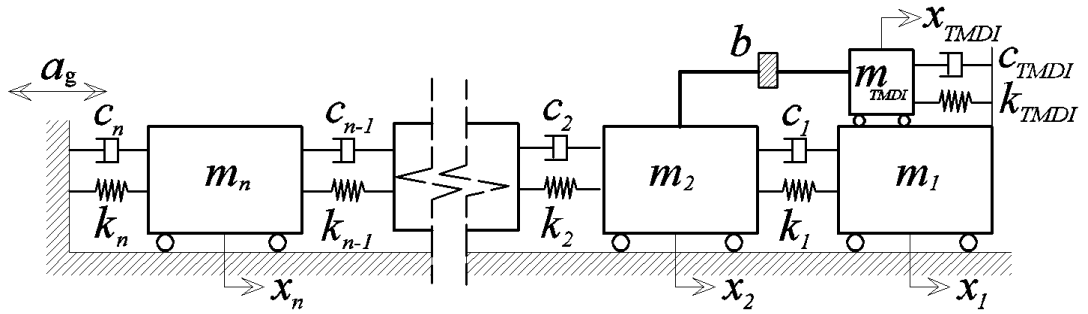


Figure 4.1. Cascaded chain-like multi-degree-of-freedom (MDOF) primary system incorporating the proposed tuned mass-damper-inerter (TMDI) configuration.

4.2 GOVERNING EQUATIONS OF MOTION

The $n+1$ equations of motion of the resulting MDOF system in Figure 4.1 subject to a lateral ground motion represented by an acceleration stochastic process $\alpha_g(t)$ are written in matrix form as:

$$\mathbf{M}\ddot{\mathbf{x}} + \mathbf{C}\dot{\mathbf{x}} + \mathbf{K}\mathbf{x} = -\mathbf{M}\delta\alpha_g(t) \quad (4-1)$$

In the above equation, δ is the unit column vector and \mathbf{x} is the vector collecting all lateral floor deflections x_i ($i=1,2,\dots,n$) and the relative to the ground displacement x_{TMDI} of the attached TMDI mass, that is,

$$\mathbf{x} = [x_{TMDI}(t) \quad x_1(t) \quad x_2(t) \quad \dots \quad x_n(t)]^T \quad (4-2)$$

where the superscript “ T ” denotes matrix transposition. Further, in Equation (4-1) the mass matrix \mathbf{M} , the damping matrix \mathbf{C} , and the stiffness matrix \mathbf{K} are given by the expressions:

$$\mathbf{M} = \begin{bmatrix} m_{TMDI} + b & 0 & -b & 0 & \dots & 0 \\ 0 & m_1 & 0 & 0 & \dots & \vdots \\ -b & 0 & m_2 + b & 0 & \dots & \vdots \\ 0 & 0 & 0 & m_3 & \dots & \vdots \\ \vdots & \vdots & \vdots & \vdots & \ddots & 0 \\ 0 & \dots & \dots & \dots & 0 & m_n \end{bmatrix} \quad (4-3)$$

$$\mathbf{C} = \begin{bmatrix} c_{TMDI} & -c_{TMDI} & 0 & \cdots & 0 \\ -c_{TMDI} & c_1 + c_{TMDI} & -c_1 & 0 & \vdots \\ 0 & -c_1 & c_1 + c_2 & -c_2 & \vdots \\ 0 & 0 & -c_2 & \ddots & 0 \\ \vdots & \vdots & \vdots & \vdots & -c_{n-1} \\ 0 & \cdots & 0 & -c_{n-1} & c_{n-1} + c_n \end{bmatrix} \quad (4-4)$$

$$\mathbf{K} = \begin{bmatrix} k_{TMDI} & -k_{TMDI} & 0 & \cdots & 0 \\ -k_{TMDI} & k_1 + k_{TMDI} & -k_1 & 0 & \vdots \\ 0 & -k_1 & k_1 + k_2 & -k_2 & \vdots \\ 0 & 0 & -k_2 & \ddots & 0 \\ \vdots & \vdots & \vdots & \vdots & -k_{n-1} \\ 0 & \cdots & 0 & -k_{n-1} & k_{n-1} + k_n \end{bmatrix} \quad (4-5)$$

respectively, where m_i , k_i , and c_i are the mass, lateral stiffness, and damping of floor i ($i=1,2,\dots,n$) and m_{TMDI} , k_{TMDI} , c_{TMDI} , and b are the TMDI mass, stiffness, damping, and inertance coefficients (see also Figure 4.1). Note that for $b=0$ Eqs. (4-1) to (4-5) govern the response of a base excited chain-like MDOF system with the classical TMD attached to its leading mass. The latter TMD topology is widely considered to control the first mode of vibration of structural systems which, in many practical cases, dominates their dynamic response to broadband base excitations such as seismically excited multi-storey buildings subjected to earthquake ground motions (e.g. Rana & Soong, 1998). The inclusion of the inerter device as shown in (4-3) alters the mass matrix which is no longer diagonal. However, the overall system remains linear and, from a practical viewpoint, the same well-established computational methods for optimal design of classical TMD can be readily applied for the optimal design of the TMDI system of Figure 4.1.

The optimal design of the TMDI for chain-like MDOF systems requires the determination of the transfer function between the input support excitation and the output displacement of the lead mass relative to the base motion x_I in Figure 4.1. This can be

achieved by first writing the $n+1$ system of second-order differential equations of Eq. (4-1) as a system of $2n+2$ first-order differential equations (state-space form):

$$\dot{\mathbf{z}} = \mathbf{A}\mathbf{z} + \mathbf{B}a_g(t) \quad (4-6)$$

where \mathbf{z} is the state vector defined as

$$\mathbf{z} = \begin{bmatrix} \mathbf{x} \\ \dot{\mathbf{x}} \end{bmatrix} \quad (4-7)$$

and \mathbf{A} and \mathbf{B} are the system matrix and input matrix, respectively, given by:

$$\mathbf{A} = \begin{bmatrix} \mathbf{0}_{n+1} & \mathbf{I}_{n+1} \\ -\mathbf{M}^{-1} \times \mathbf{K} & -\mathbf{M}^{-1} \times \mathbf{C} \end{bmatrix}, \quad (4-8)$$

$$\mathbf{B} = \begin{bmatrix} \mathbf{0}_{n+1} \\ \mathbf{I}_{n+1} \end{bmatrix} \quad (4-9)$$

It is noted \mathbf{O}_{n+1} and \mathbf{I}_{n+1} as the zero and unit square matrices respectively of dimension $n+1$. Let $Y(t)$ denote the output of the system expressed by:

$$Y(t) = C_o \cdot Z(t) \quad (4-10)$$

where C_o is defined as the measurement (output) matrix which depends on the selection of the studied output variable (e.g. displacement/velocity of the primary system).

Assuming that the initial condition state vector is homogenous, that is:

$$Z(0) = 0, \quad (4-11)$$

the Laplace transforms of Eqs.(4-6) and (4-10) are expressed after basic manipulations as:

$$s\tilde{Z}(s) - A \cdot \tilde{Z}(s) = B \cdot \tilde{A}(s) \quad (4-12)$$

$$\tilde{Y}(s) = C_o \cdot \tilde{Z}(s) \quad (4-13)$$

respectively. It is noted $\tilde{A}(s)$ as the Laplace transform of the support acceleration process $a_g(t)$ and $\tilde{Z}(s)$ as the Laplace transform of $Z(t)$. Further manipulation leads to:

$$\tilde{Z}(s) = (sI_{2(n+1)} - A)^{-1} \cdot B \cdot \tilde{A}(s) \quad (4-14)$$

Substituting the latter back into Equation (4-10) one obtains:

$$\tilde{Y}(s) = [C_o \cdot (sI_{2(n+1)} - A)^{-1} \cdot B] \cdot \tilde{A}(s) \quad (4-15)$$

Based on the above equation, the overall system transfer function that relates input base acceleration to the output is expressed by:

$$G_1(s) = \frac{\tilde{Y}(s)}{\tilde{A}(s)} = C_o \cdot (sI_{2(n+1)} - A)^{-1} \cdot B \quad (4-16)$$

Setting the output matrix C_o as:

$$C_o = [0 \ 1 \ 0 \ \dots \ 0]_{(2n+2)} \quad (4-17)$$

in Equation (4-16), the transfer function $G_I(s)$ relating the (input) support excitation in terms of acceleration to the (output) top floor mass m_I relative displacement is reached. Specifically, that is:

$$G_I(s) = \frac{\tilde{x}_1(s)}{\tilde{A}(s)}, \quad (4-18)$$

where $\tilde{x}_1(s)$ is the Laplace transform of the second element in the vector defined by Equation (4-2). Actually, the location of the non-zero element in the C_o vector identifies the location of the floor (lead mass m_I) - for which the output is sought for. Evaluation of $G_I(s)$ along the imaginary axis yields the frequency response function noted herein $G_I(\omega)$.

The following section goes through the steps taken for optimum design of the herein proposed TMDI configuration for a given MDOF primary structure and for pre-specified (fixed) values of m_{TMDI} and b .

4.3 OPTIMUM DESIGN OF TUNED-MASS-DAMPER-INERTER CONFIGURATION FOR DAMPED MULTI-DEGREE-OF-FREEDOM PRIMARY SYSTEMS

Consider the dimensionless modal mass ratio defined by:

$$\mu_M = \frac{m_{TMDI}}{M_1} \quad (4-19)$$

where M_1 is the generalized mass of the fundamental mode shape of the uncontrolled (primary) chain-like MDOF structure of Figure 4.1 given by the expression:

$$M_1 = \boldsymbol{\phi}_1^T \mathbf{M}_p \boldsymbol{\phi}_1 \quad (4-20)$$

In the last equation $\boldsymbol{\phi}_1$ is the fundamental mode shape vector (eigenvector) normalized by the modal coordinate corresponding to the lead mass m_1 (see also Rana & Soong, 1998). Further, \mathbf{M}_p is obtained from the mass matrix \mathbf{M} of Equation (4-3) by elimination of the first row and column and by setting b equal to zero. Similarly to the case of SDOF primary structures discussed in Chapter 3, a second dimensionless (modal) mass ratio involving the constant of the inerter b is defined as:

$$\beta_M = \frac{b}{M_1} \quad (4-21)$$

Let the support excitation process $a_g(t)$ be non-stationary, represented in the frequency domain by a one-sided evolutionary power spectral density function (power spectrum) $S(\omega, t)$. It is sought to determine optimal design values for the frequency ratio ν and the damping ratio ζ_{TMDI} defined in Eqs. (3-3) and (3-4), respectively, to minimize the variance of the process x_1 (relative displacement of the lead mass m_1) given the mass ratios μ_M and β_M . To this aim, the following dimensionless cost function or “performance index” (PI) is considered:

$$PI = \frac{J^{TMDI}}{J^0} \quad (4-22)$$

where J^0 and J^{TMDI} denote the relative displacement variance of the lead mass (m_1) for an uncontrolled primary structure exposed to the support acceleration $a_g(t)$ and for the same primary structure equipped with the proposed TMDI configuration, respectively. Specifically,

$$J^{TMDI} = \int_0^\infty |G_1(\omega)|^2 \max_t \{S(\omega, t)\} d\omega \quad (4-23)$$

where $|G_1(\omega)|^2$ is the squared modulus of the frequency response function (“transfer function”) between the input acceleration and the output displacement of the primary system evaluated on the imaginary axis of the Laplace s -plane. The input seismic action is represented by the non-stationary power spectrum $S(\omega, t)$. Note that, notation-wise, for $b=0$: $J^{TMDI} = J^{TMD}$ and for $b=\mu_M=0$: $J^{TMDI} = J^0$.

In all of the ensuing numerical work, a standard MATLAB® built-in “min-max” constraint optimization algorithm employing a sequential programming method is used

to minimize the PI of Equation (4-22) for the design parameters ν_{TMDI} and ζ_{TMDI} (Salvi & Rizzi, 2011). The required “seed” values of ν_{TMDI} and ζ_{TMDI} used to initiate the optimization algorithm are determined by substituting $\beta_M \rightarrow \beta$ and $\mu_M \rightarrow \mu$ in Equations (3-26) and (3-27), respectively. These values minimize the considered PI for an undamped linear SDOF primary structure under white noise support excitation, as detailed in Chapter 3. Further, the constraints

$$0.5 < \nu < 4.50 \text{ and } 0 < \zeta_{TMD} < 1.00 \quad (4-24)$$

are enforced to the sought TMDI design parameters relying on physical considerations.

4.4 NUMERICAL APPLICATION OF THE TUNED-MASS-DAMPER-INERTER FOR DAMPED MULTI-DEGREE-OF-FREEDOM PRIMARY SYSTEMS: OPTIMUM DESIGN FOR STATIONARY COLOURED NOISE SUPPORT EXCITATION

In this section optimum design parameters are derived following the procedure discussed in Section 4.3 for the TMDI passive vibration control configuration of Figure 4.1. The purpose is to demonstrate the applicability of the numerical algorithm proposed and to gauge on the effectiveness of the TMDI over the TMD to suppress the lead mass displacement for damped MDOF systems. The need for such a numerical based evaluation, as opposed to an analytical one followed in Chapter 3, stems from the fact that optimum TMDI design for damped MDOF (even when targeting to control the first mode) is a challenging task. For the more general case of coloured noise excitation is not feasible. In this respect, a judiciously chosen primary system and base excitation are considered. In particular, a 3-DOF primary system ($n=3$) is used whose inertial and elastic properties are shown in Table 4.1. The undamped natural frequencies of the considered primary system obtained from standard modal analysis are $\omega_1= 6.37\text{rad/s}$, $\omega_2= 13.02\text{rad/s}$, and $\omega_3= 20.57\text{rad/s}$. Further, the fundamental mode shape normalized by the modal coordinate of the lead mass m_1 is computed as $\boldsymbol{\phi}_1 = \{1.000 \quad 0.593 \quad 0.286\}^T$ and the corresponding generalized mass is equal to $M_I= 16.9 \times 10^3 \text{ kg}$ (Eq. (4-20)).

The damping coefficients of the considered primary structure are assumed to be stiffness proportional (“classically” damped system), determined by the expression:

$$c_j = \frac{2\zeta_1}{\omega_1} k_j \quad (j=1,2,3) \quad (4-25)$$

in which ζ_1 is the critical damping ratio of the fundamental mode shape taken equal to 0.02.

Table 4.1 Inertial and elastic properties of the considered 3-DOF primary structure

j	Mass m_j (kg)	Stiffness k_j (N/m)	Damping c_j (Ns/m)
1	10×10^3	10×10^5	6280
2	15×10^3	25×10^5	15670
3	20×10^3	35×10^5	21980

Further, the input action is represented by the stationary coloured noise stochastic process represented in the frequency domain by the power spectrum $S(\omega)$ plotted in Figure 4.2. Incidentally, this spectrum is compatible in the “mean sense” with the elastic spectrum of the European seismic code for peak ground acceleration 0.36g ($g=981\text{cm/s}^2$) and ground type “B” (Eurocode 8, 2004). It has been derived by a methodology described in (Giaralis & Spanos, 2010). However, it is noted that this spectrum has been selected to attain a single dominant frequency (spike) at the damped 2nd natural frequency. In this way, the considered spectrum can be regarded as a broadband excitation since all three modes of the system are dynamically excited. (see Figure 4.2).

Furthermore, for the herein considered base excitation, the numerator in (4-23) simplifies to:

$$J^{TMDI} = \int_0^\infty |G_1(\omega)|^2 S(\omega) d\omega \quad (4-26)$$

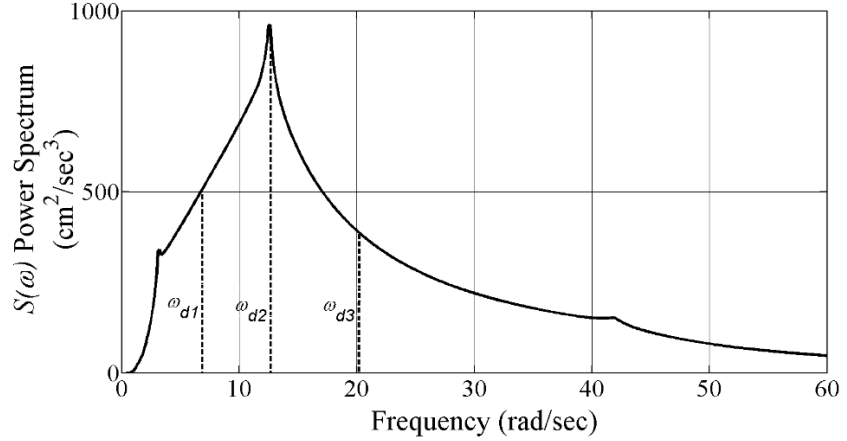


Figure 4.2. One-sided power spectrum representing the acceleration support excitation $\alpha_g(t)$.

4.4.1 OPTIMUM DESIGN OF THE CLASSICAL TUNED-MASS-DAMPER AS A SPECIAL CASE OF THE TUNED-MASS-DAMPER-INERTER CONFIGURATION

As discussed in Section 4.2, by setting $b \rightarrow 0$, or equivalently $\beta_M \rightarrow 0$ (Eq. (30)), the proposed TMDI configuration depicted in Figure 4.1 becomes the classical TMD used to suppress oscillations according to the fundamental mode of vibration for MDOF primary systems. Therefore, optimal design TMD parameters for the frequency ratio ν_{TMDI} and the damping ratio ζ_{TMDI} can be determined by following the procedure outlined in section 4.3. For example, set $\beta_M = 0$ and let the additional oscillating mass be equal to 450 kg, that is, 1% of the total mass of the 3-DOF chain-like primary system with properties given in Table 4.1. The modal mass ratio becomes $\mu_M = 0.0267$ (Eq. (4-19)). Next, the “seed” values $\nu_{TMDI} = 0.967$ and $\zeta_{TMDI} = 0.081$ are computed from Eqs. (3-26) and (3-27) respectively to initialize the adopted optimization algorithm to minimize the cost function of Equation (4-22) (see section 4.3). Similar computations are performed for different values of the TMD mass within a commonly used in engineering applications

range: 1% to 10% of the total mass of the primary structure, corresponding to 450kg to 4500kg of mass. The optimal frequency ratio ν and damping ratio ζ_{TMD} parameters obtained from the adopted optimization procedure are plotted as functions of the TMD mass in Figs. 9 and 10, respectively ($b=0$ classical TMD curve).

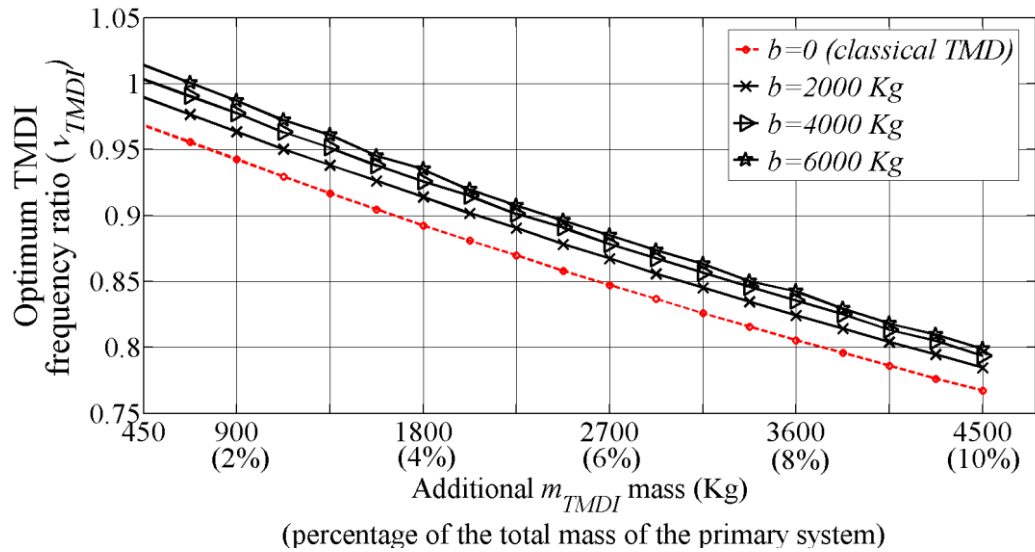


Figure 4.3. Optimum frequency ratio as a function of the TMD mass for various values of the inerter constant b to control the fundamental mode of vibration of the 3-DOF primary structure of Table 4.1

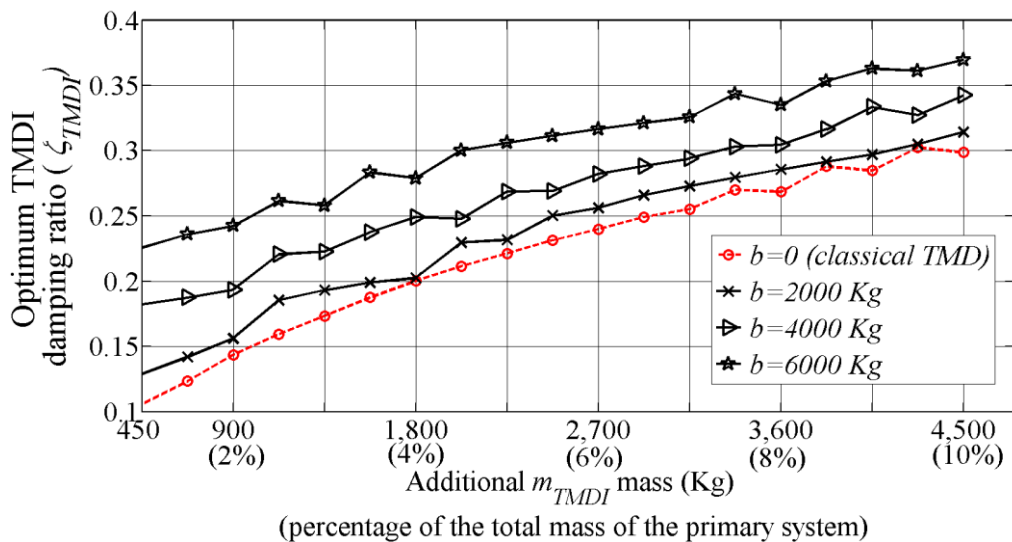


Figure 4.4. Optimum damping ratio as a function of the TMD mass for various values of the inerter constant b to control the fundamental mode of vibration of the 3-DOF primary structure of Table 4.1.

Further, the achieved value of the performance index of Equation (4-22) for the classical TMD ($b = 0$) are plotted in Figure 4.5 as a function of the TMD mass.

It is noted that the numerical data presented in Figure 4.3 and Figure 4.4 for the classical TMD are in alignment with similar results reported in the literature obtained by alternative numerical optimization techniques (see e.g. Hoang et al, 2008; Rana & Soong, 1998; Lee et al, 2006 and references therein).

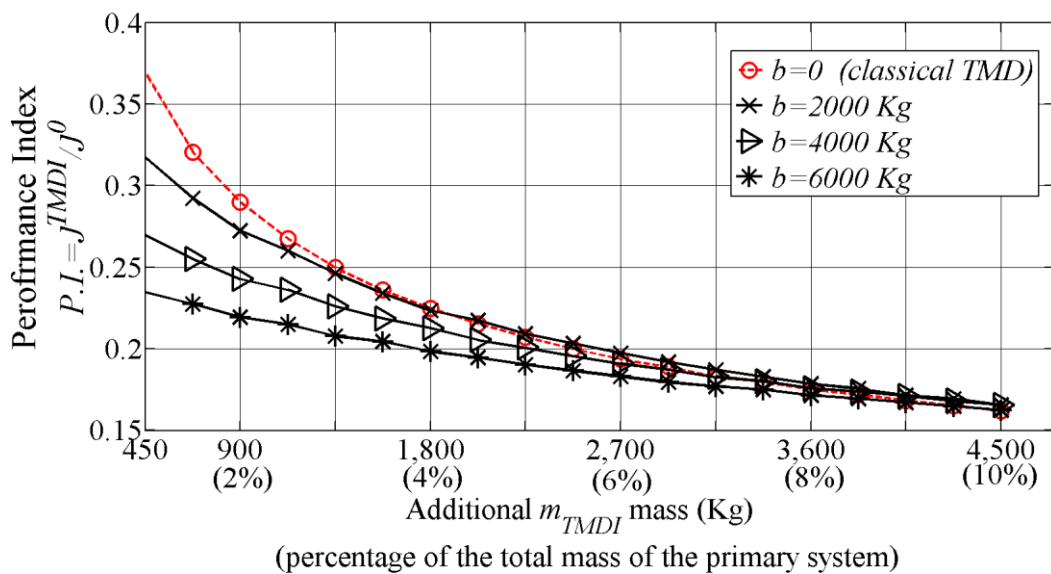


Figure 4.5. Achieved performance index versus the TMD mass for various values of the inerter constant b .

Specifically, increased values of the TMD mass require higher damping ratios ζ_{TMDI} values and lower TMD frequency ratios to achieve optimal tuning. Consequently, larger TMD mass is more effective in controlling the dynamic response of the primary structure according to its fundamental mode shape, at the cost of an increase total weight of the structural system. However, the rate of decay of the PI (proportional to the variance of the relative displacement of the m_1 mass) decreases rapidly (i.e. PI “saturates”) as the

TMD mass increases. It reaches a practically constant value for *TMD* mass larger than 5% the total mass of the considered primary structure.

4.4.2 OPTIMUM DESIGN OF THE TUNED-MASS-DAMPER-INERTER CONFIGURATION

Let an inerter device be incorporated to the considered 3-DOF mechanical primary system with the properties listed in Table 4.1 according to the proposed TMDI configuration of Figure 4.1. The previously considered optimization procedure is used to derive optimum TMDI parameters (v_{TMDI} and ζ_{TMDI}) minimizing the cost function of Equation (4-22) for the input power spectrum of Figure 4.2.

The same range of pre-specified TMD mass (1% to 10% of the total mass of the primary structure) is considered as in the previous section, while three different values of the inerter constant b are taken: 2000, 4000, and 6000 kg. Optimal TMDI parameters are plotted in Figure 4.3 and Figure 4.4 in which the case of the classical TMD ($b=0$) is also included for comparison purposes. Further, in Figure 4.5 curves of the performance index of Equation (4-22) achieved by the different TMDI systems considered are superposed to numerical results corresponding to the classical TMD ($b=0$). It can be readily seen from the herein reported numerical data that the value of the Performance Index, or equivalently the variance of the relative displacement of the m_1 mass, is reduced as the value of the inerter b increases. In fact, in all cases considered, the proposed TMDI configuration outperforms the classical TMD in terms of minimizing the adopted cost function. The achieved improved performance of the TMDI over the classical TMD is reported in the rightmost column of Table 4.2 for several selected cases.

Table 4.2. Optimal TMDI parameters, Performance Index (PI) and percentage difference of PI achieved for different values of the attached TMDI mass and the inerter constant b compared to the classical TMD ($b=0$).

m_{TMDI} (kg)	b (kg)	v_{TMDI}	ζ_{TMDI}	PI	Percentage difference of PI compared to the classical TMD (%)
450 (1%)	0	0.97	0.105	0.369	-
	2000	2.31	0.307	0.317	14.1
	4000	3.16	0.582	0.270	27.0
	6000	3.84	0.852	0.235	36.5
900 (2%)	0	0.94	0.146	0.290	-
	2000	1.73	0.280	0.272	6.1
	4000	2.28	0.454	0.243	16.3
	6000	2.73	0.671	0.220	24.4
1350 (4%)	0	0.92	0.175	0.250	-
	2000	1.48	0.310	0.246	1.4
	4000	1.89	0.452	0.226	9.5
	6000	2.24	0.615	0.208	16.8
1800 (6%)	0	0.89	0.200	0.225	-
	2000	1.32	0.301	0.224	0.6
	4000	1.66	0.455	0.213	5.4
	6000	1.94	0.594	0.198	11.8

The performance improvement is considerably higher for relatively small TMD mass values (less than about 3% of the total mass of the primary system) while it becomes less significant for attached TMDI mass values greater than 6% of the total mass of the mechanical primary system. Note that similar trends were found in the case of the undamped SDOF primary structure for which optimal TMDI parameters have been derived in closed form Figure 3.11. Therefore, it can be concluded that the effectiveness of an inerter device to suppress the displacement response variance beyond what can be achieved by the classical TMD increases for relatively small attached oscillating masses. It is also noted that the enhanced performance of the TMDI system requires that the TMD

mass is attached to the primary structure by “stiffer” connection arrangements and by considering viscous damping devices with higher damping coefficients.

More importantly, the herein furnished data demonstrate that the “mass amplifying” effect of the inerter device can be effectively used to replace part of the oscillating TMD mass and, thus, to reduce the total weight of the structural system for the same level of performance in terms of keeping the oscillatory motion of the primary system below a certain threshold. For example, as shown in Table 4.2, in the case of the considered 3-DOF chain-like cascaded mechanical system, an optimally tuned TMDI with an inerter device of “mass” constant $b=6000$ kg and an attached mass of 450kg achieves similar level of performance (more than 75% reduction to the displacement variance of the m_1 mass compared to the uncontrolled primary structure) as an optimally tuned classical TMD with four times heavier oscillating mass (1800kg). However, the physical mass of the considered inerter might be up to two orders of magnitude smaller than its b constant. Specifically, ratios of constant b over physical mass for inerters of up to 200/1 or more have been reported in the literature (Papageorgiou & Smith, 2005). Adopting this ratio, the considered inerter has a physical mass of $6000/200= 30$ kg. Therefore, the total weight of the examined TMDI system remains about four times lighter than a classical TMD for similar vibration control performance assuming that the weight of the equipment used to attach the TMD mass to the primary structure and of the viscous damping devices are similar in both cases. The latter consideration may have significant advantages in certain real-life structural passive vibration control design scenarios necessitating the use of large TMD masses to achieve the desired vibration suppression effect, as is the case of building structures excited by severe earthquake induced strong ground motions (see e.g. Hoang et al, 2008; Moutinho, 2012 and references therein).

Comprehensive numerical results are furnished along these lines in the next chapter focusing on the design and assessment of TMDI for seismic protection of multi-storey building structures.

CHAPTER 5 : DESIGN AND ASSESMENT OF THE TUNED-MASS-DAMPER-INERTER FOR SEISMIC PROTECTION OF MULTI-STOREY BUILDINGS

5.1 PRELIMINARY REMARKS

Civil engineering structures at seismically prone areas are exposed to earthquake induced ground motions of different severity levels during the structures' life service. At high levels of seismic severity, the inertial dynamic loads exerted to structures may induce permanent damage and, in extreme cases, total structural failure/collapse. Admittedly, current conventional codes of practice for earthquake resistance design are based on concepts of inelastic energy absorption through controlled localized damage, allowing ordinary structures to yield under a specified "design" seismic excitation level for the purpose of reducing initial excessive construction expenditures. Regardless of this acceptable design risk criterion, recent major seismic events incurred extensive structural damage in urban areas (e.g. Kobe- Japan 1995 and Christchurch-New Zealand 2011) where the associated cost of structural retrofit and downtime has been significant. In this respect, the incorporation of various equipment such as base isolators (Naeim & Kelly, 1999), energy dissipation devices (e.g. viscous dampers, friction dampers, etc.), and Tuned-Mass Dampers (TMD) (Chang, 1999; Spencer, 2002; Martelli & Forni, 2011) has been proposed by various researchers and has been applied in practice for the passive vibration control of civil engineering structures exposed to earthquake induced ground motions to achieve "minimal damage" structures (Karavasilis et al. 2011). Such passive vibration control devices/equipment are designed to maintain the seismic response of structures bellow certain acceptable thresholds.

Initially proposed for naval and mechanical engineering application (Ormondroyd & Den Hartog, 1928; Frahm, 1911; Den Hartog, 1956; Brock, 1956), the TMD is commonly used in present day in the field of civil engineering as a mean to mitigate wind and traffic-induced vibration, where the weight of the TMD mass commonly ranges between 1% to 10% of the total weight of the building (e.g. Chung et al, 2013; Shi & Cai, 2008). However, this passive control solution is not commonly considered for the mitigation of earthquake-induced vibrations. Instead, more involved TMD-based solutions are used such as multiple TMDs, non-linear TMDs and large mass TMDs as reviewed in Section 2.1. This is mainly due to the facts listed below:

- Dependence on the property of the primary system. Classical TMDs are effective only for a narrow band of exciting frequency, which creates difficulties in designing effective and robust TMDs, whose parameters commonly depend on structural and earthquake characteristics, both with inherent uncertainties.

- Impulsive nature of earthquake loads. Typically seismic events have large energy dissipated within a short period of time. In this case, the TMD absorbing capabilities are impaired due to the long period of time it takes to accommodate appropriate displacements with significant out-of-phase motion.

- Much larger TMD mass displacements. Since earthquake-induced vibrations impose higher displacement demands compared to with wind-induced ones, there is also a concern of practical importance whether the displacement amplitude of the additional mass, referred to as TMD stroke, can be physically accommodated within the limitations of the construction.

To this end, in this chapter the novel TMDI passive vibration control solution proposed in Chapter 4 is herein applied for the seismic protection of building structures to demonstrate its effectiveness and to explore its efficiency and usefulness in addressing

several practical disadvantages of the classical TMD, while maintaining its advantages. To this aim, seismically excited n -storey frame buildings modelled as linear proportionally damped multi-degree-of-freedom (MDOF) systems with the inertial/mass properties lumped at the floor slabs are considered. The tuned mass-damper-inerter (TMDI) is incorporated in the considered MDOF primary structure in between the top floor mass and the second to the top floor mass as shown in Figure 5.1.

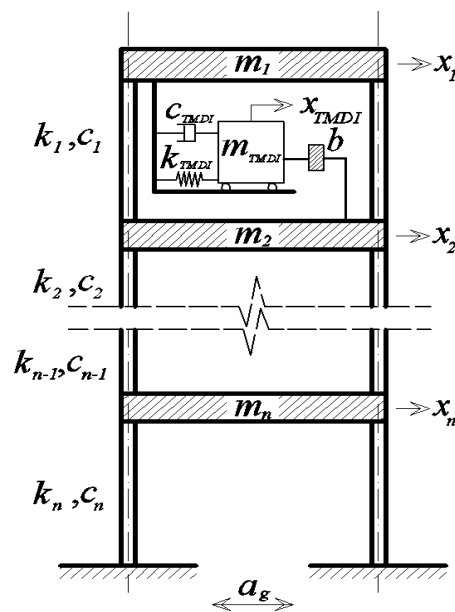


Figure 5.1. Tuned mass-damper-inerter (TMDI) equipped n -storey frame building.

As mentioned, one of the drawbacks when considering classical TMDs is the lack of robustness towards uncertainties in the properties of the primary structure which critically influence its design and control efficiency (Soto-Brito & Ruiz, 1999; Pinkaew et al, 2003). Specifically, the optimum TMD parameters are fundamentally given as dependent on the natural frequency and the mass of the primary structure (see Equation (3-4)). In this respect, alongside, a TMDI parametric efficiency study is undertaken to emphasize on the influence of the properties of the primary structures in terms of mass

and stiffness distribution along its height to the optimum design of the TMDI passive control solutions. For this purpose, several building structures have been chosen such that they vary from a uniform in elevation structure to structures with reduced top floor stiffness and structures with reduced top floor mass. For the purpose of this work, an input non-stationary stochastic process compatible with the elastic design spectrum of the European aseismic code provisions (EC8) has been assumed. The effectiveness of the proposed TMDI configuration over the classical TMD is assessed by performing response history analyses for an ensemble of EC8 spectrum compatible field recorded strong ground motions. Furthermore, the study will extend on the impact of TMDI control capabilities of higher modes.

5.2 EUROCODE 8 COMPATIBLE OPTIMUM TUNED-MASS-DAMPER-INERTER DESIGN OF BUILDING STRUCTURES

In this section optimum design parameters are derived following the procedure reviewed in Section 4.3 for the TMDI passive vibration control solution of Figure 5.1. In order to assess the influence of the stiffness and mass distribution along the height of the primary structure, three-storey buildings are considered having different inertial and elastic properties as shown in Table 5.1. Specifically, a uniform in elevation structure (Structure **I**) to structures with reduced top floor stiffness (Structures **IIa** and **IIb**) and structures with reduced top floor mass (Structures **IIIa** and **IIIb**) are considered. The characteristics of these structures are similar to those considered as test/benchmark primary structures used in the literature to study the performance and design of TMDs for earthquake engineering applications (e.g. Sadek et al, 1997, Rana & Soong, 1998; Salvi & Rizzi, 2011). Table 5.2 reports the undamped natural frequencies of the considered primary structures obtained from standard modal analysis. Further, the damping matrix of the (uncontrolled) primary structure $[C_p]$ is assumed to be proportional to the stiffness matrix of the primary structure $[K_p]$ following the expression:

$$[C_p] = \frac{2\xi_1}{\omega_1} [K_p], \quad (5-1)$$

where ω_1 is the fundamental undamped natural frequency of the primary structure and ξ_1 is the critical damping ratio of the fundamental mode shape taken equal to 0.02. In the last equation $[K_p]$ is obtained from the stiffness matrix $[K]$ of Equation (4-5) by elimination of the first row and column and by setting k_{TMDI} equal to zero.

Table 5.1. Inertial and elastic properties of the considered primary structure

Structure	Story	Mass (kg)	Stiffness (N/m)
CONSTANT PROPERTIES			
3DOF (I)	1 (top)	30 x 10 ³	30 x 10 ⁶
	2	30 x 10 ³	30 x 10 ⁶
	3	30 x 10 ³	30 x 10 ⁶
REDUCED TOP FLOOR STIFFNES			
3DOF (IIa)	1 (top)	30 x 10 ³	25 x 10 ⁶
	2	30 x 10 ³	30 x 10 ⁶
	3	30 x 10 ³	30 x 10 ⁶
3DOF (IIb)	1 (top)	30 x 10 ³	20 x 10 ⁶
	2	30 x 10 ³	30 x 10 ⁶
	3	30 x 10 ³	30 x 10 ⁶
INCREASED TOP FLOOR MASS			
3DOF (IIIa)	1 (top)	35 x 10 ³	30 x 10 ⁶
	2	30 x 10 ³	30 x 10 ⁶
	3	30 x 10 ³	30 x 10 ⁶
3DOF (IIIb)	1 (top)	40 x 10 ³	30 x 10 ⁶
	2	30 x 10 ³	30 x 10 ⁶
	3	30 x 10 ³	30 x 10 ⁶

Table 5.2. Undamped natural frequencies of the considered primary structure.

Structure	Mode	Period (s)	Frequency (rad/s)
CONSTANT PROPERTIES			
3DOF (I)	1 st	0.44	14.07
	2 nd	0.16	39.43
	3 rd	0.11	56.98
REDUCED TOP FLOOR STIFFNES			
3DOF (IIa)	1 st	0.45	13.92
	2 nd	0.17	37.40
	3 rd	0.11	55.45
3DOF (IIb)	1 st	0.46	13.69
	2 nd	0.18	34.82
	3 rd	0.02	54.16
INCREASED TOP FLOOR MASS			
3DOF (IIIa)	1 st	0.47	13.47
	2 nd	0.16	38.42
	3 rd	0.11	56.56
3DOF (IIIb)	1 st	0.49	12.93
	2 nd	0.17	37.62
	3 rd	0.11	56.27

The input seismic action is represented by the non-stationary power spectrum $S(\omega, t)$ plotted in Figure 5.2 which is compatible in the “mean sense” with the elastic spectrum of the current European aseismic code provisions (EC8) for peak ground acceleration 0.36g ($g=981\text{cm/s}^2$) and ground type “B” (CEN 2004). The considered power spectrum is derived by a methodology described in detail in (Giaralis & Spanos, 2010).

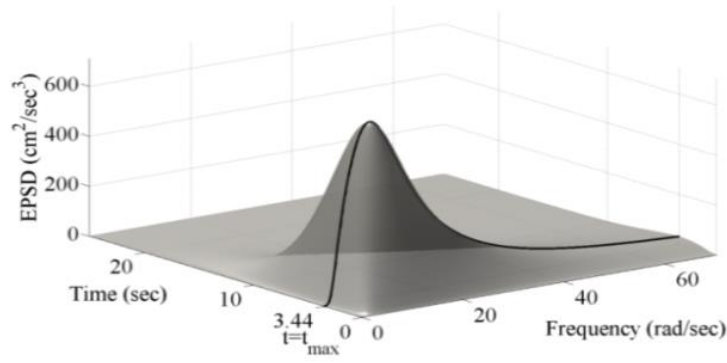


Figure 5.2. Considered EC8 compatible evolutionary power spectrum $S(\omega, t)$ for design purposes

The adopted design evolutionary power spectrum (EPS) $S(\omega, t)$ is expressed in a parametric form and, in particular, it involves a deterministic time varying envelop function proposed by (Bogdanoff et al., 1961) modulating a stationary power spectrum expressed by the Clough-Penzien (C-P) spectral form (Clough & Penzien, 1993):

$$S(\omega, t) = \left| C t \exp\left(\frac{-bt}{2}\right) \right|^2 \frac{1 + 4\zeta_g^2 \left(\frac{\omega}{\omega_g}\right)^2}{\left(1 - \left(\frac{\omega}{\omega_g}\right)^2\right)^2 + 4\zeta_g^2 \left(\frac{\omega}{\omega_g}\right)^2} \frac{\left(\frac{\omega}{\omega_f}\right)^4}{\left(1 - \left(\frac{\omega}{\omega_f}\right)^2\right)^2 + 4\zeta_g^2 \left(\frac{\omega}{\omega_f}\right)^2} \quad (5-2)$$

where parameters C and b are defining characteristics of the ground acceleration's intensity and of the envelop function's width respectively. The parameters ω_f and ζ_f of the (C-P) spectrum determine the characteristics of the high-pass filter which suppresses the low frequency allowed by $Y_{KT}(\omega)$ – the Kanai-Tajimi (K-T) spectrum (Kanai, 1957). Also, in Equation (5-2), the defining parameters ω_g and ζ_g allow for a clear physical interpretation for the influence of the site conditions on the seismic input frequency content, accounting for the 'frequency' and the 'damping' characteristics of the ground respectively.

Considering the above, for the herein considered base excitation the numerator in (4-23) becomes:

$$J^{TMDI} = \int_0^{\infty} |G_1(\omega)|^2 \max_t \{S(\omega, t)\} d\omega \quad (5-3)$$

It is defined in (5-3) t_{max} as the instant in time at which the proposed non-stationary power spectrum is maximized.

As a final note, Table 5.3 reports the parameters defining C-P EPS compatible with the EC8 spectrum for PGA= 0.36g, damping ratio 5%, soil conditions “B” (Giaralis & Spanos, 2012).

Table 5.3. Parameters for the definition of C-P evolutionary power spectrum compatible with EC8 spectra

C (cm/sec ^{2.5})	b (1/sec)	ζ_g	ω_g (rad/sec)	ζ_f	ω_f (rad/sec)
17.76	0.58	0.78	10.73	0.90	2.33

In what follows, the optimization procedure previously described in Chapter 4 is applied to derive optimum design parameters v_{TMDI} and ζ_{TMDI} for the considered primary structures, at the time the input power spectrum of Figure 5.2 is maximized and for various values of μ_M and b .

5.2.1 OPTIMUM TUNED MASS-DAMPER-INERTER DESIGN PARAMETERS

The normalized by the top floor value of the first mode shape vector and the corresponding generalised masses for the considered three DOF primary structures are summarised below in Table 5.4. The optimization procedure described in Section 4.3 is used to derive optimum TMDI parameters for both $b=0$ and $b>0$ while considering a same range of pre-specified additional m_{TMDI} mass values commonly used.

Table 5.4. The normalized by the top floor value of the first mode shape vector and the corresponding generalised masses

Structure	Normalized by the top floor value of the first mode shape vector	Generalized Mass (Kg)
3DOF (I)	$\{\Phi_{1_I}\}=\{1 \ 0.802 \ 0.445\}^T$	55235
3DOF (IIa)	$\{\Phi_{1_{IIa}}\}=\{1 \ 0.815 \ 0.412\}$	55019
3DOF (IIb)	$\{\Phi_{1_{IIb}}\}=\{1 \ 0.832 \ 0.370\}$	54872
3DOF (IIIa)	$\{\Phi_{1_{IIIa}}\}=\{1 \ 0.788 \ 0.434\}^T$	59278
3DOF (IIIb)	$\{\Phi_{1_{IIIb}}\}=\{1 \ 0.777 \ 0.424\}^T$	63501

Given the primary frame structures studied, the trends of the derived optimum parameters which minimise the cost function of Equation (4-22) (frequency ratio ν_{TMDI} and damping ratio ζ_{TMDI}) are given in Figure 5.3, Figure 5.4 and Figure 5.5. These parameters are plotted as functions of the additional mass m_{TMDI} , for the particular case of $b=0$ (TMD) which are superposed to the optimum parameters obtained for several a-priori specified b values (TMDI) (thin dashed line for TMD; marked lines for TMDI) for the sake of comparison. Figure 5.6, Figure 5.7 and Figure 5.8 plot the optimum parameters in terms of stiffness k_{TMDI} and damping value c_{TMDI} .

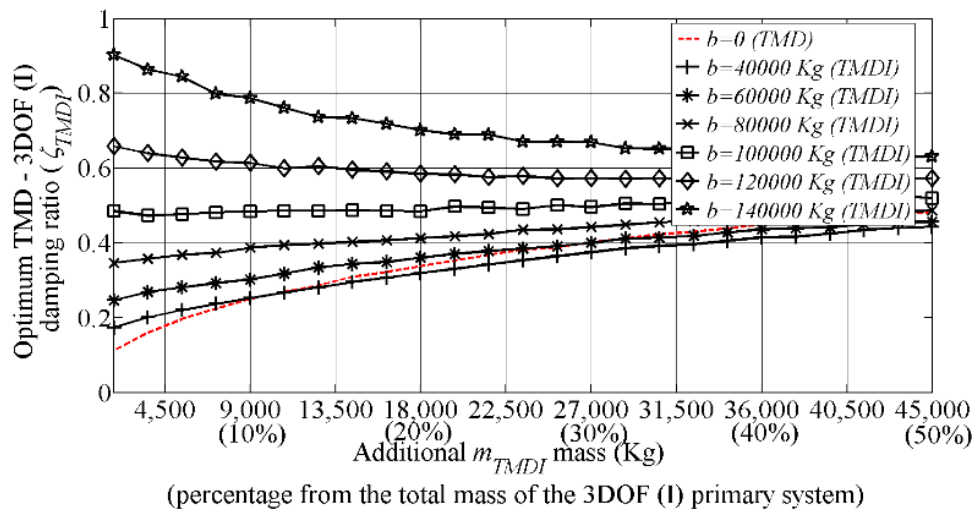
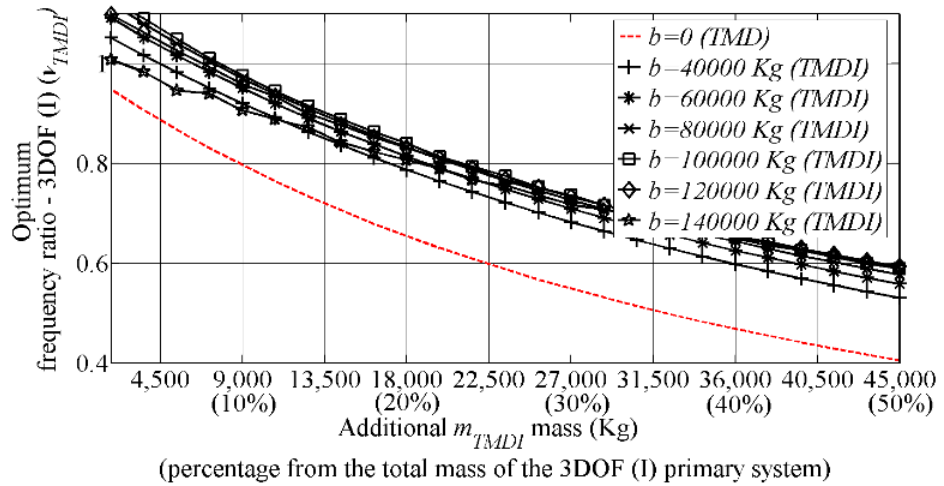
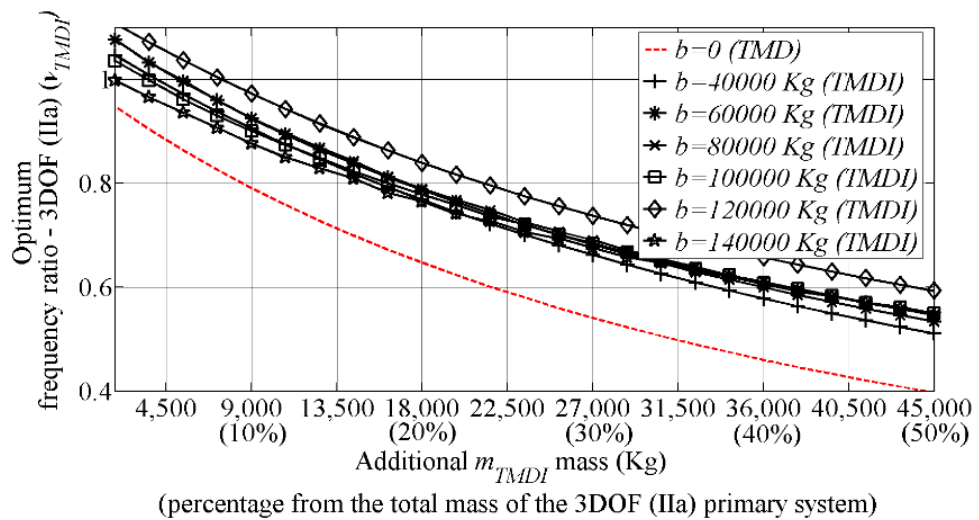


Figure 5.3. Three DOF primary structure (I). Optimum TMDI parameters. Frequency ratio (a) and TMDI damping ratio (b), versus the additional m_{TMDI} mass for various values of b .



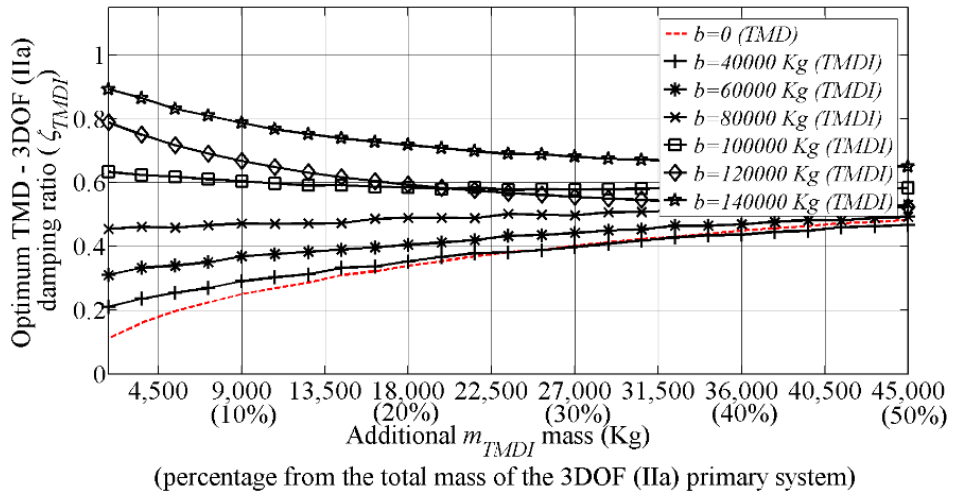


Figure 5.4. Three DOF primary structure (IIa). Optimum TMDI parameters. Frequency ratio (a) and TMDI damping ratio (b), versus the additional m_{TMDI} mass for various values of b .

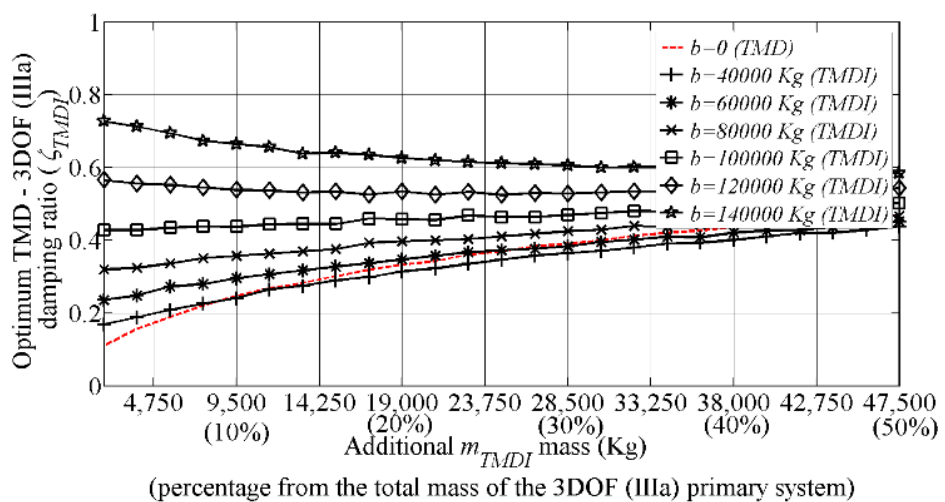
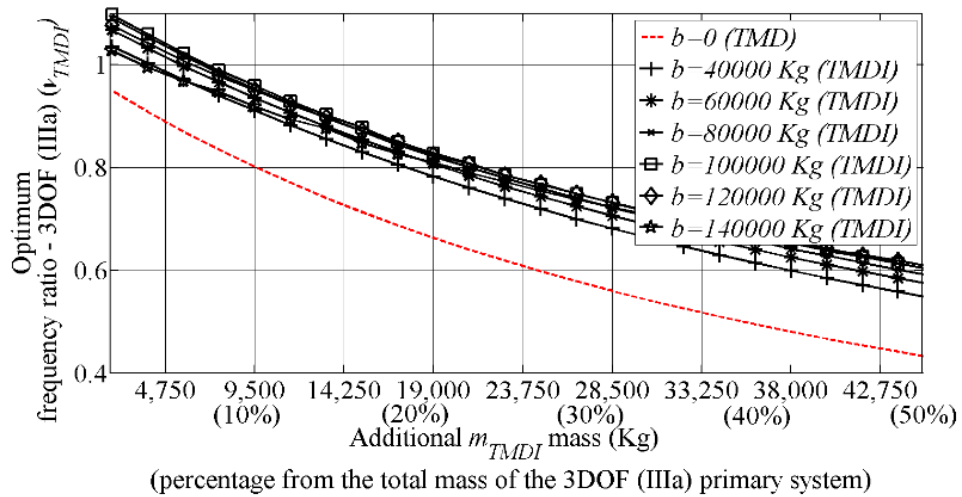


Figure 5.5. Three DOF primary structure (IIIa). Optimum TMDI parameters. Frequency ratio (a) and TMDI damping ratio (b), versus the additional m_{TMDI} mass for various values of b .

For the particular case of classical TMD ($b=0$), the numerical data presented are in alignment with similar results reported in the literature obtained by alternative numerical optimization techniques (see e.g. Rana & Soong, 1998; Salvi & Rizzi, 2011; Brown & Singh, 2010 and references therein). Specifically, increased values of the assumed attached m_{TMDI} mass necessitate higher ζ_{TMDI} values and lower frequency ratios to achieve optimal tuning.

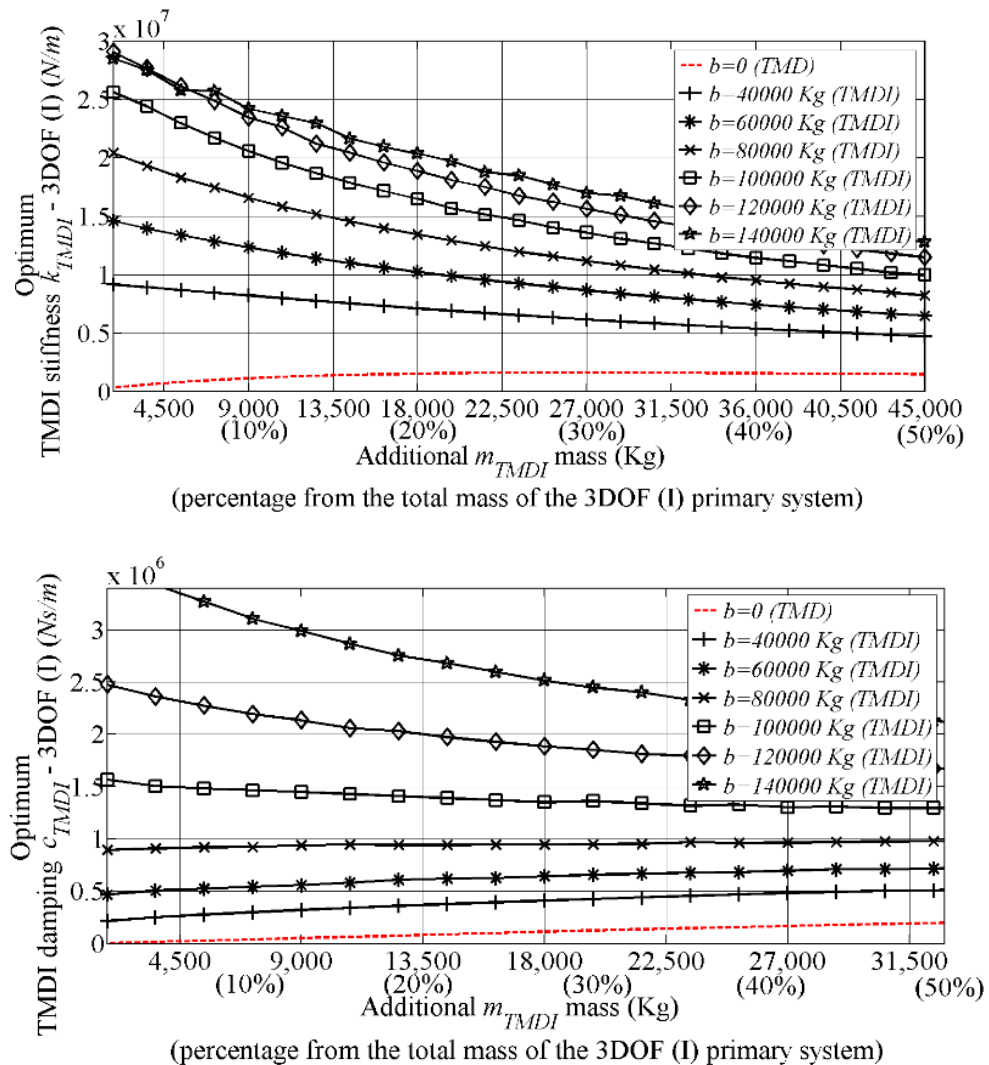


Figure 5.6. Three DOF primary structure (I). Optimum TMDI parameters. TMDI stiffness value (a) and TMDI damping value (b), versus the additional m_{TMDI} mass for various values of b .

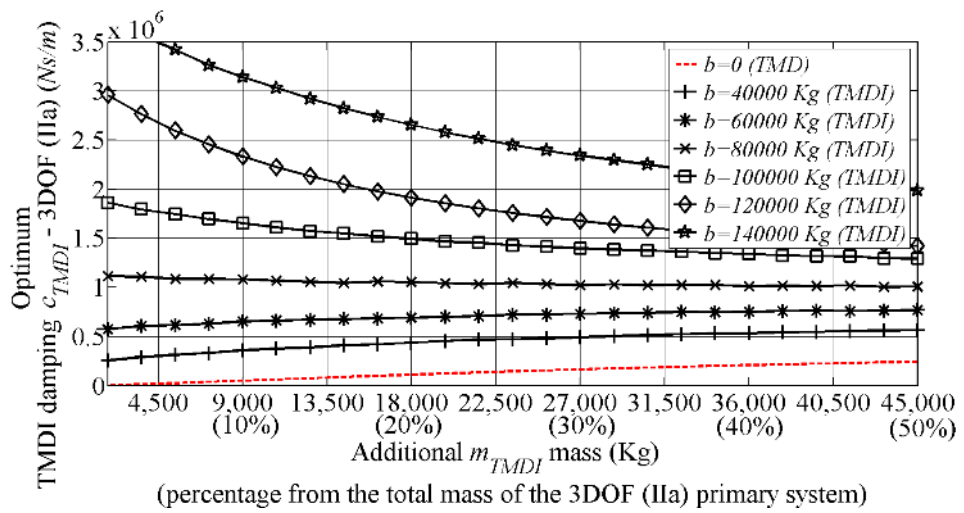
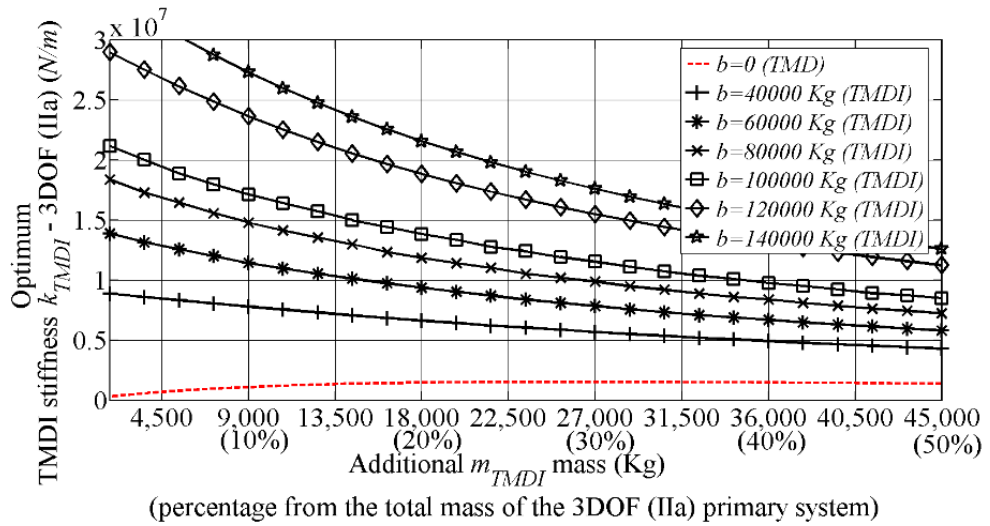


Figure 5.7. Three DOF primary structure (IIa). Optimum TMDI parameters. TMDI stiffness value (a) and TMDI damping value (b), versus the additional m_{TMDI} mass for various values of b .

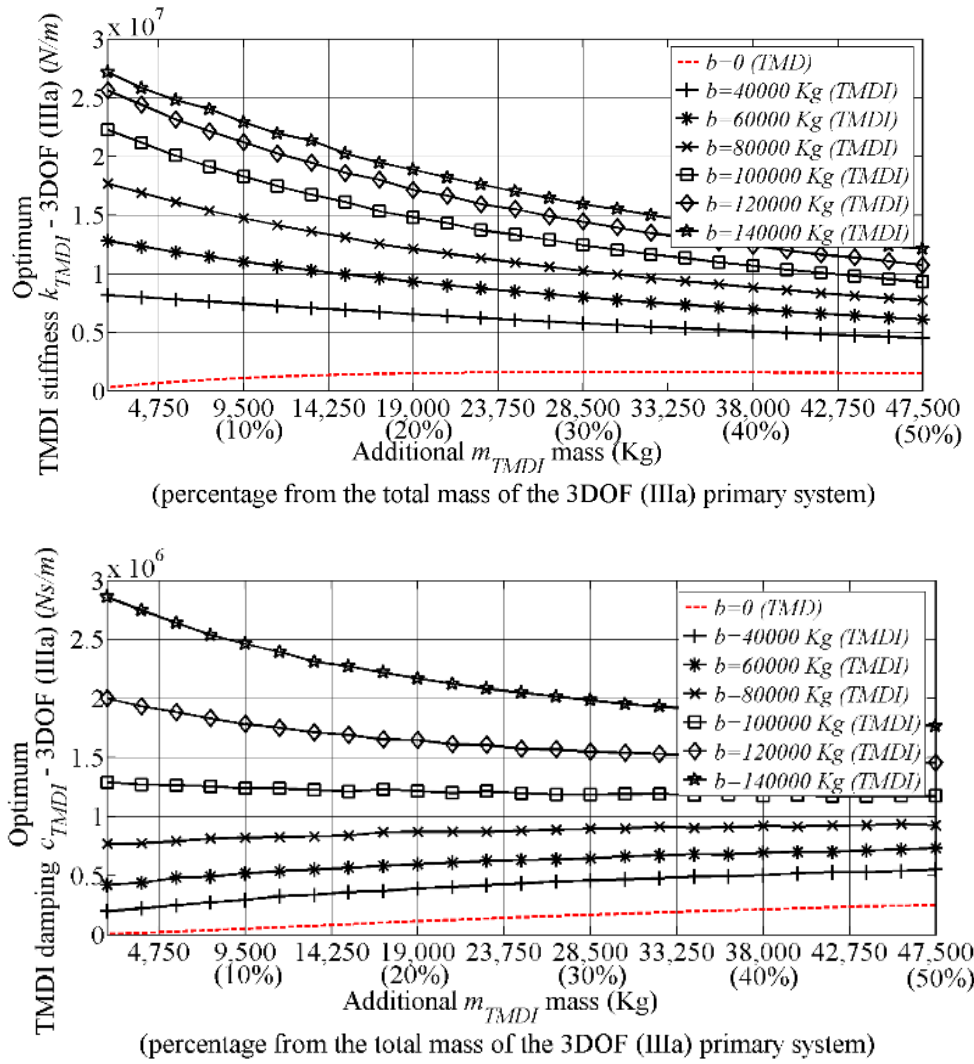


Figure 5.8. Three DOF primary structure (IIIa). Optimum TMDI parameters. TMDI stiffness value (a) and TMDI damping value (b), versus the additional m_{TMDI} mass for various values of b .

When the inerter is incorporated in the proposed TMDI configuration (for $b > 0$), numerical data evidence that optimum design requires higher k_{TMDI} and damping c_{TMDI} values for the elements connecting the attached mass to the primary structure compared with classical TMD. Furthermore, these values also increase as the b value increases, similar to the case of TMDI equipped SDOF.

It is also noted that as the mass of the top floor is increased (primary structures IIIa and IIIb), a reduction in the optimum frequency and damping values are observed for the same constant b and attached mass m_{TMDI} value. Furthermore, reducing the stiffness of the top floor (primary structures IIa and IIb), will require the use of higher damping

forces introduced by the dashpot c_{TMDI} and lower stiffness values in order to achieve optimum control. This can be clearly seen in Figure 5.9 and Figure 5.10 which plot the optimum TMDI stiffness and damping values respectively versus the additional m_{TMDI} mass for all primary structures considered.

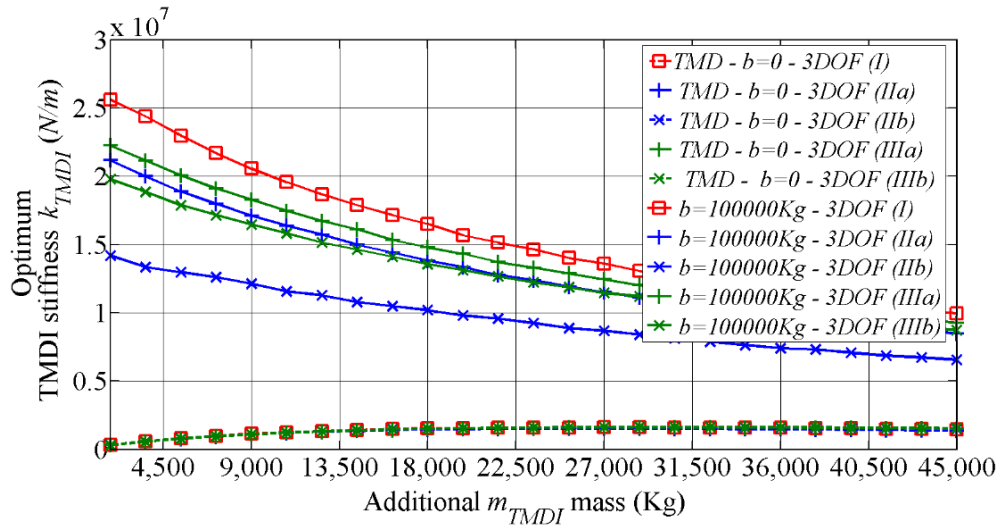


Figure 5.9. Optimum TMDI parameters. Comparison of TMDI stiffness value versus the additional m_{TMDI} mass for all primary structures considered.

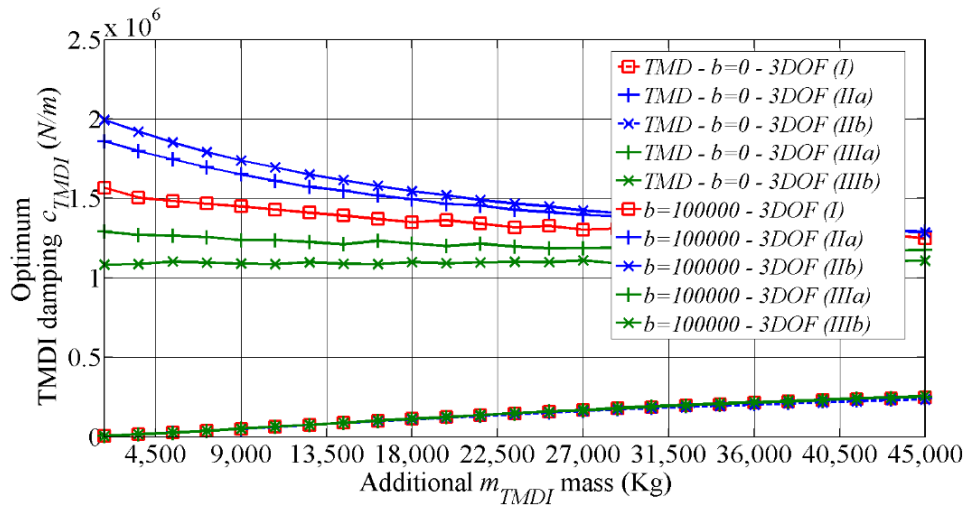


Figure 5.10. Optimum TMDI parameters. Comparison of TMDI damping value versus the additional m_{TMDI} mass for all primary structures considered

It can also be observed in the last figures that, for classical TMDs, the changes occurring in the properties of the primary system have a much smaller impact on the range of required parameters for optimum design, compared with the TMDI. This suggests that the TMDI is more robust compared with classical TMD to deviations in the optimum parameters.

5.2.2 TOP FLOOR DISPLACEMENT VARIANCE OF OPTIMALLY DESIGNED TUNED-MASS-DAMPER-INERTER ($b > 0$) VERSUS TUNED-MASS-DAMPER ($b = 0$) FOR EUROCODE 8 COMPATIBLE STOCHASTIC EXCITATION.

Given the optimum design parameters derived in the previous sub-section, numerical results obtained from the adopted optimization procedure are plotted, in terms of the PI of Equation (4-22) and for the given input non-stationary power spectrum for all 3DOF primary structures herein considered.

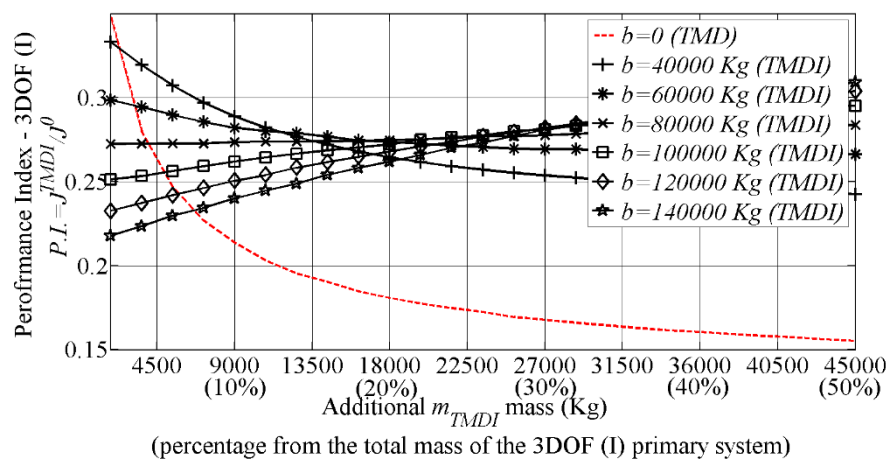


Figure 5.11. Three DOF primary structure - 3DOF (I). Performance index versus the additional m_{TMDI} mass for various values of b .

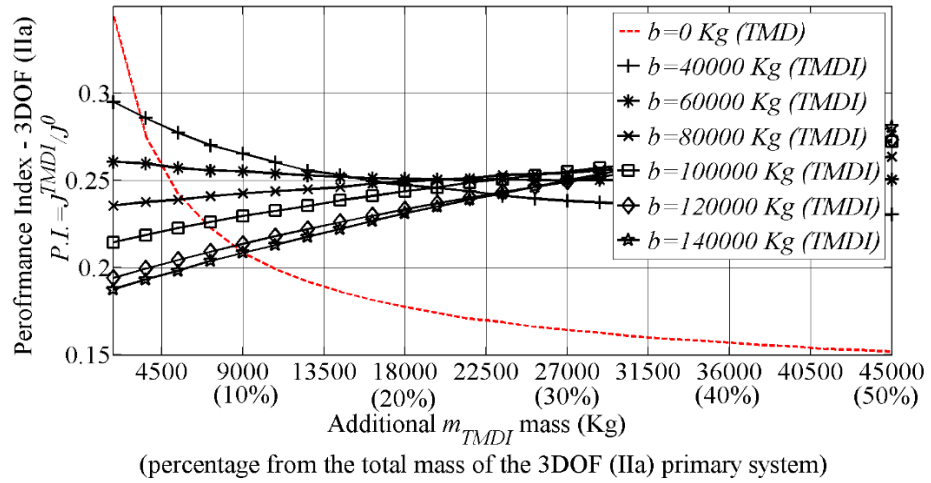


Figure 5.12. Three DOF primary structure - 3DOF (IIa). Performance index versus the additional m_{TMDI} mass for various values of b .

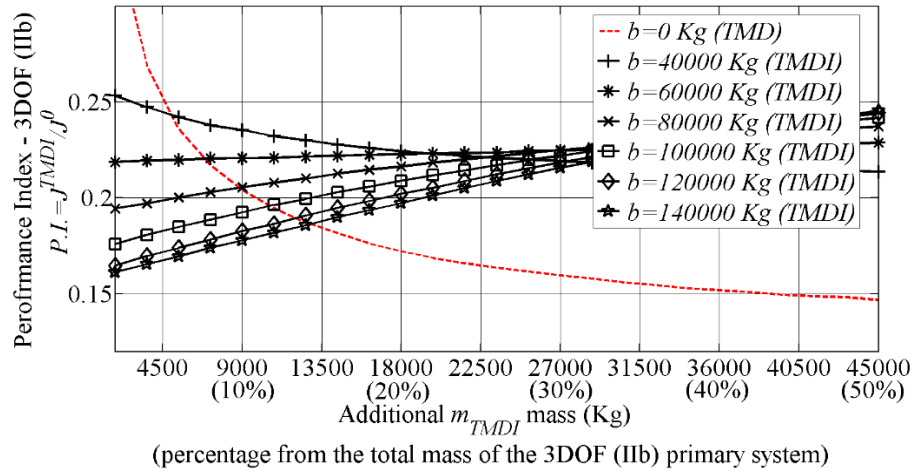


Figure 5.13. Three DOF primary structure - 3DOF (IIb). Performance index versus the additional m_{TMDI} mass for various values of b .

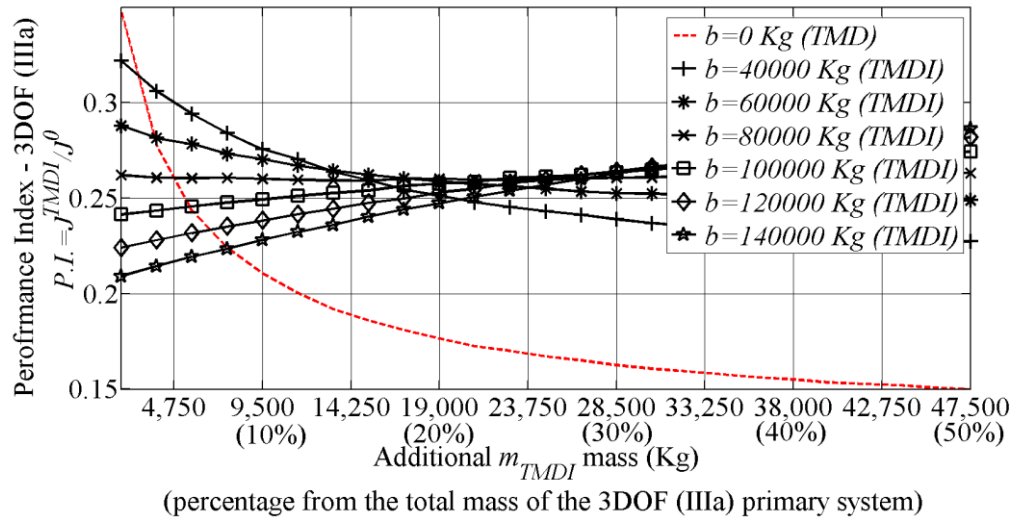


Figure 5.14. Three DOF primary structure - 3DOF (IIIa). Performance index versus the additional m_{TMDI} mass for various values of b .

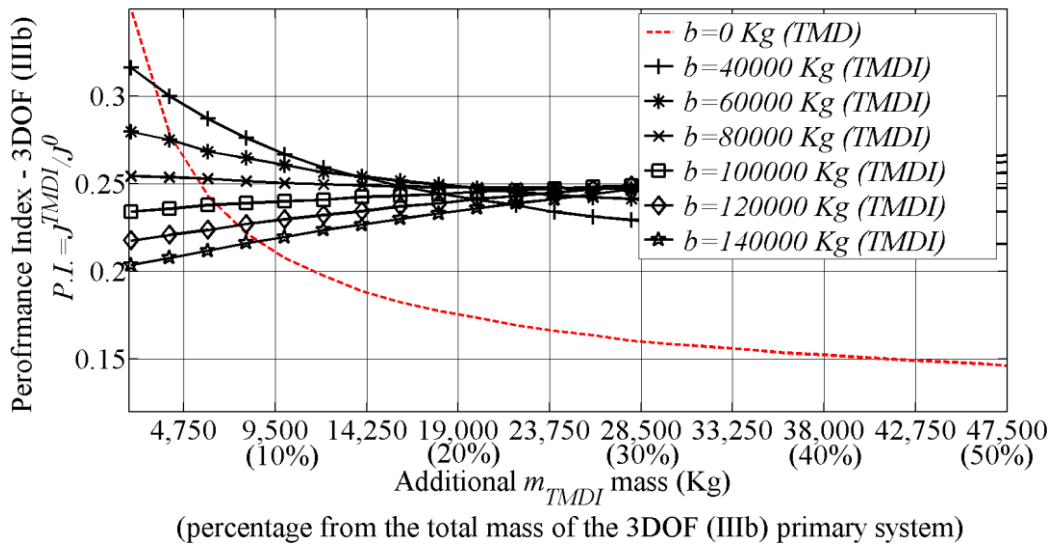


Figure 5.15. Three DOF primary structure - 3DOF (IIIb). Performance index versus the additional m_{TMDI} mass for various values of b .

For the case of classical TMD (thin dashed line), it is obvious that larger values for the attached mass are more effective in controlling the dynamic response of the primary structure of interest related to its fundamental (and dominant) mode shape. However, the rate of decrease of the PI decreases rapidly (PI “saturates”) as the TMD mass increases.

It reaches an almost flat plateau for m_{TMD} values larger than 25% the total mass of the considered primary structure.

For b values greater than zero, it can be readily deduced from the reported numerical data that the proposed TMDI configuration reduces the value of the Performance Index as the value of b increases or equivalently, the variance of the relative displacement of the top floor mass is reduced as the value of the inerter b increases, for TMD mass values less than about 10% of the total mass of the primary structure). However, it is noted that this enhanced performance comes at the cost of higher damping and stiffness values for the elements connecting the TMD mass to the primary structure. The same data are provided in tabular form, as well (Table 5.5).

Importantly, as the stiffness of the top floor is reduced (structures 3DOF IIa and IIb), and similarly, as the mass of the top floor is increased (structures 3DOF IIIa and IIIb), better performance of the TMDI is observed.

Table 5.5. TMDI parameters and Performance Index for different values of the additional m_{TMDI} mass and of the inerter constant b .

	m_2 (kg) [% total mass]	b (kg)	v_{TMDI}	k_{TMDI} (10^6 N/m)	ζ_{TMDI}	c_{TMDI} (10^5 Ns/m)	PI	Percentage difference of PI compared to the classical TMD (%)
3DOF (I)	5400 [6%]	0(w/o TTF)	0.8671	0.803	0.1961	0.2583	0.2472	-
		80000	1.040	18.29	0.3679	9.196	0.2728	-10%
		100000	1.049	22.97	0.4768	14.84	0.2564	-4%
		120000	1.026	26.11	0.6284	22.74	0.2419	2%
		140000	0.946	25.76	0.8445	32.69	0.2298	7%
3DOF (IIa)	5400 [6%]	0(w/o TTF)	0.8633	0.779	0.1961	0.2570	0.2425	-
		80000	0.9971	16.45	0.4583	10.87	0.2391	1%
		100000	0.9615	18.88	0.6187	17.45	0.2228	8%
		120000	1.037	26.12	0.7171	25.96	0.2044	16%
		140000	0.7436	15.58	0.937	34.21	0.1982	18%
3DOF (IIIa)	5700 [6%]	0(w/o TTF)	0.8695	0.782	0.1883	0.2514	0.2436	-

	80000	1.018	16.11	0.3367	7.91	0.2605	-7%
	100000	1.022	20.05	0.4346	12.65	0.2457	-1%
	120000	1.008	23.15	0.5522	18.84	0.2318	5%
	140000	0.9684	24.79	0.6943	26.39	0.2192	10%

The most significant PI reduction is observed for the structure with reduced top floor stiffness (IIa) while the structure with regular distribution in elevation of mass and stiffness achieves the smallest improvement for the same b values. These results, as expected, emphasise on the importance of stiffness and mass distribution for exploiting the maximum control capabilities of passive systems, including the herein considered TMDI. Actually, it can be observed from Figure 5.11 as well as Table 5.5 that for the 3DOF structure with uniform mass and stiffness distribution (3DOF -I), when considering an oscillating added mass of 6% from the total mass of the primary system, the TMDI does not outperform the traditional TMD solution for lower b values.

Similar to the above, referring to the unit value as the threshold where the performance of a TMDI is equal to that of a classical TMD, both optimally designed, Figure 5.16 plots the Performance Index ratio J^{TMDI} / J^{TMD} for an m_{TMDI} mass equal to 10% from the total mass of the primary system and for increasing values of b , when considering all five structures studied. It can be seen that, in order to achieve a better TMDI response compared to classical TMD (values on the vertical axis below unity) a certain interval of b values needs to be considered. For b values above or below this interval, the TMDI will become less effective than the TMD for the same attached m_{TMDI} mass. More so, when considering the structure 3DOF-I, with regular mass and stiffness conformation, for an m_{TMDI} mass equal to 10% there is no such b value for which the TMDI will outperform the TMD configuration.

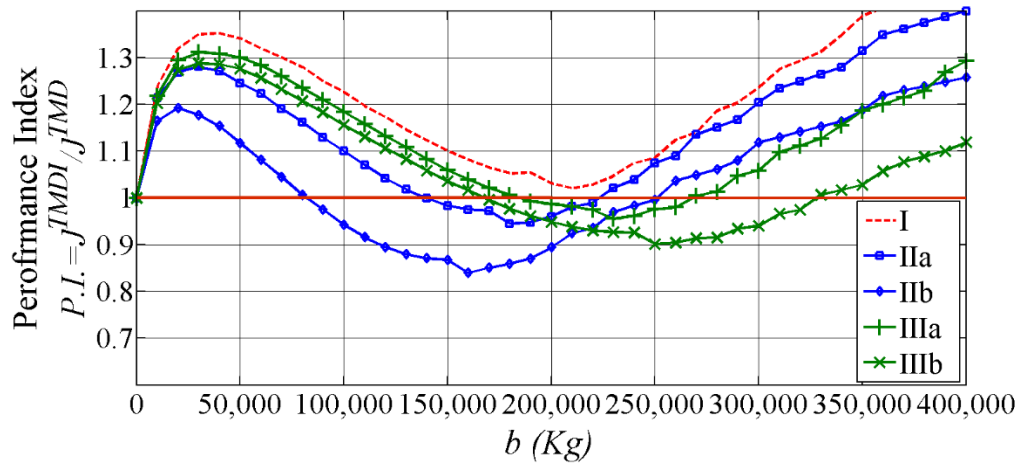


Figure 5.16. Performance index ratio between an optimum designed TMD and an optimum designed TMDI for an m_{TMDI} mass of 10% from the total mass of the primary structure and for various values of b .

It is also observed from Figure 5.16 that, as the primary structure stiffness and mass shifts away from a uniform distribution in elevation, the TMDI becomes more effective in comparison with the classical TMD for the same m_{TMDI} mass. Specifically, as the flexibility of the top floor is reduced, the b interval of TMDI effectiveness versus TMD enlarges and the performance index ratio reduces. It is noted that better results can be obtained by considering primary structures with a flexible top floor storey.

In addition, referring to Figures 5.11 to 5.15, the ‘flat’ characteristic of the TMDI $P.I.$ curves, even for small oscillating additional masses, suggests an improved robustness over the classical TMD. This is better exemplified in Figure 5.17 which plots the same $P.I.$ curves when considering an off-tuning effect for both TMD and TMDI control solution. Specifically, a variation in estimating the characteristics of the primary structures is assumed by considering frequency ratio values above and below the optimum. The figure shows that, the performance of the classical TMD ($b=0$) is drastically reduced, especially when considering small additional oscillating masses. For example, when considering an oscillating mass of 6% the total mass of the primary

system, a 20% positive detuning effect implies a reduction of about 25% in the control capabilities of the classical TMD. However, changes in the optimum control frequency have a much less significant impact on the TMDI performance, which varies with less than 10% in all cases considered.

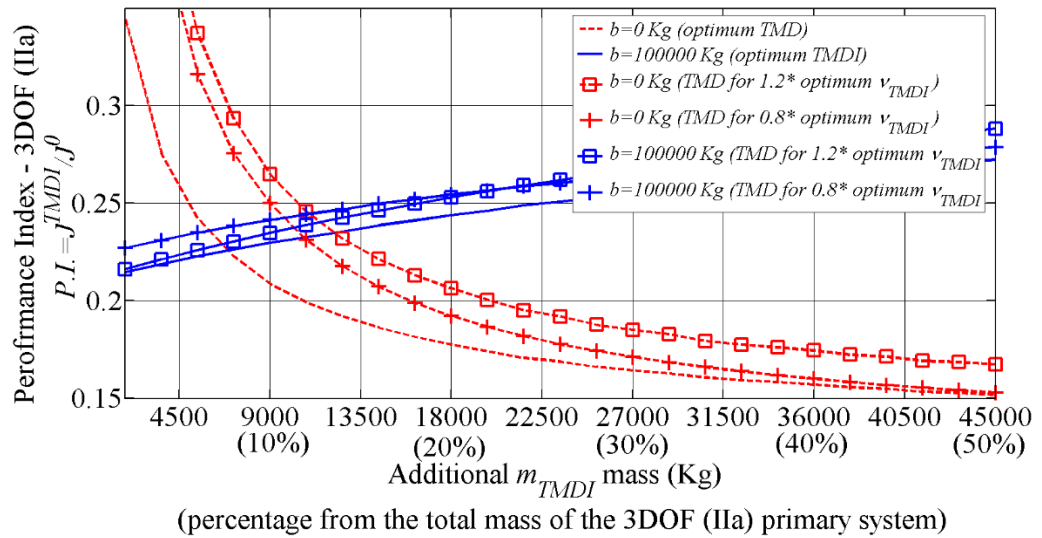


Figure 5.17. Three DOF primary structure - 3DOF (IIa). Performance index versus the additional m_{TMDI} mass for various values of b . Robustness assessment of optimal TMDI on structures with uncertainty in natural frequency.

This clearly suggests an improved robustness of the TMDI towards estimating the properties of the primary structure over classical TMDs.

To shed more light on the TMDI-TMD performance comparisons, Figure 5.18 plots the transfer function between the input ground acceleration and the output top floor displacement for the uncontrolled (primary) structure 3DOF IIa, for an optimal TMD and an optimal TMDI.

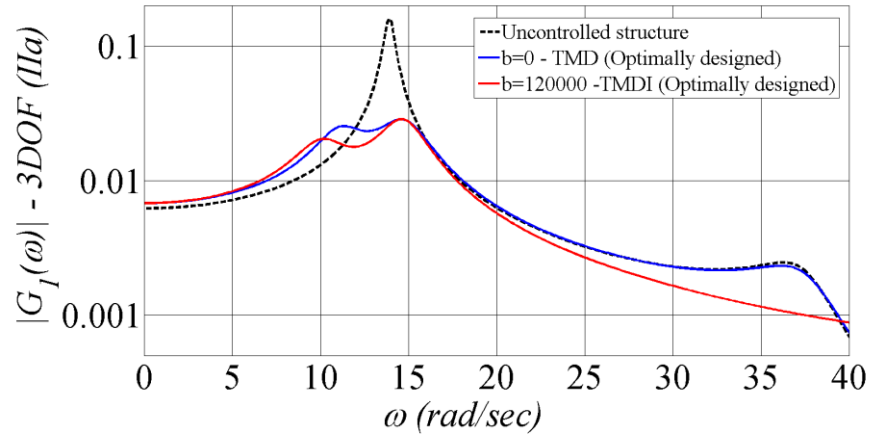


Figure 5.18. Absolute transfer function between the input ground acceleration and the output top floor displacement for the uncontrolled (primary) structure 3DOF IIa, structure equipped with optimal TMD and structure equipped with optimal TMDI

It is observed that, similar to the case of TMDI equipped SDOF presented in section 3.3, the TMDI effectiveness extends over a considerable range of frequencies allowing for efficient passive control of higher modes. This is not the case with the classical TMDs which can target only a single mode they are tuned to control it.

5.2.3 ON THE WEIGHT REDUCTION OF THE TUNED-MASS-DAMPER-INERTER ($b > 0$) VERSUS THE CLASSICAL TUNED-MASS-DAMPER ($b = 0$)

The data furnished in the previous sub-chapter demonstrates the applicability of using the “mass amplifying” effect of the TTF/inerter device to replace part of the oscillating mass of the TMD. This may be a significant advantage in certain real-life earthquake resistance design scenarios. For example, in the case of the herein considered 3 DOF primary structure (IIa) and EC8 compatible seismic excitation, the use of a inerter with a “mass” constant of $b=120000$ kg in combination with a TMD mass of 5400kg

achieves improved level of response in terms of top floor deflection variance as the classical TMD two times heavier oscillating mass (10500kg). However, the physical mass of the employed inerter might be up to two orders of magnitude smaller than its b constant as explained in Chapter 2.2, that is, about 400 kg (Smith, 2002). Thus, the total weight of the examined TMDI system becomes about two times lighter than the classical TMD. The ‘weight reduction’ capacity of the TMDI solution is better exemplified in Figure 5.19, Figure 5.20 and Figure 5.21 where the m_{TMDI} values required for achieving a certain level of response, evaluated by means of the PI of Equation (4-22), are plotted.

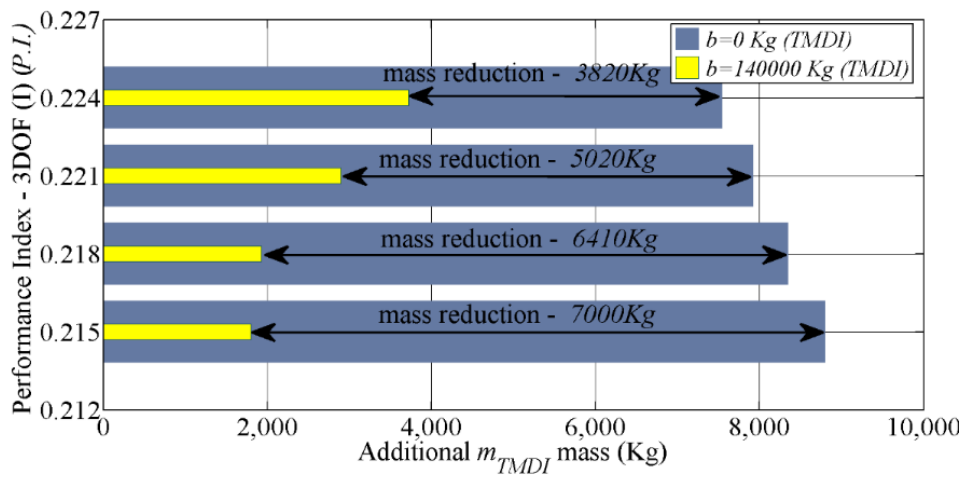


Figure 5.19. Additional m_{TMDI} mass values required for achieving the same level of performance index for the proposed TMDI configuration ($b>0$) and for classical TMD ($b=0$). Three DOF primary structure - 3DOF (I).

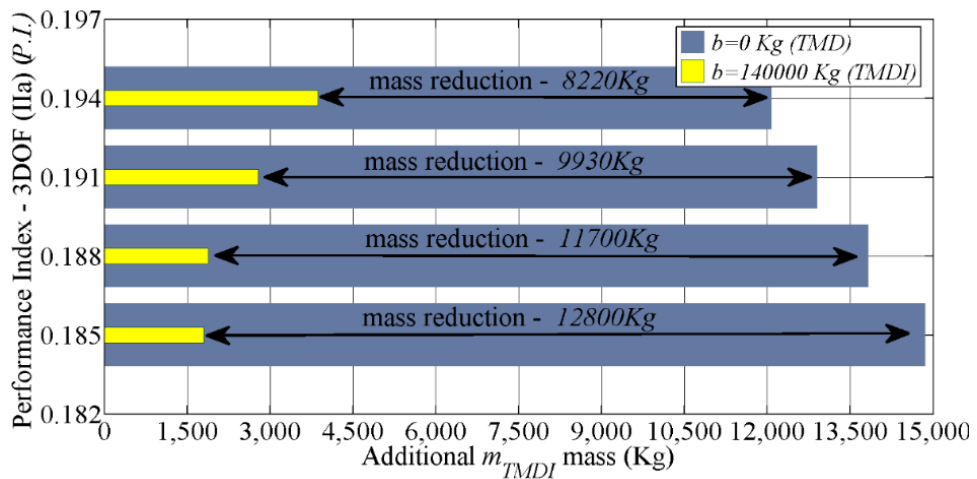


Figure 5.20. Additional m_{TMDI} mass values required for achieving the same level of performance index for the proposed TMDI configuration ($b>0$) and for classical TMD ($b=0$). Three DOF primary structure - 3DOF (IIa).

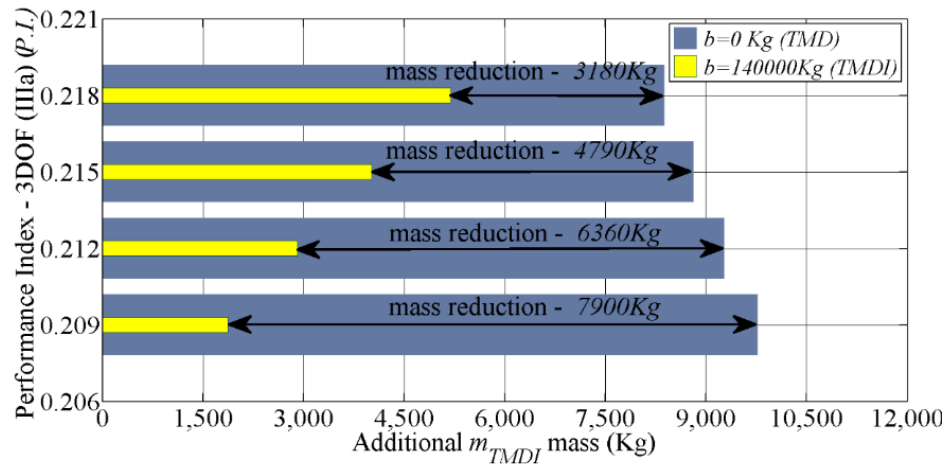


Figure 5.21. Additional m_{TMDI} mass values required for achieving the same level of performance index for the proposed TMDI configuration ($b>0$) and for classical TMD ($b=0$). Three DOF primary structure - 3DOF (IIIa).

The latter consideration may have significant advantages in certain real-life structural passive vibration control design scenarios necessitating the use of large additional vibrating masses to achieve robust and efficient vibration suppression effect of building structures excited by severe earthquake induced strong ground motions (see e.g. Feng & Mita, 1995; Moutinho, 2012; Angelis et al 2012; Hoang et al, 2008; Matta & DeStefano, 2009; Matta & DeStefano., 2009).

It is also noted that, when considering the last figures, the most significant mass reduction for the same $P.I.$ value occurs for the primary structure with reduced top floor stiffness (3DOF - IIa) while structures with uniform distribution of mass and stiffness will allow for the smallest TMDI/TMD reductions in the weight of the required oscillating masses.

5.3 PERFORMANCE ASSESMENT OF OPTIMALLY DESIGNED TUNED - MASS - DAMPER - INERTER EQUIPPED STRUCTURES USING FIELD RECORDED EUROCODE 8 COMPATIBLE ACCELEROGRAMS

This section furnishes pertinent numerical results to quantify the effectiveness of the herein proposed TMDI configuration vis-à-vis the classical TMD for passive vibration control of building structures. To this aim, the peak top floor deflection of the previously described primary structure herein noted as 3DOF IIa is obtained for an ensemble of 7 filed recorded accelerograms. A comparison is conducted between the uncontrolled (primary) structure, structure equipped with optimal TMD and structure equipped with optimal TMDI, for the same additional m_{TMDI} mass. The two considered passive vibration control systems have been optimally designed for the stochastic input compatible with the EC8 spectrum of Figure 5.2 as detailed in the Section 4.3 (see also Table 5.5).

The top row of Table 5.6 reports the properties considered for the two systems. Further, the same table lists the considered 7 accelerograms: they have been selected out of a data-bank specifically proposed to be used as input for the design and assessment of passively controlled civil structures (Naeim & Kelly 1999). The original records have been scaled in a non-uniform manner using a harmonic wavelet-based approach (Giaralis & Spanos 2009, Giaralis & Spanos 2012) to become compatible with the target EC8 spectrum of Figure 5.2 according to EC8 compatibility criteria. Specifically, their average response spectral ordinates are greater than 90% of the target spectrum within a $[0.2T_1, 2T_1]$ period interval where $T_1=1s$ is the fundamental natural period of the considered primary structure (Figure 5.22). This numerical study is motivated by the fact that EC8 prescribes using the *average* of pertinent peak response quantities for design purposes

when at least 7 response history analyses are performed for spectrum compatible accelerograms.

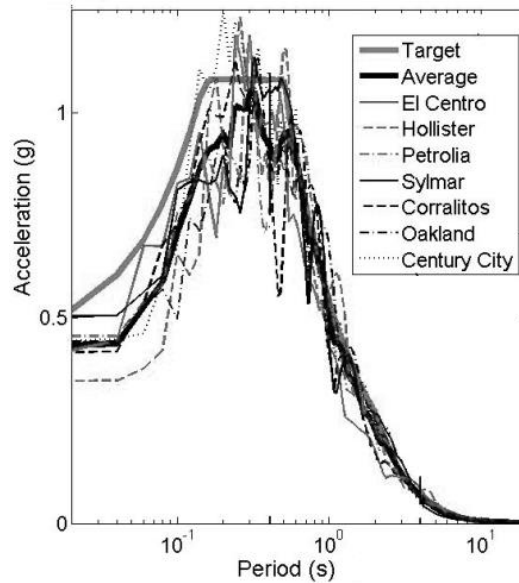


Figure 5.22. Response spectra of the considered EC8 compatible field recorded accelerograms listed in Table 5.6

Table 5.6. Maximum top floor displacements (cm) for 3DOF Structure IIa

Recorded strong ground motion component.	(Uncontrolled) Primary structure	TMD (m=5400 Kg, b=0 Kg)	TMDI (m=5400 Kg, b=80000 Kg)	TMDI (m=5400 Kg, b=100000 Kg)	TMDI (m=5400 Kg, b=120000 Kg)
Petrolia- 90° 1992- Petrolia	8.21	4.86	5.54	4.08	4.69
Corralitos- 90° Eureka Canyon 1989-Loma Prieta	10.68	4.79	5.09	3.91	6.08
El Centro #6-230° Huston Rd. 1979-Imperial Val.	8.28	5.51	4.72	4.15	4.01
Hollister-90° South St & Pine Dr 1989- Loma Prieta	9.87	6.38	5.23	4.38	4.23
Oakland-35° Outer harbor wharf 1989- Loma Prieta	9.91	5.01	4.43	7.18	4.03
Century City-90° LACC North (1994- Northridge)	7.6	4.97	5.52	3.78	3.41
Sylmar- 90° County Hospital (1994- Northridge)	7.85	5.65	6.68	3.58	4.56
Average	8.91	5.3	5.31	4.44	4.43

When considering the 3 DOF structure IIa, on average (Table 5.6), the TMD ($b=0$) achieves 60% peak response reduction compared to the uncontrolled primary structure, while the TMDI achieves 50% reduction. This additional peak response reduction accomplished by the herein proposed configuration is due to the virtual “mass amplifying effect” of the inerter which can accommodate, in an optimal manner, a damper with an order of magnitude higher damping coefficient (c_{TMDI}) for the same m_{TMDI} mass. However, as detailed in Chapter 2.2, the added actual physical mass of the inerter in this case is much smaller than the b value. Figure 5.23 and Figure 5.24 show the time history top floor displacement and acceleration respectively for the structure during the Century City Earthquake.

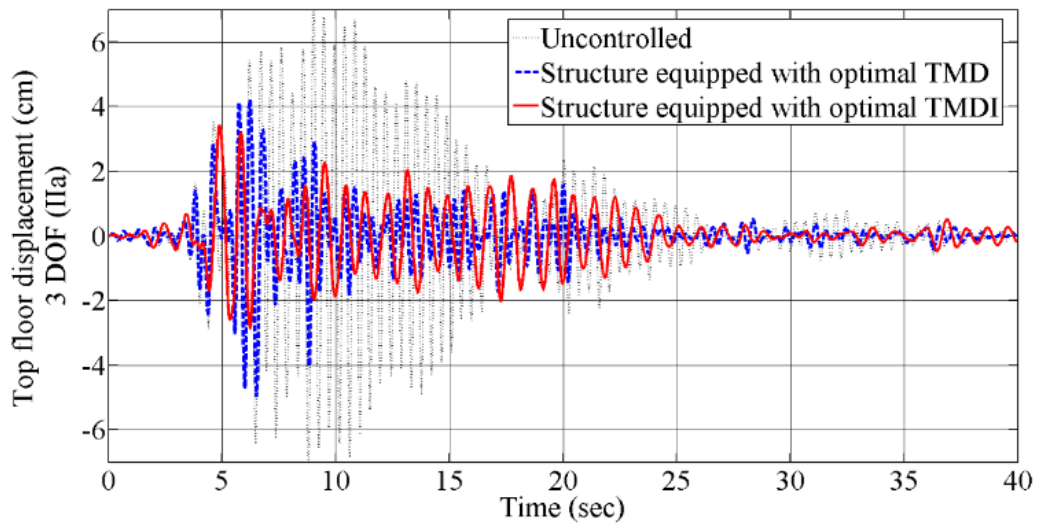


Figure 5.23. Three DOF primary structure IIa. Top floor displacement responses for uncontrolled structure, structure equipped with optimal TMD and structure equipped with optimal TMD and TTF device.

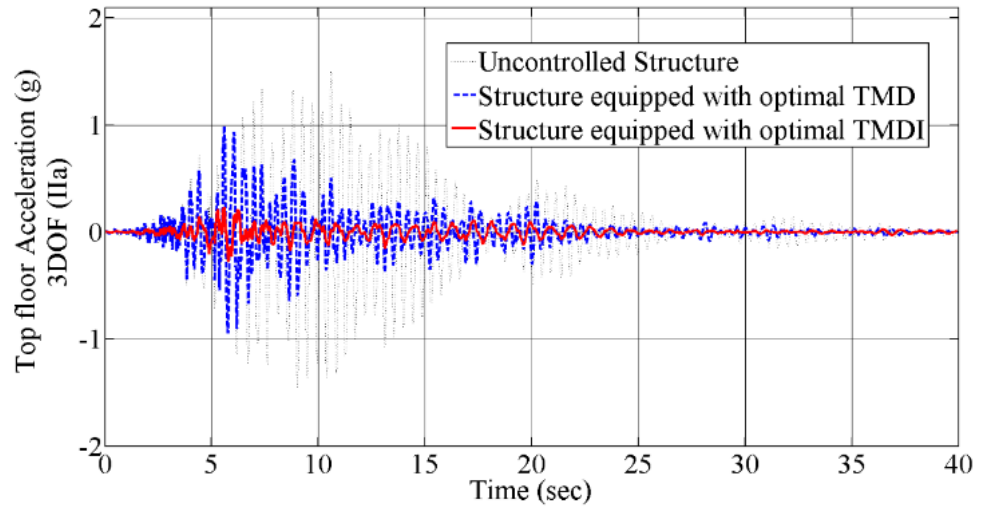


Figure 5.24. Three DOF primary structure IIa. Top floor acceleration responses for uncontrolled structure, structure equipped with optimal TMD and structure equipped with optimal TMDI and TTF device.

These are obtained by standard numerical integration of the linear equations of motion for the uncontrolled and the two controlled cases considered in Table 5.6. The proposed TMDI configuration controls better the displacement throughout the duration of the strong ground motion. Similar conclusions are drawn from response histories obtained for the other 6 EC8 compatible accelerograms.

Inertial dynamic loads exerted to structures are proportional to the absolute horizontal accelerations experienced by each floor of the building. Thus, the maximum floor acceleration is an important factor in evaluating the level of resident comfort. To this aim, Table 5.7 reports the maximum top floor acceleration for the considered ensemble of 7 accelerograms and for the same characteristics of the TMD/TMDI passive vibration control solutions.

Table 5.7. Maximum top floor acceleration (g) for 3DOF Structure IIa

Recorded strong ground motion component .	Uncontrolled structure	TMD ($m_{TMDI}=5400$ Kg, $b=0$ Kg)	TMDI ($m_{TMDI}=5400$ Kg, $b=80000$ Kg)	TMDI ($m_{TMDI}=5400$ Kg, $b=100000$ Kg)	TMDI ($m_{TMDI}=5400$ Kg, $b=120000$ Kg)
Petrolia- 90° 1992- Petrolia	1.59	1.07	0.57	0.33	0.32
Corralitos- 90° Eureka Canyon 1989-Loma Prieta	2.25	0.97	0.44	0.35	0.31
El Centro #6-230° Huston Rd. 1979-Imperial Val.	1.53	0.92	0.44	0.38	0.33
Hollister-90° South St & Pine Dr 1989- Loma Prieta	1.97	1.22	0.4	0.31	0.3
Oakland-35° Outer harbor wharf 1989- Loma Prieta	1.97	1.42	0.34	0.37	0.24
Century City-90° LACC North (1994- Northridge)	1.5	0.99	0.45	0.32	0.27
Sylmar- 90° County Hospital (1994- Northridge)	1.58	1.12	0.55	0.3	0.31
Average	1.77	1.1	0.46	0.34	0.3

The numerical result in Table 5.7 show that the TMDI control solution efficiently reduces the top floor accelerations. For the 3 DOF structure considered, this is reduced from 62% in case of classical TMD to 17% when an inerter with $b=120000$ Kg is considered in the TMDI configuration.

In addition, it is of interest to also evaluate the time history displacements of the additional oscillating mass m_{TMDI} , as a comparison between the two vibration control solutions proposed. This is because the TMD mass displacement or ‘TMD stroke’ can be an important issue of concern, especially for earthquake-induced vibrations with much larger amplitudes compared with wind-induced ones (e.g., Lin et al, 2010; Wang et al, 2009). In this respect, it is shown in Table 5.8 that, on average, the TMDI configuration achieves around 35% reduction in the maximum displacement of the oscillating mass for

the 7 response history analyses performed. Similar results are found for other primary structures.

Table 5.8. Maximum m_{TMDI} mass displacements (cm)

Recorded strong ground motion component .	TMD ($m_{TMDI}=5400$ Kg, b=0 Kg)	TMDI ($m_{TMDI}=5400$ Kg, b=80000 Kg)	TMDI ($m_{TMDI}=5400$ Kg, b=100000 Kg)	TMDI ($m_{TMDI}=5400$ Kg, b=120000 Kg)
Petrolia- 90° 1992- Petrolia	13.74	6.41	4.22	4.79
Corralitos- 90° Eureka Canyon 1989-Loma Prieta	11.62	5.61	4.25	6.49
El Centro #6-230° Huston Rd. 1979-Imperial Val.	13.22	5.27	4.52	4.28
Hollister-90° South St & Pine Dr 1989- Loma Prieta	15.03	6.00	4.78	4.70
Oakland-35° Outer harbor wharf 1989- Loma Prieta	10.09	5.06	7.82	4.32
Century City-90° LACC North (1994- Northridge)	15.34	6.28	4.03	3.56
Sylmar- 90° County Hospital (1994- Northridge)	13.80	7.57	4.14	4.83
Average	13.26	6.03	4.82	4.71

It can thus be concluded that the inclusion of the inerter in the proposed TMDI configuration reduces not only the top floor displacement variance, but also accelerations and TMDI mass displacement.

5.4 ON THE CONTROL OF HIGHER MODES USING THE TUNED-MASS-DAMPER-INERTER PASSIVE CONTROL SOLUTION

This section emphasises on the capabilities of the TMDI passive solution for controlling higher modes. As detailed in the previous section, the efficiency of the TMDI critically depends on the choice of the primary structure it is applied to. For buildings with regular distribution of stiffness and mass along its height, the TMDI might not always outperform the traditional TMD configuration, as is the case of the 3DOF structure – 3DOF (I) previously studied. However, it is important to note that, as suggested in Figure 5.18 for the case of 3DOF primary structure, the TMDI control solution also allows for efficient passive control of higher than the first modes. Along these lines, Figure 5.26 reports the absolute transfer function between the input ground acceleration and the output top floor absolute displacement of a regular 10DOF primary structure whose characteristics are detailed in Table 5.9 and Table 5.10 (Taflanidis & Giaralis, 2015).

Table 5.9. Inertial and elastic properties of the considered primary structure

Structure	Story	Mass (kg)	Stiffness (N/m)
10DOF	1 (top)	900×10^3	470×10^6
	2	900×10^3	470×10^6
	3	900×10^3	470×10^6
	4	900×10^3	630×10^6
	5	900×10^3	630×10^6
	6	900×10^3	630×10^6
	7	900×10^3	780×10^6
	8	900×10^3	780×10^6
	9	900×10^3	780×10^6
	10	900×10^3	780×10^6

Table 5.10. Undamped natural frequencies of the considered primary structure.

Structure	Mode	Period (s)	Frequency (rad/s)
10DOF	1 st	1.50	4.19
	2 nd	0.54	11.52
	3 rd	0.33	18.87
	4 th	0.24	26.34
	5 th	0.19	32.19
	6 th	0.17	38.09
	7 th	0.14	42.22
	8 th	0.13	46.84
	9 th	0.12	50.72
	10 th	0.11	56.24

These curves were derived following the optimisation procedure described in Section 4.3. Specifically, the following are considered:

Table 5.11. Inertial and elastic properties of the considered primary structure

	m_{TMDI} (kg)	b (kg)	v_{TMDI}	k_{TMDI} (10^6 N/m)	ζ_{TMDI}	c_{TMDI} (10^5 Ns/m)	PI	Improvement (%)
10DOF	45000	0(w/o TTF)	0.9850	0.766	0.0514	0.191	0.8011	-
		240×10^4	2.2260	20.91	0.9694	43.46	0.8013	0%

Notably, given the increased overall total mass and rigidity of the primary structure, considerably larger b values are required for optimum design compared with the previously studied examples.

The last column of Table 5.11 shows that, given the regular distribution of mass and stiffness of the structure considered, and as expected from the findings of the previous section, the TMDI does not outperform the TMD when evaluating the control capabilities at the fundamental mode shape of vibration. Actually, the choice of b has been made such that both TMD and TMDI obtain similar performance in terms of top floor response. With respect to Figures 5.11 to 5.15, the values of the performance index in Table 5.11 can be viewed as the point of intersection of the TMDI-TMD performance curves.

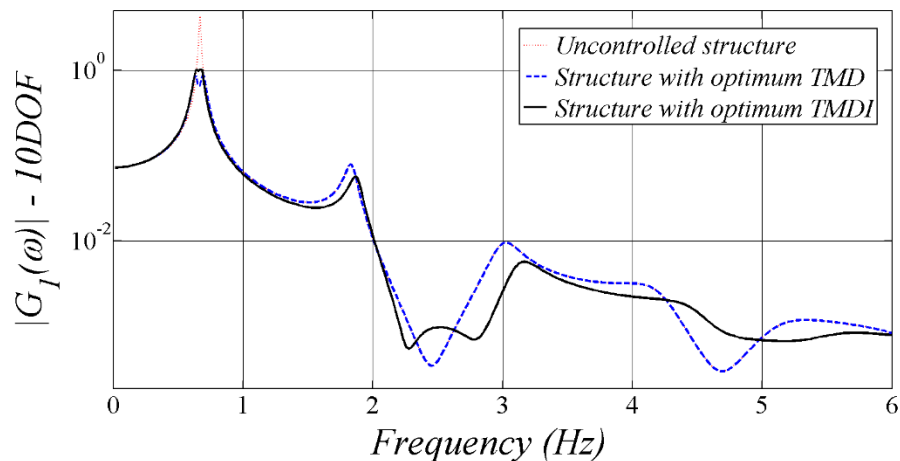


Figure 5.25. Absolute transfer function between the input ground acceleration and the output top floor displacement for the 10DOF uncontrolled (primary) structure, structure equipped with optimal TMD and structure equipped with optimal TMDI

It can be seen that, although both control solutions have been optimally design such that they achieve similar response variance (i.e. equal areas under graphs of Figure 5.25), at the fundamental frequency the TMD solution offers negligible improvements compared with TMDI. More importantly, when analysing higher modes, Figure 5.25 suggests a reduction in the overall response amplitudes for the TMDI compared with traditional TMD. Given the broad-band influence of the TMDI as compared with classical one-frequency targeted control of the TMD, this suggests the practical applicability of the TMDI for medium-height to tall structures where large response amplitudes can be observed at frequencies higher than the fundamental one.

In addition, it is also useful to consider the absolute transfer function between the input ground acceleration and the output top floor acceleration for the regular 10DOF, as reported in Figure 5.26. It can be seen that, although both control solutions offer identical control performance in terms of top floor displacement variance, an overall reduction in the acceleration response of higher modes can be observed. This has an important significance in real-life scenarios where acceleration-sensitive non-structural components can have a major effect on the safety of occupants and integrity of facilities (Petrone et al, 2015).

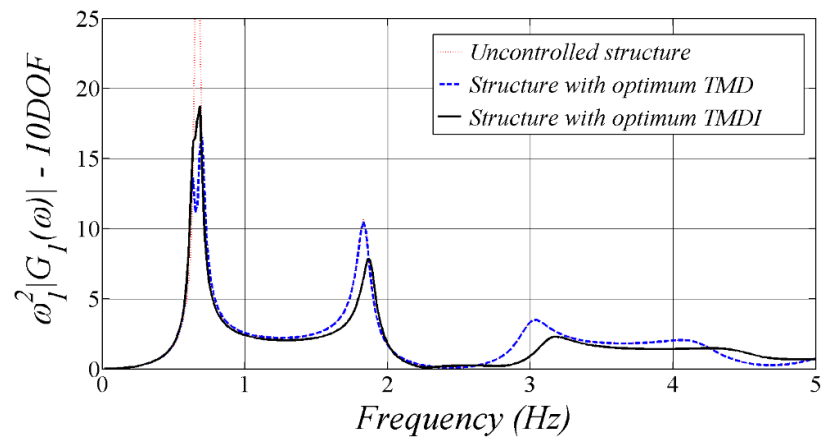


Figure 5.26. Absolute transfer function between the input ground acceleration and the output top floor acceleration for the regular 10DOF uncontrolled (primary) structure, structure equipped with optimal TMD and structure equipped with optimal TMDI

Along the same lines, Table 5.12 reports the average displacement, acceleration and added oscillating mass displacement for the studied 10DOF uncontrolled structure, structure equipped with classical TMD ($b=0$) and structure equipped with TMDI ($b>0$) when considering the recorded strong ground motions detailed of Table 5.6.

Table 5.12. Maximum top floor and next-to-top floor displacements (cm) and accelerations for the 10DOF primary structure

	(Uncontrolled) Primary structure		TMD ($m=45000$ Kg, $b=0$ Kg)		TMDI ($m=45000$ Kg, $b=240*10^4$ Kg)	
	Top floor	Next-to-top floor	Top floor	Next-to-top floor	Top floor	Next-to-top floor
Average Displacement (cm) (Improvement)	46.08	44.33	37.33 (19%)	35.87 (19%)	37.78 (18%)	36.09 (19%)
Average Acceleration (g) (Improvement)	1.30	1.17	1.20 (8%)	1.11 (5%)	1.08 (17%)	1.05 (10%)
Average TMD displacement (cm) (Improvement)	-		198.2		37.5 (81%)	

When comparing the TMD-TMDI responses in Table 5.12, it can be observed that, as suggested by the *P.I.* of Table 5.11, similar responses are obtained in terms of displacement responses for bot top and next-to-top floors. However, the TMDI achieves a much greater reduction in terms of floor acceleration compared with TMD. Furthermore, an even more significant reduction is achieved in terms of the displacement requirements for the additional oscillating mass thus demonstrating the superiority of the herein proposed TMDI over classical TMDs.

CHAPTER 6 : SIMULTANEOUS VIBRATION SUPPRESSION AND ENERGY HARVESTING USING THE TUNED-MASS- DAMPER-INERTER

6.1 PRELIMINARY REMARKS

As described in previous chapters, TMDs are widely used today in a plethora of different applications in civil engineering to mitigate undesirable vibrations due to dynamic loads caused by different sources such as traffic, wind, and earthquakes (e.g. Shi & Cai, 2008; Chung et al, 2012; Angelis et al 2013). In addition, the potential of energy harvesting from TMD equipped civil structural facilities has been recently recognized and explored to some extent (Zuo & Tang, 2013; Gonzalez-Buelga et al 2014, Tang & Zuo 2012; Adhikari & Ali, 2013). It relies on the idea of using certain devices capable of transforming kinetic into electric energy in order to link the attached mass to the primary structure as opposed to using only a damper at which kinetic energy is “lost” into radiating heat.

In this context, a “tuned mass damper/harvester” (TMD/H) control configuration is proposed in (Gonzalez-Buelga et al, 2014) where an electromagnetic motor consisted of a magnet travelling within a constant magnetic field is considered, along with a linear spring and a damper, to link the attached mass to the primary structure. Pertinent numerical and experimental results furnished evidence that sufficient energy can be generated from harmonic force or support excitation such that the proposed configuration can perform as a self-tuned regenerative semi-active vibration control solution. Along similar lines, an electromagnetic transducer connected to an energy harvesting enabled

circuit is used to transform kinetic energy into electric power and to provide controlled force vibrations mitigation for TMD equipped multi-storey buildings structures in (Tang & Zuo, 2012). Experimental results demonstrate the effectiveness of the thus created self-powered active TMD to achieve vibration suppression. Further, an “energy harvester-dynamic vibration absorber” (EHD-VA) configuration is employed in (Tang & Zuo, 2012), in which electric energy is generated from strains developed in layers of piezoelectric material mounted onto the attached vibrating mass of a TMD. An approximate formulation based on Den Hartog fixed point theory is used to derive closed form expressions for optimal design parameters of the proposed EHD-VA.

In this chapter, the TMDI is applied to achieve simulations vibration suppression and energy harvesting for harmonically excited structures. In particular, the potential of optimally designed TMDIs for energy harvesting using a linear electromagnetic motor acting in parallel with the standard dashpot of the TMDI is explored, as this is commonly considered in the literature for energy scavenging. This study is motivated by the fact that in considering a passive TMD-based harvester device, as the oscillating TMD mass increases, better primary structure response reduction is achieved but at the cost of reduced available energy for harvesting (Gonzalez-Buelga et al, 2014; Adhikari & Ali, 2013). However, this trade-off between better vibration suppression vis-à-vis energy harvesting may be controlled by considering inerters with varying inertance and therefore TMDIs with varying inertial properties.

6.2 MECHANICAL DESCRIPTION AND CHARACTERISATION OF THE PROPOSED ENERGY HARVESTING ENABLED TUNED-MASS-DAMPER-INERTER

Having established the effectiveness of the TMDI system for vibration suppression and weight reduction for harmonically excited structures in section 3.3, this section assesses its potential for energy harvesting by relying on the use of an electromagnetic linear motor (EM) to harness electric energy from low-frequency vibrations. The idea is to channel part of the kinetic energy of the attached mass to the EM to transform part of the kinetic into electric energy. Therefore, not all of the kinetic energy is “lost” (dissipated) in the form of radiating heat at the TMDI damper. In this context, the energy harvesting enabled TMDI system shown in Figure 6.1 is herein proposed which incorporates an EM connected in parallel with a spring and a damper to the attached TMDI mass. The herein considered EM comprises a moving magnet DC voice coil linear actuator connected to a resistance emulator circuit (see e.g. Gonzalez-Buelga et al, 2014). The moving magnet observes the relative motion of the primary structure and of the attached mass and travels within a magnetic field of constant flux density J generating voltage V expressed as:

$$V = J(\dot{x}_1 - \dot{x}_2) \quad (6-1)$$

In this manner, the considered electromagnetic energy harvester achieves kinetic to electrical energy conversion. In particular, the harvester “resists” the relative motion between the primary structure and the attached mass by developing an additional electromechanical “damping” force F_{EM} . This force is expressed in the “mechanical domain” shown in Figure 6.1 by the equation:

$$F_{EM} = c_{EM} (\dot{x}_1 - \dot{x}_2) \quad (6-2)$$

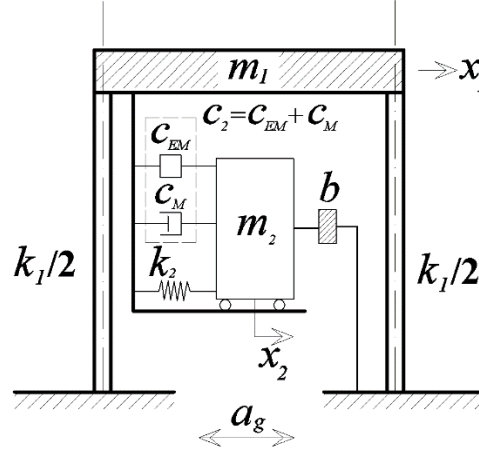


Figure 6.1 Single-degree-of-freedom (SDOF) primary structure incorporating the proposed tuned mass-damper-inerter-harvester (TMDI-H) configuration.

where c_{EM} is the electromechanical damping coefficient. Further, the above damping force F_{EM} generated by the considered device is linearly proportional to the generated electric current intensity I , that is,

$$F_{EM} = J I \quad (6-3)$$

Using (6-2) and (6-3) in conjunction with Ohm's law $I=V/R$, which relates the electric current I through a circuit with resistance R due to a voltage V across R , the electromechanical damping coefficient c_{EM} is expressed as (Gonzalez-Buelga et al, 2014):

$$c_{EM} = \frac{J^2}{(R_C + R_L)} \quad (6-4)$$

In the last equation, R_C represents the internal "parasitic" resistance of the electromechanical device which models the overall energy losses within the device. Further, R_L is the resistive load due to the resistance emulator circuit proposed in (Gonzalez-Buelga et al, 2014) harvesting kinetic energy from the dynamic mechanical

system of Figure 6.1. By comparing the latter system with the TMDI system of Figure 6.1 it is readily seen that the total damping coefficient c_2 of the energy harvesting enabled TMDI is given by the sum of the electromechanical damping coefficient with the damping c_M of the TMDI linear damper. That is,

$$c_2 = c_{TMDI} = c_{EM} + c_M \quad (6-5)$$

6.3 QUANTIFICATION OF ENERGY SCAVENGED BY THE PROPOSED TUNED-MASS-DAMPER-INERTER ELECTROMAGNETIC HARVESTER DEVICE

In this section, the energy (or the power) available to harvest from the vibrating system of Figure 6.1 is quantified by assuming that the energy harvesting enabled TMDI system is optimally designed for vibration suppression of a harmonically base-excited primary structure as detailed in section 3.3. To this aim, it is noted that the power P that can be harvested from the mechanical domain vibrations is given by the resistive load R_L of the electromechanical harvester. Therefore, it is given by the standard relationship:

$$P = I^2 R_L \quad (6-6)$$

Use of Eq. (6-1) to Eq. (6-5) in conjunction with the above relationship yields the following expression of the power P that can be harvested from the considered harmonically support-excited structural system of Figure 6.1

$$P(\omega) = \frac{J^2}{(R_C + R_L)^2} |G_{RV}(\omega)|^2 R_L \quad (6-7)$$

In the above equation, G_{RV} is the relative velocity FRF between the m_1 mass of the primary structure and the attached m_2 mass given as:

$$G_{RV}(\omega) = i\omega \frac{G_1(\omega) - G_2(\omega)}{\omega_1^2} \quad (6-8)$$

where the FRFs G_1 and G_2 have been defined in (3-5) and (3-6), respectively.

In Figure 6.2, the magnitude of the G_{RV} FRF is plotted as a function of the input harmonic excitation normalized by the natural frequency of the uncontrolled primary structure ω_1 for an optimally designed TMDI equipped undamped SDOF primary structure with mass ratio $\mu=0.1$ and for different values of the inertance ratio β using the optimum parameters in (3-15) and (3-17). The amplitude of $|G_{RV}|$ reduces as higher β values are used (for a fixed μ) and, therefore, enhanced vibration suppression is achieved (see also Figure 3.5). However, the reduction of $|G_{RV}|$ is not beneficial in terms of energy harvesting as is readily inferred from (6-7).

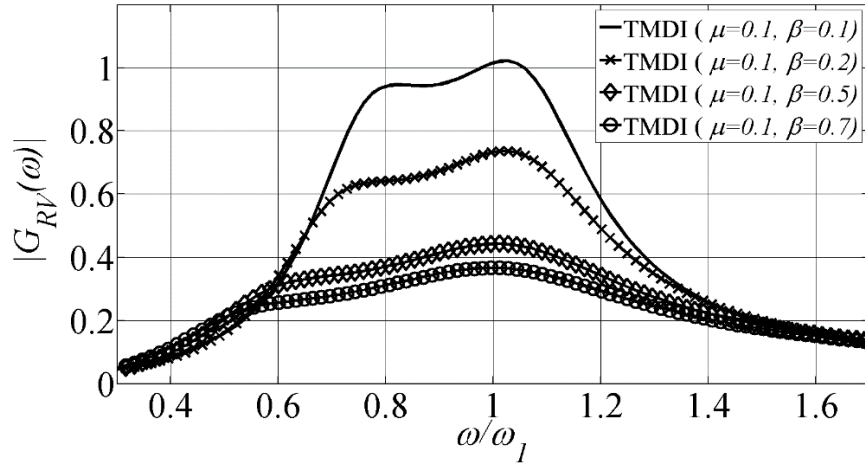


Figure 6.2. Normalized relative velocity amplitude for an undamped structure equipped with optimal TMDI configuration

This effect of the inertance ratio β on the energy harvesting capabilities of the TMDI system of Figure 6.1 is further quantitatively illustrated in Figure 6.3 which plots the magnitude of the power in (6-7) normalized by the amplitude of the input harmonic support acceleration. The latter plots have been obtained by taking $J=11.34$ N/A and $R_c=2.96\Omega$, and by assuming that $c_M=c_{EM}$ (Gonzalez et al, 2014). Further, the optimal c_2 value has been obtained by use of (3-3), (3-17), (6-4) and (6-5).

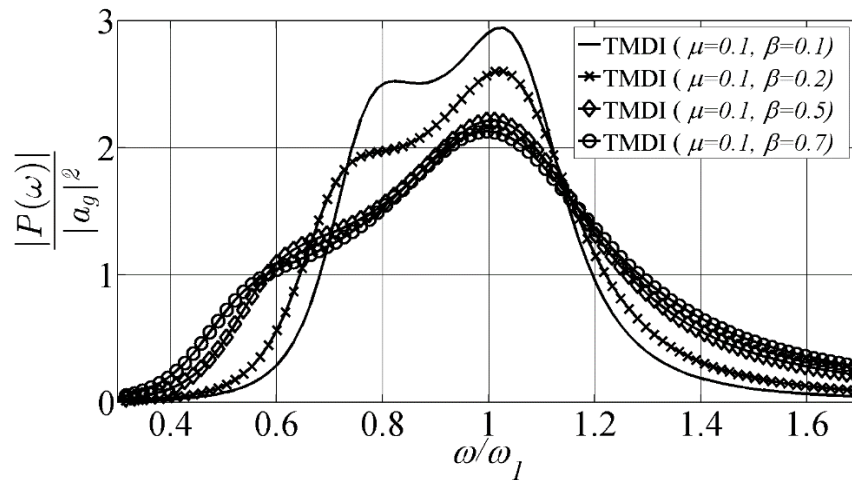


Figure 6.3. Normalized power harvested from various TMDI systems optimally designed for vibration suppression.

Focusing on Figure 6.3, it is seen that the increase of the ratio β has a negative effect in terms of the available energy for harvesting close to the natural period of the uncontrolled primary structure. However, similarly to what has been observed and discussed in view of Fig. 5, the effect of β to the peak values of the magnitude of FRFs saturates for $\beta > 0.5$, while the range of frequencies that the FRFs take on non-negligible values increases (i.e., the FRF curves become flatter). In every case, Figure 3.5 and Figure 6.3 confirm what has been reported in the literature for the case of the classical TMD: “an optimal absorber is not an optimal harvester” (Gonzalez et al, 2014). Still, the herein considered TMDI system is not necessarily confined by an *a priori* fixed mass ratio μ , as the classical TMD. This aspect is addressed in the next section.

6.4 SIMULTANEOUS ENERGY HARVESTING AND VIBRATION SUPPRESSION FOR TUNED-MASS-DAMPER-INERTER EQUIPPED SYSTEMS WITH VARYING INERTANCE

The inertance value b of the flywheel-based inerter shown schematically in Figure 6.1 can change at will, without changing the total physical mass or weight of the TMDI, by considering a relatively simple stepped gearbox (see e.g. Papageorgiou & Smith, 2005). In this manner, the sequence and/or the ratio of gears linking the flywheel to the rack can change in a passive/adaptive mode and, consequently, the inertance b computed by Eq. (2-1). This consideration allows for increasing the potential amount of energy that can be harvested from a TMDI optimally designed for vibration suppression for fixed attached mass spring and damper coefficients. This is exemplified in Figure 6.4 and Figure 6.5 which plot the dynamic amplification factor spectra and, respectively, the normalized energy harvested spectra for an optimally designed TMDI for vibration suppression with mass ratio $\mu= 0.1$ and inertance ratio $\beta=0.6$ having optimal TMDI parameters $v_{TMDI}=0.5651$ and $\zeta_{TMDI}=0.4132$ (see Equations (3-5) and (6-7)).

It is observed that as β reduces, the (sub-optimal) TMDI becomes less effective for vibration suppression at the ω_1 frequency, for fixed μ , v_{TMDI} and ζ_{TMDI} parameters. However, as reduced β values are used (for a fixed μ , v_{TMDI} and ζ_{TMDI}) the TMDI allows for increased energy to be harvested at excitation frequencies equal to the natural frequency of the uncontrolled system ω_1 , (see Figure 6.5).

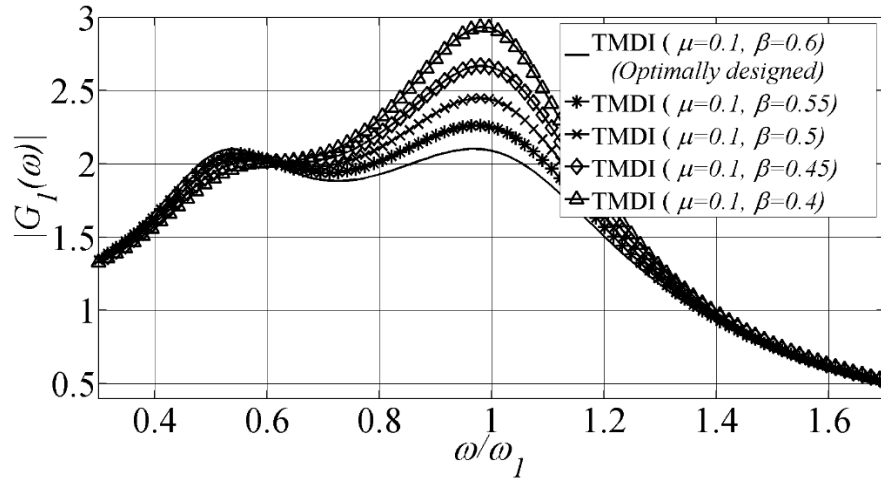


Figure 6.4. Dynamic amplification factor spectra (left panel) for an optimally designed TMDI system for vibration suppression with $\mu=0.1$ and $\beta=0.6$ (fixed $\nu_{TMDI}=0.5651$ and $\zeta_{TMDI}=0.4132$) and for several values of inertance.

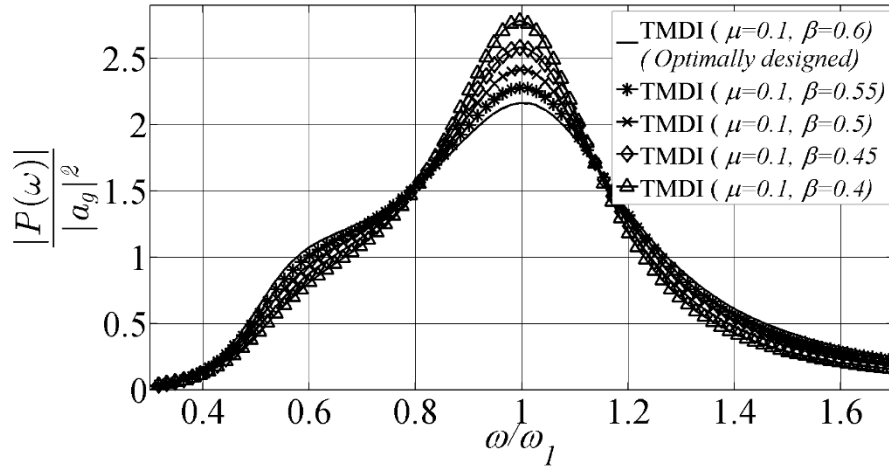


Figure 6.5. Normalized power harvested spectra for an optimally designed TMDI system for vibration suppression with $\mu=0.1$ and $\beta=0.6$ (fixed $\nu_{TMDI}=0.5651$ and $\zeta_{TMDI}=0.4132$) and for several values of inertance.

Therefore, by keeping constant the weight of the TMDI, changes in the inertance b allows for controlling the trade-off between energy harvesting and vibration suppression in the range of excitation frequencies between 70%~90% of the ω_1 frequency.

This can be clearly seen in Figure 6.6 which plots the peak response amplitude of the non-optimal TMDI configuration normalised by the peak response amplitude of the optimally designed TMDI with $\beta=0.6$, as the inertia ratio β changes for four different

values of the mass ratio μ and for constant optimal TMDI parameters ν_{TMDI} and ζ_{TMDI} as exemplified in Table 6.1.

Table 6.1 Optimal TMDI parameters derived for $\beta=0.6$ and several mass ratio μ values

	Frequency ratio ν_{TMDI}	Damping ratio ζ_{TMDI}
$\mu = 0.2$	0.5512	0.4497
$\mu = 0.4$,	0.4226	0.5227
$\mu = 0.6$	0.3484	0.6026
$\mu = 0.8$	0.2846	0.6990

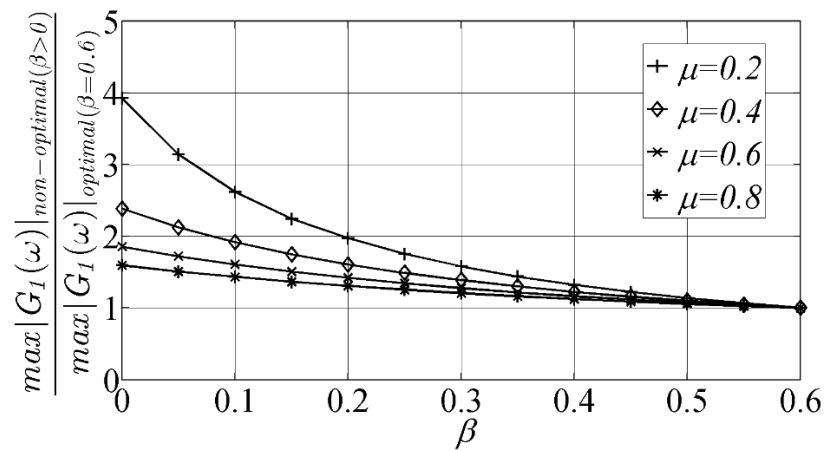


Figure 6.6. Peak dynamic amplification factor for the *non-optimal* TMDI configurations normalized by the maximum of the dynamic amplification factor for optimally designed TMDI (for $\beta=0.6$) as functions of the inertance ratio β

The last figure also suggests that as the ratio β shifts from the value the TMDI was optimally designed against, the non-optimal configurations obtained are less effective for vibration suppression, as β decreases ($\beta < 0.6$). Furthermore, increasing the m_{TMDI} mass provides less fluctuations on the performance of the TMDI configuration, as β varies (almost flat performance curves). Similarly, the same type of performance robustness can be observed when considering β values closer to the optimum.

Lastly, Figure 6.7 plots the maximum power available to be harvested from a *non-optimal* TMDI configuration normalized by the maximum power available to be

harvested for an optimally designed TMDI for vibration suppression (for $\beta=0.6$), as function of the inertance ratio β and for several mass ratio μ values.

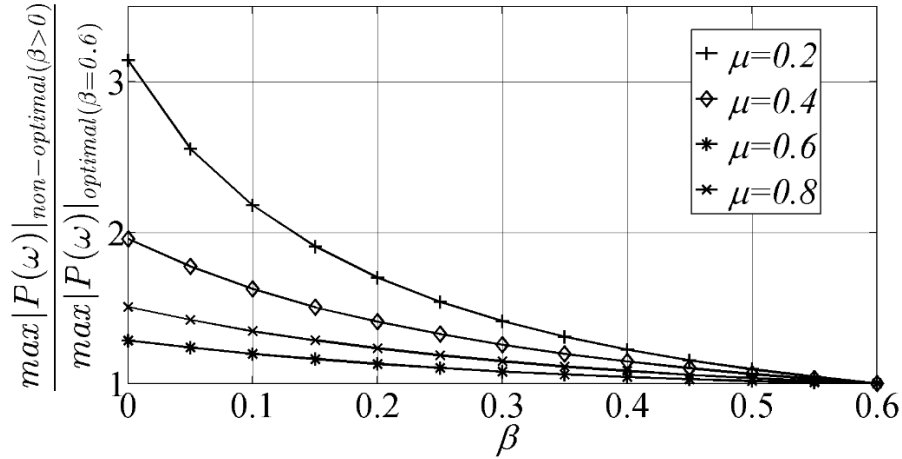


Figure 6.7. Peak normalized potential harvesting power for the *non-optimal* TMDI configurations normalized by the maximum of the dynamic amplification factor for optimally designed TMDI (for $\beta=0.6$) as functions of the inertance ratio β

Specifically, the curves in Figure 6.7 are obtained by varying the inerter constant b while keeping constant the optimum c_{TMDI} and k_{TMDI} values for several μ values in order to demonstrate the benefits of considering inerters with varying inertance. It readily be observed that, as β reduces from the value for which the TMDI was optimally designed ($\beta=0.6$), more power will be available for harvesting. Furthermore, when considering both Figure 6.6 and Figure 6.7 it can be observed that, for larger μ values, the changes in the inertance values will imply less variations in the power harvested as well as less variation in the control performance of the TMDI.

All the above suggest the applicability of considering TMDIs with varying inertance according to pre-set optimally tuned values for different objectives such as optimal vibration suppression or energy harvesting. The above findings also motivate future research directions by suggesting in a progressive manner semi-actively controlled TMDI with varying b , c_{TMDI} and even k_{TMDI} .

CHAPTER 7 : CONCLUDING REMARKS

A novel passive vibration control configuration, namely the tuned mass-damper-inerter (TMDI) has been proposed in this work. Initially, the TMDI was developed for single-degree-of freedom (SDOF) primary systems where its performance superiority over classical tuned-mass-dampers (TMDs) was analytically proven. Similarly, following a standard optimisation procedure, TMDI benefits in terms in vibration suppression and weight reduction has been demonstrated for multi-degree-of freedom (MDOF) primary systems. Next, the TMDI was applied for seismic protection of building structures where it was shown that it allows for significant reductions in terms of displacements, accelerations and TMDI ‘stroke’ compared with classical TMDs. Further, it was shown that by assuming TMDI with varying inertance, simultaneous vibration suppression and energy harvesting can be achieved.

Following from Table 1.1 – Matrix of Thesis Contribution, the above can be further elaborated into:

(I) Development of the TMDI for Single Degree of Freedom Primary Systems (SDOF)

The herein proposed TMDI configuration for SDOF primary systems takes advantage of the “mass amplification effect” of the inerter, a two terminal mechanical element of negligible mass/weight developing an internal (resisting) force proportional to the relative acceleration of its terminals which are free to move independently, by using it as an additional connective element between the TMD oscillating mass and the ground for SDOF primary systems. For both ground and force excitation, the governing differential equations of motion have been derived in the time and in the frequency

domain for TMDI equipped damped linear SDOF primary structures. The TMDI system has been herein considered for vibration control of harmonically and white noise support-excited structures. Closed-form analytical expressions for optimal TMDI parameters have been derived by application of a semi-empirical approach extensively used for the “optimum” design/tuning of the classical TMD to suppress the motion of harmonically excited undamped SDOF primary structures. Furthermore, optimal TMDI design parameters minimizing the relative displacement variance of undamped SDOF primary structures under white noise support excitation have been derived analytically in closed form as functions of the TMD mass and the inerter properties.

The main conclusion drawn from the above development stage can be summarised as:

- The TMDI can be viewed as a generalization of the classical TMD for both primary mass or support excited SDOF primary structures. Therefore, all established in the literature procedures for optimum design (“tuning”) of the classical TMD are readily applicable to achieve “optimal” performance for the new TMDI configuration.

- It was analytically shown that the TMDIs perform better than the classical TMDs for passive vibration control of harmonically excited undamped SDOF systems, for the same attached oscillating mass. The TMDI system is more effective than the classical TMD to suppress vibrations close to the natural frequency of the uncontrolled harmonically excited primary structure, while it is more robust to de-tuning effects.

- It was analytically shown that the TMDI configuration is more effective than the classical TMD for a fixed value of the TMD mass in suppressing the displacement variance of white noise excited undamped SDOF primary structures (based on optimally derived closed form design parameters). Further, the effectiveness of the TMDI increases for relatively low values of the TMD mass.

-It was proven that an optimum designed TMDI can achieve a significantly lighter passive vibration control solution (TMD mass replacement effect) for achieving equal levels of primary structure's response.

(II) Development of the TMDI for Multi Degree of Freedom Primary Systems (MDOF)

The TMDI is developed for MDOF systems by taking advantage of the 'mass amplification' effect of the inerter which is placed in between the TMD oscillating mass and the lead mass in mechanical chain-like (cascaded) primary structures. The governing differential equations of motion have been derived in the Laplace domain for damped chain-like MDOF primary structures incorporating a TMDI to suppress the fundamental mode of vibration. A standard optimization procedure has been considered to obtain optimum TMDI and classical TMD designs (as a special case of a TMDI with $b=0$) which minimize the displacement variance of the "lead" mass (most remote mass from the support) of the primary structure base excited by a stationary coloured stochastic process. Pertinent numerical data for the case of a 3-DOF damped primary structure base excited by a stationary coloured stochastic process reported that:

- The TMDI can be viewed as a generalization of the classical TMD for support excited MDOF primary structures and all optimum tuning approaches used in the literature for the TMD hold.

- The variance of the relative displacement of the lead mass, is reduced as the value of the inerter constant of proportionality increases.

- The TMDI configuration can either replace part of the TMD vibrating mass to achieve a significantly lighter passive vibration control solution (TMD mass replacement

effect), or improve the TMD performance for a fixed TMD mass (TMD mass amplification effect).

- The TMDI is more effective for relatively small attached masses in which case the inclusion of the inerter accommodates viscous dampers with much higher damping coefficients and “stiffer” connection arrangements compared to an optimally tuned classical TMD. The TMDI effectiveness becomes less significant for attached TMDI mass values greater than 6% of the total mass of the mechanical primary system.

(III) Application of the TMDI for Multi Degree of Freedom Primary Systems (MDOF) - Earthquake Protection of Multi-Storey Buildings

The TMDI has been applied for vibration control of seismically excited MDOF building structures. For this purpose the TMDI was placed in-between the top floor mass and the second to the top floor mass to control the fundamental mode of vibration. The governing differential equations of motion have been derived in time and frequency domain for TMDI equipped damped building structures ideally modelled as frames. A standard optimisation criterion has been adopted to obtain optimum TMDI parameters which minimize the mean square top floor displacement of low-height frame buildings base excited by a stationary stochastic process. Alongside, a TMDI parametric efficiency study has been undertaken, in order to emphasize on the importance of the primary structures’ properties when designing the TMDI passive control solutions. For this purpose, several building structures have been chosen such that they vary from a uniform in elevation structure to structures with reduced top floor stiffness and structures with reduced top floor mass. An input non-stationary stochastic process compatible with the elastic design spectrum of the European aseismic code provisions (EC8) has been assumed. Furthermore, the effectiveness of the proposed TMDI configuration over the

classical TMD has been demonstrated by performing response history analyses for an ensemble of 7 EC8 spectrum compatible field recorded strong ground motions.

(IIIa) When considering **EUROCODE 8 compatible design**, the main conclusions of the proposed TMDI application can be summarised as:

- It was proven that the TMDI outperforms the classical TMD mass for the same value of the additional oscillating mass when considering linear seismically excited MDOF buildings.

- It was numerically evidenced that, when the inerter is incorporated in the proposed TMDI configuration, that optimum design requires higher stiffness and damping values for the elements connecting the attached mass to the primary structure compared with classical TMD. Furthermore, these values also increase as the inerter constant of proportionality increases.

- It was proven that, the changes occurring in the properties of the primary system have a higher impact on the range of required TMDI parameters for optimum design, compared with the classical TMDI.

- The TMDI is most efficient for top-storey variance reduction of seismically excited structures with reduced top floor stiffness ('soft' top storey).

- It was proven that, changes in the optimum control frequency have a less significant impact on the TMDI performance compared with TMD, thus clearly suggesting an improved robustness of the TMDI towards estimating the properties of the primary structure over classical TMDs.

- It was shown that the TMDI effectiveness extends over a considerable range of frequencies allowing for efficient passive control of higher modes. This is drastically

opposed to classical TMDs which traditionally target only the mode they are tuned against.

- The TMDI system represents a significantly lighter passive vibration control solution compared with classical TMDs when considering linear seismically excited MDOF buildings.

(IIIb) When assessing the Performance of the proposed TMDI application using **field recorded EUROCODE 8 compatible accelerograms** the main conclusions can be summarised as:

- The optimally tuned TMDI solution achieves considerable reduction of the peak average top floor displacement and accelerations of the considered primary structures compared to the ones achieved by the optimally designed classical TMD, assuming the same additional mass in both cases.

- The TMDI configuration achieves significant reduction in the maximum displacement of the additional oscillating mass.

- The TMDI offers a broad-band influence compared with classical one-frequency targeted control of the TMD, thus justifying the practical applicability of the TMDI for medium-height to tall structures where large response amplitudes can be observed at frequencies higher than the fundamental one.

- Even though the TMDI achieves similar performance with the TMD when evaluating the displacement control capability, the TMDI allows for a significant reduction of floor accelerations.

(IV) Application of the TMDI for Single Degree of Freedom Primary Systems (SDOF) - Energy harvesting and vibration suppression.

The TMDI was applied for simultaneous energy harvesting and vibration suppression. The energy harvesting enabled TMDI system was thus proposed which incorporates a typical electromagnetic (EM) motor for electric energy generation connected in parallel with a spring and a damper to the attached TMDI mass. The herein considered EM comprises a moving magnet DC voice coil linear actuator connected to a resistance emulator circuit. The energy (or the power) available to harvest from the system has been parametrically and numerically quantified for an optimally designed TMDI for vibration suppression. The main conclusions of the proposed TMDI application can be summarised as:

- It was shown that the inerter constant b leverages the available power to be harvested in an optimally designed TMDI for vibration suppression. The larger the inerter constant b is, the less the available energy to be harvested. Therefore, the fact that an optimum vibration absorber is not an optimum energy harvester is confirmed.

- In the case of the energy harvesting enabled TMDI system, the value of b can change by considering flywheel-based inerters combined with a gearbox thus allowing a trade-off in between vibration control and energy harvesting capabilities.

- The applicability of considering TMDIs with varying inertance according to pre-set optimally tuned values for different objectives such as optimal vibration suppression or energy harvesting was proven.

Aiming to counteract some of the limitations of the present work, **further studies** can be directed towards:

- For SDOF Primary Systems:
 - Consideration of other optimisation methodologies/criteria for deriving closed form TMDI parameters in addition to Den Hartog's empirical method such as energy based methods.
 - Extend current study to nonlinear and damped SDOF primary structures to allow for a better analysis and interpretation of the TMDI robustness superiority over classical TMDs.
 - Consideration of non-linear dampers as opposed to linear ones used in the present study.
 - Establishing alternative configurations/topologies to combine TMDs with inerter devices to control the dynamic response of SDOF primary systems.

- For MDOF Primary Systems:
 - Establishing alternative configurations/topologies to combine TMDs with inerter devices to control the dynamic response of various mechanical and civil engineering structures and structural systems for stochastic and deterministic excitations and for various response minimization criteria.
 - A further extension of this work could consider placing the TMDI in-between not-consecutive floors, thus taking advantage of much-larger relative acceleration which implies greater forces generated by the inerter. Indeed, drawing on the findings herein, this solutions has already been introduced for the case of reliability-based Design of TMDI frame buildings under Seismic Excitation (Giaralis & Taflanidis, 2015).

-
- For application of the TMDI in seismically excited structures:
 - The present study can be extended to 3D primary building structures in order to capture torsional effects.
 - Consideration of pulse-like earthquakes.
 - Alternative work could also focus on the use of semi-active TMDIs which could be designed by considering alternative optimisation criteria (e.g. acceleration based, life-cycle costs analysis and others)

 - For application of the TMDI for simultaneous vibration control and energy harvesting
 - Extend present study and explore electric energy harvesting from the kinetic energy generated by the rotation of the inerters' flywheel.
 - Explore other connectivity arrangements of spring-mass-damper-inerter and electric motor harvester.
 - Consider the dynamics/coupling between the electric motor, energy harvesting circuit in the study.

Furthermore, in addition to the above, further research could focus on:

- TMDI for vibration control and energy harvesting of wind excited structures.
- TMDI for medium to high-rise structures.
- Prototyping and experimental work thus validating the herein reported numerical results.

APPENDIX I - ALTERNATIVE CONNECTIVITY ARRANGEMENTS OF SPRINGS, DAMPERS AND INERTERS

Alternative connectivity arrangements of spring-damper and inerter device have also been explored in addition to the proposed TMDI configuration, as suggested by Figure 0.1.

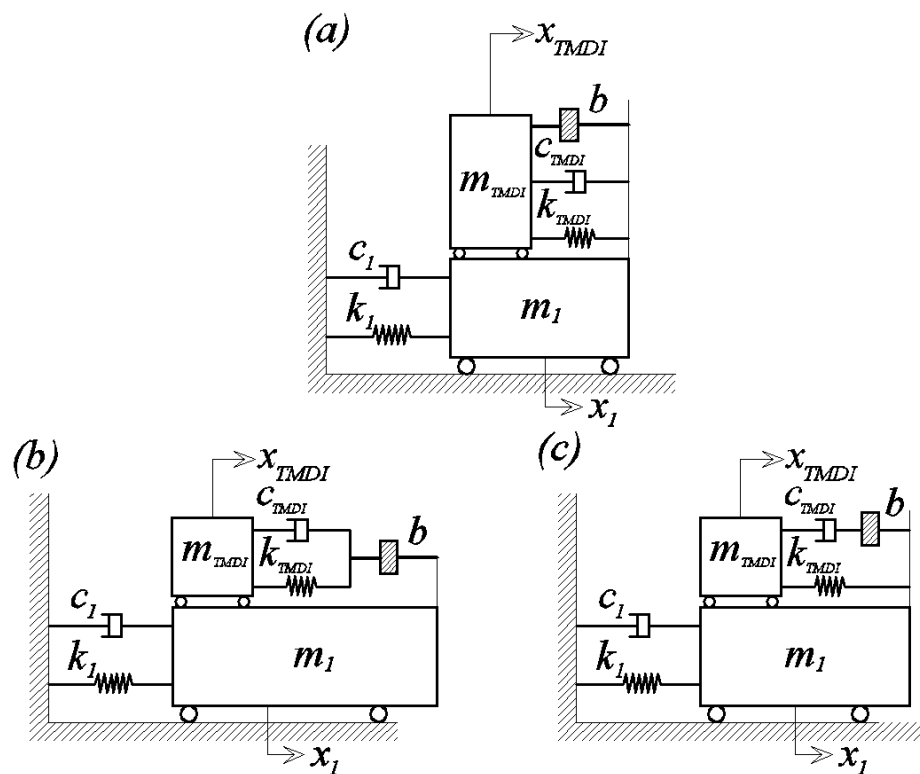


Figure 0.1. Alternative connectivity arrangements of TMD-inerter considered

Specifically, a parallel connection of spring-damper-inerter as described in Figure 0.1 was adopted. Also the inclusion of an inerter device to the classical TMD configuration was considered by introducing the inerter in series with a parallel connection of spring and damper as shown in Figure 0.1b. Furthermore, a series connection of damper and inerter device in parallel with spring was explored as shown in Figure 0.1c. For this alternative arrangements, the inclusion of an inerter device under the

proposed configurations does not outperform the classical TMD in controlling the dynamic behaviour of the primary system.

For example, considering the configuration given by Figure 0.1a, it can be shown following the methodology described in detail in Chapter 3.3 that the optimum frequency ratio can be expressed as:

$$v_{TMDI} = \frac{\sqrt{1 + \beta + \mu}}{1 + \mu} \quad (0-1)$$

Furthermore, the maximum dynamic amplification factor achieved at the points P_1 and P_2 (see Chapter 3.3) can be obtained as:

$$\max_{\omega} \{|G_1(\omega)|\} = |G_1(\omega_{P_1})| = |G_1(\omega_{P_2})| = \sqrt{\frac{2\beta\mu + 2\beta + \mu + 2}{\mu}} \quad (0-2)$$

For the case of traditional TMD configuration, the Dynamic amplification factor which can be achieved at the two points is expressed as:

$$\max_{\omega} \{|G_1(\omega)|\} = |G_1(\omega_{P_1})| = |G_1(\omega_{P_2})| = (1 + \mu) \sqrt{\frac{2}{\mu}} \quad (0-3)$$

Based on the above, it can be deduced that:

$$\sqrt{\frac{2\beta\mu + 2\beta + \mu + 2}{\mu}} > (1 + \mu) \sqrt{\frac{2}{\mu}}, \quad \forall (\beta, \mu) \quad (0-4)$$

Thus, for all values of β (and thus for all values of inerter constant of proportionality, b) the inclusion of parallel combination of spring, damper and inerter

device to connect the primary system to the TMD does not have an improved effect on the response of the primary system, compared with the classical case of TMD. Only when $b = 0$, the Dynamic Amplification Factor becomes equal for both cases, and for any values of $b > 0$ we have the inequality in Equation (0-4). Furthermore, the above results can be supplemented by the graph in Figure 0.2.

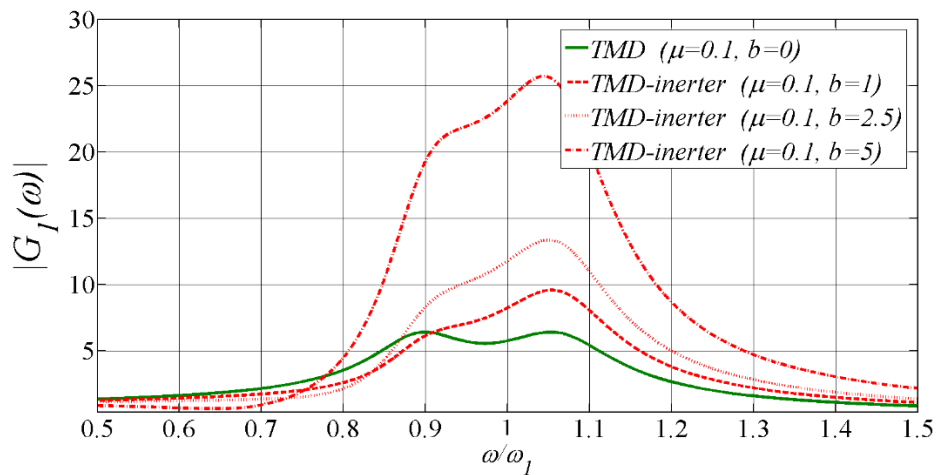


Figure 0.2. Dynamic amplification factor for the system equipped with TMD and for the same system equipped with TMD-inerter, for varying values of b

Following a similar approach, it can be proved the inclusion of the inerter in all other configuration explored does not outperform the traditional TMD.

APPENDIX II – TUNED-MASS-DAMPER-INERTER EQUATIONS OF MOTION USING A SYSTEM NETWORK APPROACH

As an alternative approach to Newton’s method used in Section 4.2, the derivation of the governing equations of motion of the linear dynamical structural system of Figure 4.1 can be obtained by considering passive mechanical “admittances” Q defined as the ratio of force over velocity in the Laplace domain (e.g. Hixson, 1961). This is a common practice in topology studies of mechanical system networks. In this respect, the considered MDOF primary structure equipped with the TMDI configuration of Figure 4.1 can be interpreted as a system of $n+1$ masses inter-connected by “networks” represented by admittances Q as shown in Figure 0.3.

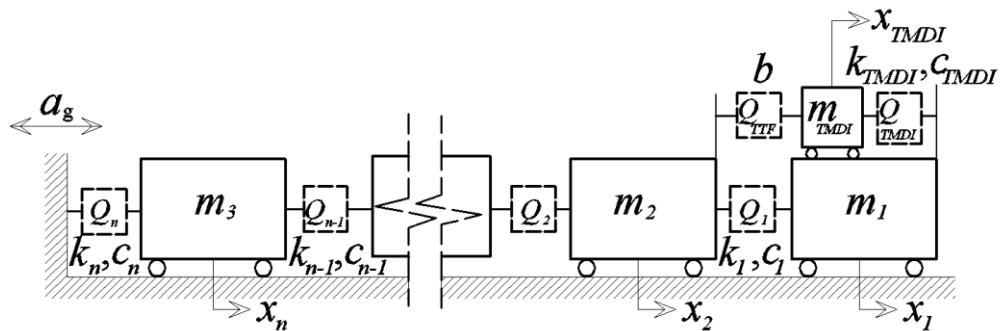


Figure 0.3. Multi-degree-of-freedom (MDOF) primary structure incorporating the proposed tuned mass-

In particular, the mechanical admittances shown in Figure 0.3 are expressed in terms of the standard Laplace variable s by:

$$Q_{TTF}(s) = bs \quad ; \quad Q_{TMDI}(s) = \frac{k_{TMDI}}{s} + c_{TMDI} \quad ; \quad Q_j(s) = \frac{k_j}{s} + c_j \quad (j = 1 \dots n) \quad (0-5)$$

where Q_{TTF} is the admittance corresponding to the inerter (two terminal flywheel), Q_{TMDI} is the admittance corresponding to the mass-spring-and-damper-in-parallel “network”

connecting the additional attached mass to the lead mass m_1 of the primary structure and Q_j are the admittances of the n spring-plus-dashpot-in-parallel “networks” linking the n masses of the primary mechanical system together and with the ground (see Figure 4.1 and Figure 0.3). By relying on the previous expressions, the $n+1$ equations of motions of the linear MDOF dynamical system of Figure 4.1 can be written in the Laplace domain as:

$$Q(s) \tilde{\mathbf{X}}(s) = -\mathbf{M}_s \delta \tilde{A}(s) \quad (0-6)$$

where :

$$Q = \begin{bmatrix} m_{TMDI}s^2 + (Q_{TMDI} + Q_{TTF})s & -Q_{TMDI}s & -Q_{TTF}s & 0 & \cdots & 0 & 0 \\ -Q_{TMDI}s & m_1s^2 + (Q_1 + Q_{TMDI})s & -Q_1s & 0 & \cdots & 0 & 0 \\ -Q_{TTF}s & -Q_1s & m_2s^2 + (Q_1 + Q_2 + Q_{TMDI})s & -Q_2s & \cdots & 0 & 0 \\ 0 & 0 & -Q_2s & m_3s^2 + (Q_2 + Q_3)s & \ddots & \vdots & \vdots \\ 0 & 0 & 0 & -Q_3s & \ddots & -Q_{n-2}s & 0 \\ \vdots & \vdots & \vdots & \vdots & \ddots & \vdots & \vdots \\ 0 & 0 & 0 & 0 & \cdots & m_n s^2 + (Q_{n-1} + Q_n)s & -Q_{n-1}s \\ & & & & & -Q_{n-1}s & m_n s^2 + (Q_{n-1} + Q_n)s \end{bmatrix} \quad (0-7)$$

δ is the unit column vector, $\tilde{A}(s)$ is the Laplace transform of the support acceleration process $a_g(t)$, \mathbf{M}_s is the diagonal mass matrix of the primary system written as:

$$\mathbf{M}_s = \begin{bmatrix} m_{TMDI} & 0 & \cdots & 0 \\ 0 & m_1 & \cdots & \vdots \\ \vdots & \vdots & \ddots & 0 \\ 0 & \cdots & 0 & m_n \end{bmatrix} \quad (0-8)$$

and $\tilde{\mathbf{X}}(s)$ is the Laplace transform of the vector:

$$\mathbf{x} = \{x_{TMDI}(t) \quad x_1(t) \quad x_2(t) \quad \cdots \quad x_n(t)\}^T \quad (0-9)$$

collecting the relative displacements of the $n+1$ masses included in the considered system. In the latter equation, the superscript “ T ” denotes matrix transposition.

The frequency response function (FRF) $G_1(\omega)$ relating the (input) support excitation in terms of acceleration to the (output) relative displacement of the lead mass m_1 of the primary structure is reached by evaluating the ratio:

$$G_1(s) = \frac{\tilde{x}_1(s)}{\tilde{A}(s)} \quad (0-10)$$

along the imaginary axis $s=i\omega$. In the latter equation, $\tilde{x}_1(s)$ is the Laplace transform of $x_1(t)$ which is analytically found by solving Equation (0-6). That is,

$$\tilde{\mathbf{X}}(s) = -\mathcal{Q}^{-1}(s)\mathbf{M}_s\delta\tilde{A}(s) \quad (0-11)$$

Note that, the transfer function in Section 4-6 yields the same results as in Equation (0-11) but uses a different approach to evaluate the denominator.

REFERENCES

- Ali, S. F., & Adhikari, S. (2013). Energy harvesting dynamic vibration absorbers. *Journal of Applied Mechanics*, 80(4), 041004.
- De Angelis, M., Perno, S., & Reggio, A. (2012). Dynamic response and optimal design of structures with large mass ratio TMD. *Earthquake Engineering & Structural Dynamics*, 41(1), 41-60.
- Asami, T., Nishihara, O., & Baz, A. M. (2002). Analytical solutions to H_∞ and H_2 optimization of dynamic vibration absorbers attached to damped linear systems. *Journal of vibration and acoustics*, 124(2), 284-295.
- Ayorinde, E. O., & Warburton, G. B. (1980). Minimizing structural vibrations with absorbers. *Earthquake Engineering & Structural Dynamics*, 8(3), 219-236.
- Bakre, S. V., & Jangid, R. S. (2007). Optimum parameters of tuned mass damper for damped main system. *Structural Control and Health Monitoring*, 14(3), 448-470.
- Bogdanoff, J. L., Goldberg, J. E., & Bernard, M. C. (1961). Response of a simple structure to a random earthquake-type disturbance. *Bulletin of the Seismological Society of America*, 51(2), 293-310.
- Brock, JE. (1946). A note on the damped vibration absorber. *Journal of Applied Mechanics*, 13(4): A-284.

Brown, B., & Singh, T. (2011). Minimax design of vibration absorbers for linear damped systems. *Journal of Sound and Vibration*, 330(11), 2437-2448.

CEN. Eurocode 8. (2004). Design of structures for earthquake resistance –part 1: general rules, seismic actions and rules for buildings. EN 1998-1, 2004. Brussels: Comité Européen de Normalisation.

Chang, C. C. (1999). Mass dampers and their optimal designs for building vibration control. *Engineering Structures*, 21(5), 454-463.

Chen, M. Z., Hu, Y., Huang, L., & Chen, G. (2014). Influence of inerter on natural frequencies of vibration systems. *Journal of Sound and Vibration*, 333(7), 1874-1887.

Cheung, Y. L., & Wong, W. O. (2011). H-infinity optimization of a variant design of the dynamic vibration absorber—revisited and new results. *Journal of sound and vibration*, 330(16), 3901-3912.

Li, C., Liang, M., Wang, Y., & Dong, Y. (2011a). Vibration suppression using two-terminal flywheel. Part I: Modeling and characterization. *Journal of Vibration and Control*, 18(8):1096-1105.

Li, C., Liang, M., Wang, Y., & Dong, Y. (2011b). Vibration suppression using two-terminal flywheel. Part II: application to vehicle passive suspension. *Journal of Vibration and Control*, 18(8):1353-1365.

Chung, L. L., Wu, L. Y., Yang, C. S. W., Lien, K. H., Lin, M. C., & Huang, H. H. (2013). Optimal design formulas for viscous tuned mass dampers in wind-excited structures. *Structural Control and Health Monitoring*, 20(3), 320-336.

Clough, RW & Penzien, J. (1993). Dynamics of Structures. Second Edition. *McGraw-Hill*, New York.

Den Hartog, JP. (1956). Mechanical Vibrations. 4th Edition. *McGraw-Hill*. New York

Evangelou, S., Sharp, R. S., & Smith, M. C. (2004, December). Steering compensation for high-performance motorcycles. In *Decision and Control, 2004. CDC. 43rd IEEE Conference on* (Vol. 1, pp. 749-754). IEEE.

Feng, M. Q., & Mita, A. (1995). Vibration control of tall buildings using mega subconfiguration. *Journal of Engineering Mechanics*, 121(10), 1082-1088.

Frahm, H. (1911) Device for Damping Vibrations of Bodies, *U.S. Patent*, 989958.

Garrido, H., Curadelli, O., & Ambrosini, D. (2013). Improvement of tuned mass damper by using rotational inertia through tuned viscous mass damper. *Engineering Structures*, 56, 2149-2153.

Ghosh, A., & Basu, B. (2007). A closed-form optimal tuning criterion for TMD in damped structures. *Structural Control and Health Monitoring*, 14(4), 681-692.

Giaralis, A., & Spanos, P. D. (2009). Wavelet-based response spectrum compatible synthesis of accelerograms—Eurocode application (EC8). *Soil Dynamics and Earthquake Engineering*, 29(1), 219-235.

Giaralis, A., & Spanos, P. D. (2012). Derivation of response spectrum compatible non-stationary stochastic processes relying on Monte Carlo-based peak factor estimation. *Earthquake and Structures*, 3(3-4), 581-609.

Giaralis, A., & Spanos, P. D. (2010). Effective linear damping and stiffness coefficients of nonlinear systems for design spectrum based analysis. *Soil Dynamics and Earthquake Engineering*, 30(9), 798-810.

Giaralis, A & Taflanidis, A.A. (2015 July 12-15). Reliability-based Design of Tuned Mass-Damper-Inerter (TMDI) Equipped Multi-storey Frame Buildings under Seismic Excitation. *12th International Conference on Applications of Statistics and Probability in Civil Engineering, ICASP12*. Vancouver, Canada.

Gonzalez-Buelga, A., Clare, L. R., Cammarano, A., Neild, S. A., Burrow, S. G., & Inman, D. J. (2014). An optimised tuned mass damper/harvester device. *Structural Control and Health Monitoring*, 21(8), 1154-1169.

Hixson, E.L. (1961). Mechanical Impedance and Mobility. In C. M. Harris, A.G. Piersol (Eds.), *Shock and Vibration Handbook*, McGraw-Hill Book Company Inc., New York, chap. 10.

Hoang, N., & Warnitchai, P. (2005). Design of multiple tuned mass dampers by using a numerical optimizer. *Earthquake engineering & structural dynamics*, 34(2), 125-144.

Hwang, J. S., Kim, J., & Kim, Y. M. (2007). Rotational inertia dampers with toggle bracing for vibration control of a building structure. *Engineering structures*, 29(6), 1201-1208.

Hoang, N., Fujino, Y., & Warnitchai, P. (2008). Optimal tuned mass damper for seismic applications and practical design formulas. *Engineering Structures*, 30(3), 707-715.

Ikago, K., Saito, K., & Inoue, N. (2012). Seismic control of single-degree-of-freedom structure using tuned viscous mass damper. *Earthquake Engineering & Structural Dynamics*, 41(3), 453-474.

Roberts, J. B. & Spanos, P. D. (2003). *Random Vibration and Statistical Linearization*, Dover Publications, New York.

Kanai, K. (1957) Semi-empirical formula for the seismic characteristics of the ground. University of Tokyo, *Bulletin of the Earthquake Research Institute*; 35, 309-32.

Karavasilis, T. L., Krawala, S., & Hale, E. (2012). Hysteretic model for steel energy dissipation devices and evaluation of a minimal-damage seismic design approach for steel buildings. *Journal of Constructional Steel Research*, 70, 358-367.

Krenk, S., & Høgsberg, J. (2008). Tuned mass absorbers on damped structures under random load. *Probabilistic Engineering Mechanics*, 23(4), 408-415.

Krenk, S. (2005). Frequency analysis of the tuned mass damper. *Journal of applied mechanics*, 72(6), 936-942.

Lazar, I. F., Neild, S. A., & Wagg, D. J. (2014a). Using an inerter-based device for structural vibration suppression. *Earthquake Engineering & Structural Dynamics*, 43(8), 1129-1147.

Lazar, I. F., Neild, S. A., & Wagg, D. J. (2014b). Inerter-based vibration suppression systems for laterally and base-excited structures. *Proceedings of EUROODYN 2014*, 1525-1530.

Lee, C. L., Chen, Y. T., Chung, L. L., & Wang, Y. P. (2006). Optimal design theories and applications of tuned mass dampers. *Engineering structures*, 28(1), 43-53.

Leung, A. Y. T., & Zhang, H. (2009). Particle swarm optimization of tuned mass dampers. *Engineering Structures*, 31(3), 715-728.

Lin, C. C., Wang, J. F., Lien, C. H., Chiang, H. W., & Lin, C. S. (2010). Optimum design and experimental study of multiple tuned mass dampers with limited stroke. *Earthquake Engineering & Structural Dynamics*, 39(14), 1631-1651.

Liu, K., & Liu, J. (2005). The damped dynamic vibration absorbers: revisited and new result. *Journal of Sound and Vibration*, 284(3), 1181-1189.

Marian, L., & Giaralis, A. (2014). Optimal design of a novel tuned mass-damper–inertor (TMDI) passive vibration control configuration for stochastically support-excited structural systems. *Probabilistic Engineering Mechanics*, 38, 156-164.

Martelli, A., Forni, M., & Clemente, P. (2012, September). Recent worldwide application of seismic isolation and energy dissipation and conditions for their correct use. In *Proceedings on electronic key of the 15th World conference on earthquake engineering (15WCEE), Lisbon, Conference programme* (Vol. 52, pp. 24-28).

Matta, E., & De Stefano, A. (2009a). Robust design of mass-uncertain rolling-pendulum TMDs for the seismic protection of buildings. *Mechanical Systems and Signal Processing*, 23(1), 127-147.

Matta, E., & De Stefano, A. (2009b). Seismic performance of pendulum and translational roof-garden TMDs. *Mechanical Systems and Signal Processing*, 23(3), 908-921.

Moutinho, C. (2012). An alternative methodology for designing tuned mass dampers to reduce seismic vibrations in building structures. *Earthquake Engineering & Structural Dynamics*, 41(14), 2059-2073.

Naeim, F., & Kelly, J. M. (1999). *Design of seismic isolated structures: from theory to practice*. John Wiley & Sons.

Nishihara, O., & Asami, T. (2002). Closed-form solutions to the exact optimizations of dynamic vibration absorbers (minimizations of the maximum amplitude magnification factors). *Journal of Vibration and Acoustics*, 124(4), 576-582.

Ormondroyd, J. (1928). Theory of the dynamic vibration absorber. *Transaction of the ASME*, 50, 9-22.

Ozbulut, O. E., Bitaraf, M., & Hurlebaus, S. (2011). Adaptive control of base-isolated structures against near-field earthquakes using variable friction dampers. *Engineering Structures*, 33(12), 3143-3154.

Papageorgiou, C., & Smith, M. C. (2005, December). Laboratory experimental testing of inerters. In *Decision and Control, 2005 and 2005 European Control Conference. CDC-ECC'05. 44th IEEE Conference on* (pp. 3351-3356). IEEE.

Petrone, C., Magliulo, G., & Manfredi, G. (2015). Seismic demand on light acceleration-sensitive nonstructural components in European reinforced concrete buildings. *Earthquake Engineering & Structural Dynamics*, 44(8), 1203-1217.

Pinkaew, T., Lukkunaprasit, P., & Chatupote, P. (2003). Seismic effectiveness of tuned mass dampers for damage reduction of structures. *Engineering Structures*, 25(1), 39-46.

Rana, R., & Soong, T. T. (1998). Parametric study and simplified design of tuned mass dampers. *Engineering structures*, 20(3), 193-204.

Ricciardelli, F., & Vickery, B. J. (1999). Tuned vibration absorbers with dry friction damping. *Earthquake engineering & structural dynamics*, 28(7), 707-723.

Rüdinger, F. (2006). Optimal vibration absorber with nonlinear viscous power law damping and white noise excitation. *Journal of engineering mechanics*, 132(1), 46-53.

Sadek, F., Mohraz, B., Taylor, A. W., & Chung, R. M. (1997). A method of estimating the parameters of tuned mass dampers for seismic applications. *Earthquake Engineering and Structural Dynamics*, 26(6), 617-636.

Salvi, J., & Rizzi, E. (2011). Minimax optimization of Tuned Mass Dampers under seismic excitation. In *EURODYN 2011: 8th International Conference on Structural Dynamics, Leuven, Belgium, 4-6 July 2011* (pp. 1892-1899).

Shi, X., & Cai, C. S. (2008). Suppression of vehicle-induced bridge vibration using tuned mass damper. *Journal of Vibration and Control*, 14(7), 1037–1054.

Smith, M. C. (2002). Synthesis of mechanical networks: the inerter. *Automatic Control, IEEE Transactions on*, 47(10), 1648-1662.

Soong, T. T., & Dargush, G. F. (1999). Passive energy dissipation and active control. *Structural Engineering Handbook*. CRC Press LLC, Boca Raton.

Spencer Jr, B. F., & Nagarajaiah, S. (2003). State of the art of structural control. *Journal of structural engineering*, 129 (7), 845-856.

Soong, T. T., & Spencer, B. F. (2002). Supplemental energy dissipation: state-of-the-art and state-of-the-practice. *Engineering Structures*, 24(3), 243-259.

Soto-Brito, R., & Ruiz, S. E. (1999). Influence of ground motion intensity on the effectiveness of tuned mass dampers. *Earthquake engineering & structural dynamics*, 28(11), 1255-1271

Swift, S. J., Smith, M. C., Glover, A. R., Papageorgiou, C., Gartner, B., & Houghton, N. E. (2013). Design and modelling of a fluid inerter. *International Journal of Control*, 86(11), 2035-2051.

Takewaki, I., Murakami, S., Yoshitomi, S., & Tsuji, M. (2012). Fundamental mechanism of earthquake response reduction in building structures with inertial dampers. *Structural Control and Health Monitoring*, 19(6), 590-608.

Tang, X., & Zuo, L. (2012). Simultaneous energy harvesting and vibration control of structures with tuned mass dampers. *Journal of Intelligent Material Systems and Structures*, 23(18), 2117-2127.

Wang, F. C., Chen, C. W., Liao, M. K., & Hong, M. F. (2007, December). Performance analyses of building suspension control with inerters. In *Decision and Control, 2007 46th IEEE Conference on* (pp. 3786-3791). IEEE.

Wang, F. C., Hong, M. F., & Chen, C. W. (2010). Building suspensions with inerters. *Proceedings of the Institution of Mechanical Engineers, Part C: Journal of Mechanical Engineering Science*, 224(8), 1605-1616.

Wang, F. C., Hong, M. F., & Lin, T. C. (2011). Designing and testing a hydraulic inerter. *Proceedings of the Institution of Mechanical Engineers, Part C: Journal of Mechanical Engineering Science*, 225(1), 66-72.

Wang, J. F., Lin, C. C., & Lian, C. H. (2009). Two-stage optimum design of tuned mass dampers with consideration of stroke. *Structural Control and Health Monitoring*, 16(1), 55-72.

Warburton, G. B. (1982). Optimum absorber parameters for various combinations of response and excitation parameters. *Earthquake Engineering & Structural Dynamics*, 10(3), 381-401.

Wong, W. O., & Cheung, Y. L. (2008). Optimal design of a damped dynamic vibration absorber for vibration control of structure excited by ground motion. *Engineering Structures*, 30(1), 282-286.

Yamaguchi, H., & Harnpornchai, N. (1993). Fundamental characteristics of multiple tuned mass dampers for suppressing harmonically forced oscillations. *Earthquake engineering & structural dynamics*, 22(1), 51-62.

Yoshioka, H., Ramallo, J. C., & Spencer Jr, B. F. (2002). “Smart” base isolation strategies employing magnetorheological dampers. *Journal of engineering mechanics*, 128(5), 540-551.

Zuo, L., & Tang, X. (2013). Large-scale vibration energy harvesting. *Journal of intelligent material systems and structures*, 24(11), 1405-1430.